Universita' degli Studi di Padova
Facoltà di Scienze MM.FF.NN.

Dipartimento di Astronomia
Scuola di Dottorato in Astronomia

ARCS: THE ASIAGO RED CLUMP SPECTROSCOPIC SURVEY AND ITS FIRST APPLICATIONS

Ph. D. Thesis of:
Marica Valentini

Supervisor:
Prof. **Ulisse Munari**

To my family...

CONTENTS

LIST OF FIGURES

LIST OF TABLES

1 RED CLUMP STARS

Contents

1.1 INTRODUCTION

Red Clump stars are of strong interest: their near-constant luminosity, high brightness and the fact that this phase of stellar evolution is usually well populated makes the Red Clump a reliable distance indicator and an useful tool for investigating the three-dimensional kinematics and properties of various Galactic subsystems.
We aim to create an accurate catalog for a sample of Red Clump stars belonging to the Solar Neighbourhood. This catalog contains accurate multi-epoch radial velocities, atmospheric parameters (T_{eff}, *logg*, [M/H]) and space velocities (U,V,W) for a well selected sample of ~300 equatorial Red Clump stars belonging to the solar neighbourhood.
We observed with the Asiago 1.82m + Echelle spectrograph an highly pruned sample of Red Clump stars. Radial velocities are obtained via cross-correlation against synthetic templates. We derived atmospheric parameters thought a fitting of the stellar spectra against a synthetic grid of spectra built from the library of Munari et al. (2005).
We obtained accurate radial velocities ($\sigma_{Vrad} \leq 0.5$ Km/s) and precise atmospheric parameters ($\sigma_{T_{eff}} \leq 50$ K, $\sigma_{logg} \leq 0.12$ dex,

$\sigma_{M/H} \leq 0.11$ dex) for 300 Red Clump stars of the Solar Neighbourhood. We also deeply tested the χ^2 method we adopted, demonstrating its reliability.
At the end we study some properties of the Solar Neighborhood by using ARCS Red Clump stars.

1.2 THE RED CLUMP

Red Clump stars take their name from their position in the HR diagram: they form a clump on the giant branch.

This feature is easily recognizable in the Hertzsprung-Russel diagrams built with stars of the Hipparcos Catalog (Perryman et al.,1997) in Fig. 1: it is the overdensity on the Red Giant branch. The Red Clump is considered the metal-rich counterpart to the horizontal branch of older and metal poorer clusters. This period in a star evolution corresponds to the core helium-burning phase, whereas the main sequence is the core hydrogen-burning phase.
Since the pioneering work of Cannon (1970) and Faulkner and Cannon (1973) the clump of red giants in the colour-magnitude diagram (CMD) of intermediate-age and old open clusters was recognized as being formed by stars in the stage of central helium burning. They correctly interpret the near constancy of the clump absolute magnitude as the result of He ignition in an electron-degenerate core. Under these conditions, He burning cannot start until the stellar core mass attains a critical value of about 0.45 $M_\odot$. It then follows that low-mass stars developing a degenerate He core after H exhaustion, have similar core masses at the beginning of He burning, and hence similar luminosities.
Their abundance, the presence of good parallaxes in the Hipparcos catalog, luminosities and the little spread in absolute luminosities distribution, make this type of star good standard candle candidate for estimating astronomical distances both within our galaxy and to nearby galaxies and clusters.

1.3 STRUCTURE AND EVOLUTION OF RED CLUMP STARS

The Red Clump is mainly composed by low-intermediate mass stars that are experiencing the core helium burning. This section briefly explains the evolution of an intermediate mass star after the exhaustion of the hydrogen burning in the core.

During the main sequence phase, because of the absence of convection, the star burns H more rapidly in the core than in the outer regions, so there is a chemical gradient with hydrogen de-

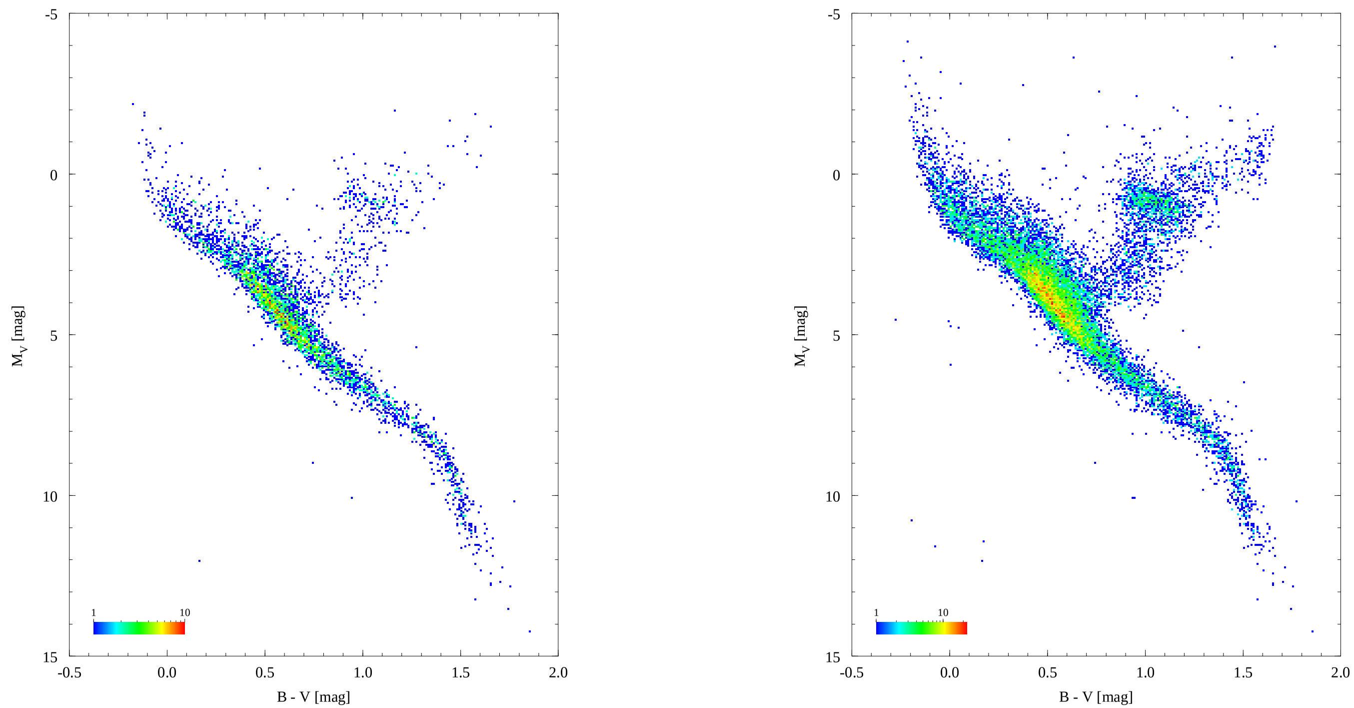

Figure 1: Hertzsprung-Russell (M_V, B-V) diagrams for the 4902 (a) and 16631 (b) stars from the Hipparcos Catalog (Perryman et al., 1997) with relative distance precision of $\sigma_{pi}/\pi < 0.05$ (a) and $\sigma_{pi}/\pi < 0.1$, and $\sigma_{B-V} \leq 0.025$ mag. Colors (gray graduate shading from black to white) indicates number of stars in a cell of 0.01 mag in (B-V) and 0.01 mag in M_V. The Red Clump is the overdensity on the Red Giant branch recognizable in the box $0.7 \leq B-V \leq 1.2$ and $-1.5 \leq M_V \sim 0$.

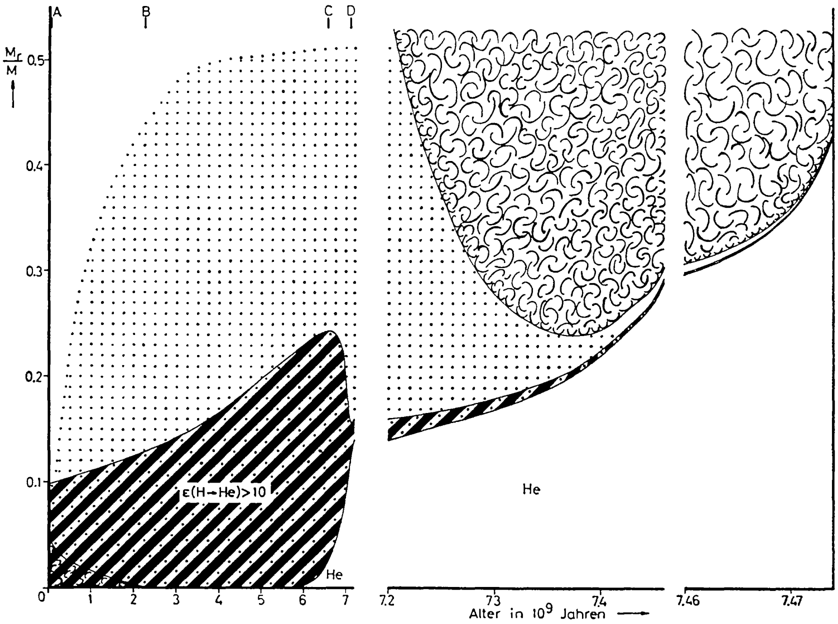

Figure 2: The evolution of the internal structure of a star of 1.3 $M_\odot$ in function of the time, till the He flash. The x-axis gives the time in 10^9 yrs after the ignition of hydrogen, in the y-asses is plotted the ratio m/M. The main region of hydrogen burning is hatched, "cloudy" areas indicate convection. Regions of variable hydrogen content are dotted. From Thomas (1967).

creasing toward the center. After central H burning, the star has a He core, which, in the absence of energy sources, tends to be isothermal. The central H burning moves into a shell that moves outwards. The shell become thinner as it moves outside, the core contracts and the envelope expands. In Fig. 2 (Thomas, 1967) is illustrated the evolution of the internal structure of a star of 1.3 $M_\odot$: the abscissa gives the age after the ignition of H in units of 10^9 yrs: the hydrogen burning in the core happens to point A to point D.
When the star reaches the Hayashi line, the envelope become convective, the luminosity increase while the T_{eff} is constant: in the HR diagram the star is rising the Red Giant Branch (RGB), as evidenced in Fig. 3. In 2 (Thomas, 1967) this phase is illustrated after the point D: is evidenced the quiescent He core, the H-burning shell that is moving outwards and the convective region.

At the end of the RGB, low-mass stars ignite He in a degenerate shell through a relatively strong He flash and then quiescently burn it in a convective central region, as shown in Fig. 3 and Fig. 5. The onset of electron degeneracy after the central H-exhaustion postpones the He-ignition until the core mass grows to about $M_c \simeq 0.45 M\odot$. Since the He-flash in a degenerate gas starts at $M_c \simeq 0.45 \div 0.55 M\odot$ for all the stars (except for a little dependence on metallicity) all these stars has the same superficial luminosity. This is clearly visible in Fig. 4: ZAHB models with masses 0.7 $M_\odot$ $\leq$ M $\leq$2 M_{Hef} describe a kind of semi-circle in both diagrams. The small range of luminosities reflects the small range of core mass at the moment of He ignition . That is confirmed by CMD of Globular Clusters: all RGB finish at the same luminosity.

The maximum mass of stars that follows this evolutionary scheme is denoted as M_{Hef} (Chiosi, 1992). Stars of masses slightly above M_{Hef} have a weakly degenerate core, and are able to ignite helium with a lower core mass (about 0.33 $M_\odot$). Therefore their lifetime in the RGB is significantly abbreviated. For stars of higher masses, the core mass at the He ignition becomes an increasing function of stellar mass and the phase in the RGB is practically missing. The value of M_{Hef} depends in the extent of convective cores during the main sequence phase: for solar composition models and for the classical Schwartzchild criterion for convective instability $M_{Hef} \sim 2.4 M_\odot$ (Castellani, 1992).
At this point the star is in the Horizontal Branch. It produces nuclear energy in two different places: in the core (helium burning) and in a shell (hydrogen burning).

The distribution of these stars in the CMD is very narrow in luminosity, but they may have a large extension in T_{eff}, hence the

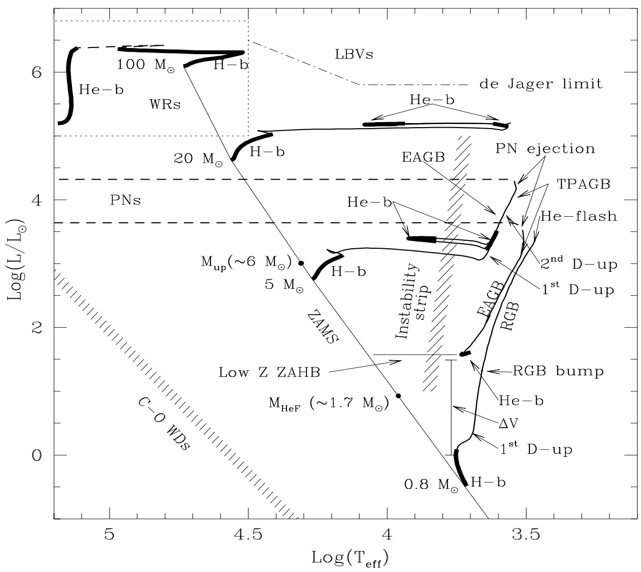

Figure 3: The evolutionary paths in the Hertzsprung Russel Diagram of model stars of composition [Z=0.008, Y=0.25] and of initial mass 0.8 $M_{\odot}$, 5 $M_{\odot}$, 20 $M_{\odot}$ and 100 $M_{\odot}$. The models are calculated with the overshoot scheme for central convection. M_{Hef} and M_{up} are, respectively, the masses separating low-mass stars from intermediate-mass stars and intermediate-mass stars from massive ones. For low- and intermediate-mass stars the tracks go from the Zero Age Main Sequence to the end of Asymptotic Giant Branch (AGB) phase, whereas for massive stars tracks reach the stage of C-ignition in the core. H-b and He-b stand for core H- and He-burning. He-flash indicates the stage of violent ignition of central He-burning in low-mass stars at the tip of the Red Giant Branch (RGB). The main episodes of external mixing (1^{st} and 2^{nd} dredge-up) are indicated as 1^{st}D-up and 2^{nd}D-up. The horizontal line labeled ZAHB indicates the locus of the Zero Age Horizontal Branch - core helium burning models- of low mass stars with composition typical of globular clusters. The shaded vertical band show the instability strip of Cepheid and RR Lyrae stars. The thick portions of the tracks indicates the stages of slow evolution, where the majority of stars are observed.(from C. Chiosi online lessons)

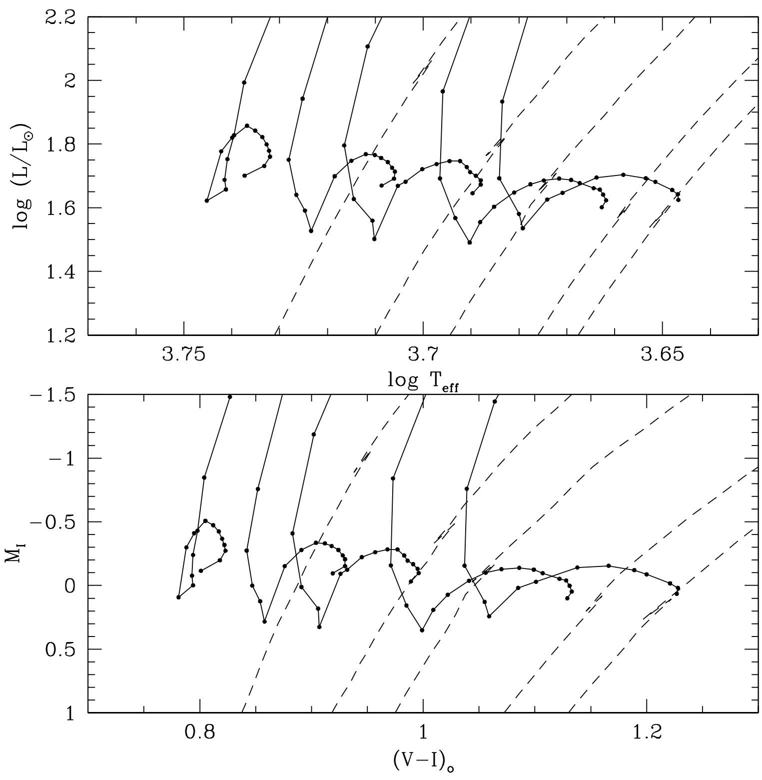

Figure 4: Position of the ZAHB (onset of quiescent He burning) for stellar evolutionary tracks of different masses and metallicities. The upper panel shows the position of ZAHB in the HR diagram; the lower panel in the M_I vs $V - I$ diagram. Dots represent the computed models at mass intervals of 0.1 $M_{\odot}$ for 0.7 $M_{\odot}$ $\leq$ M $\leq$2 $M_{\odot}$, and 0.2 to 0.5 $M_{\odot}$ for M$\geq$2 $M_{\odot}$. Metallicities are the continuous lines, from left to right: Z= 0.001, 0.004, 0.008, 0.019, 0.03 . The dashed line is the RGBs of 4 Gyr isochrones with the same values of metallicities. Is visible that ZAHB models with masses 0.7 $M_{\odot}$ $\leq$ M $\leq$2 M_{Hef}describe a kind of semi-circle in both diagrams: the small range of luminosities reflects the small range of core mass at the moment of He ignition. Figure taken from Girardi (1999).

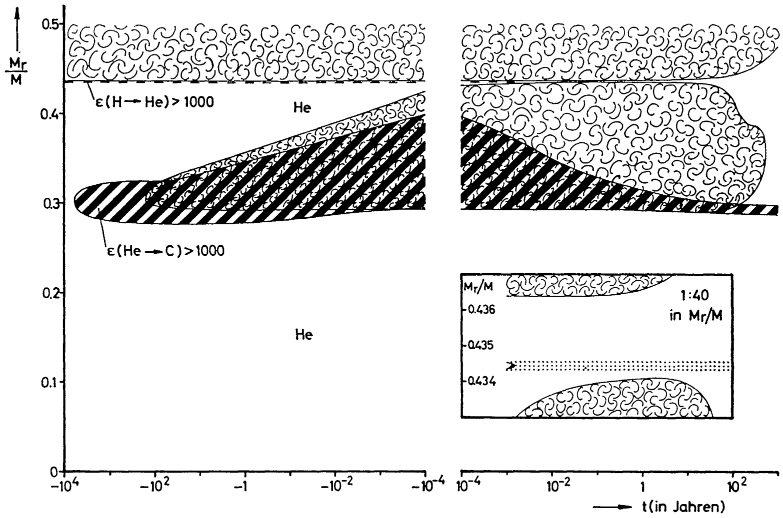

Figure 5: The evolution of the internal structure of a star of 1.3 $M_\odot$ in function of the time during the He flash. The x-axis gives the time in yrs after the He flash, in the y-axis is plotted the ratio m/M. The main regions of nuclear energy release are hatched: the central He burning and the shell H burning (that appears as a broken line). The H burning in the shell extinguishes after $t \sim 10^{-3}$yrs. 'Cloudy' areas indicate convection. In the window is drawn the close approach of the outer convective envelope and the convective region above the He-burning shell, the dotted area is the transition region of the chemical composition left by the hydrogen-burning shell. Although during the flash helium is ignited in a shell, it will also burn in the central region after some time. From Thomas (1967).

name Horizontal Branch. The T_{eff} in the HB depends on factors as metallicity and the H-rich envelope mass. The envelope mass is determined by the initial mass of the star, but also by mass loss during the RGB and the He-flash.
Lower metallicities and high mass envelope causes bluer HB, otherwise high metallicities and lower envelope mass causes a redder HB. The Red Clump on the HB is formed by stars with masses 1 $M_\odot \leq M \leq M_{HeF}$ or by lower mass stars in metal rich systems.
Subsequently, clump stars evolve toward the asymptotic giant branch during the phase of helium shell burning.
Concluding, as shown in Fig. 2, a Red Clump star is a evolved star, with mass between 0.8 ÷ 3 $M_\odot$ and of intermediate age. It burns helium in a convective core and hydrogen in a shell.

1.3.1 *The Fine Structure*

Thanks to the dependence of absolute luminosity on the mass of the helium core at the moment of the He ignition, the Red Clump has a fine structure. That dependence results from the dependence of the luminosity on the age and chemical abundances of the galaxy or cluster in which RC stars are detected.
Girardi et al.(1998) and Girardi (2000) investigated this fine structure with the aid of evolutionary models and isochrone calculations. They observed that:

- stars with $M \leq 2\ M_\odot$ constitute most of the clump, distributed over a very narrow interval on T_{eff} and with an almost constant luminosity. They form the *main red clump* feature that we observe in CMDs.
- stars with $M \simeq 2\ M_\odot$ occupy a particular region in the HR diagram, about 0.4 mag fainter than the main red clump. These stars define a fainter *secondary red clump.*
- stars with $M \geq 2\ M_\odot$ are fewer and has higher luminosities. They may originate a plume of bright clump stars.

The same features appear at different metallicities.

In open clusters, the red clump presents typically a very small dispersion in color and magnitude. This results from the small spread in age and metallicities. On the contrary, red clump stars in galaxy fields present a significant spread in age and metallicity.

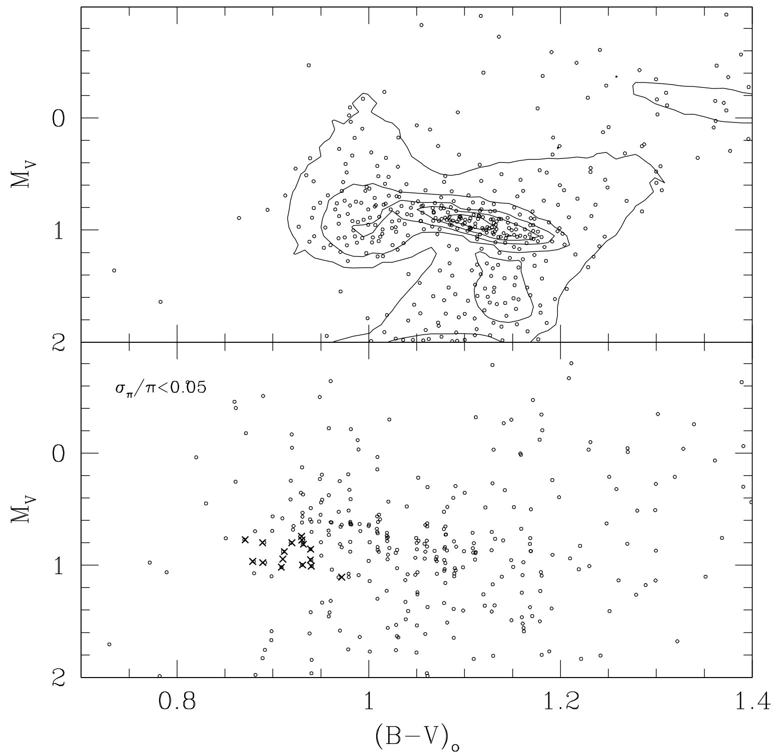

Figure 6: Distribution of clump stars in the M_V vs $B-V$ diagram, from theoretical models (upper panel) and from Hipparcos data (bottom panel), from Girardi (1999). Upper panel:Theoretical distribution was built with 400 stars, belonging to a model for a composite stellar population with constant SFR in the interval 0.1< (t/Gyr)<10 and mean solar metallicity; the contour levels delimit regions with the same density of stars. Lower panel: stars in this diagram are stars with parallax error σ_π/π < 0.05. In the diagram built with theoretical models the substructure is clearly visible: the secondary clump on the left (caused by stars with masses M≥ M_{Hef}). In the bottom panel stars that belong to the secondary clump are indicated by crosses.

1.4 PROPERTIES

Red Clump stars in the CMD M_I vs $V - I$ occupy a magnitude interval of $-0.6 \leq M_I \leq 1$ and a color interval of $0.8 \leq V - I \leq 1.3$. By using Straizys & Kuriliene (1981) criteria RC stars are red giant stars of spectral type between G8II and K2III with 4500 K $\leq$ T_{eff} $\leq$ 5300K (from Zhao et al.,2001; Soubiran et al.,2003).
The luminosity of a Red Clump star (hereafter RC star), is due to the luminosity of He burning core plus the luminosity of the H-burning shell:
$L \ L_H \ L_{He}$
L_{HE} is nearly constant, it depends on the M_{core}, that depends on metallicity: M_{core} decrease with [Fe/H]. L_H depends on the mass and metallicity. It increases monotonically with the mass, because the luminosity of the H-burning shell increases with the envelope mass; additionally the efficiency of the H-burning shell decreases with [Fe/H]. Studies on atmospheric properties of RC stars started since the first publication of Hipparcos data (Perryman, 1997), with the aim of finding any dependence of absolute magnitudes on atmospheric parameters such as metallicity, temperature and gravity.
High resolution spectroscopic observations of local Red Clump stars was done by Zhao et al. (2001), Zhao (2001), Soubiran et al. (2003) and Liu et al. (2005). Zhao et al. (2001), Zhao et al. (2001) and Liu et al. (2005) observed a sample of 39 Hipparcos RC stars. They obtained values of T_{eff} and *logg* through photometry while [Fe/H] and $[\alpha/Fe]$ by comparing FWHM of the spectrum lines with a synthetic template. They obtained T_{eff} from color index $B - V$ and *logg* from Hipparcos parallaxes and magnitudes, by combining $g \ GM/R^2$ and $L \ 4\pi R^2 \sigma T^4_{eff}$ (in which R= stellar radius, L= absolute luminosity, M = stellar mass).
Soubiran et al. (2003) obtained atmospheric parameters of 16 Tycho2 RC stars via spectroscopic analysis by fitting spectra with the method of minimum distance a template of stars with well known atmospheric parameter.
The results of these studies are summarized in Tab. 1.4.

1.5 THE RED CLUMP IN HIPPARCOS

The existence of core He-burning stars has been known for decades in the color magnitude diagrams of open clusters and nearby galaxies. Sturch (1971) first discovered Helium-core burning giants in the Galactic field. The first theoretic evidence of a clump in the Giant Branch was made by Thomas (1967) and Iben (1968). King (1985) made the first observational confirm on the existence of

	Catalogue	observed RC	$T_{\rm eff}$ K	$\log g$	[Fe/H] dex	[α/H] dex
Zhao (2001) Zhao et al. (2001) and Liu (2005)	Hip.	39	4400 - 5300	1.90 - 3.1	- 0.1 - +0.35	-0.45 - 0.44
Soubiran et al. (2003)	Tycho-2	16	4700 - 5300	2.51 - 3.26	-0.54 - 0.15	-

Table 1: Atmospheric parameters of Red Clump stars present in literature. They were obtained from high resolution spectra of a sample of RC. Zhao et al. (2001), Zhao (2001) and Liu et al. (2005) observed a sample of 36 Hipparcos clump stars. They obtained T_{eff} from color index $B-V$ and $logg$ from Hipparcos parallaxes and magnitudes, and [Fe/H][α/Fe] via spectroscopic analysis. Soubiran (2003) observed a sample of 16 RC stars taken from Tycho2 catalog. They derived their values by fitting spectra with the method of minimum distance a template of stars with well known atmospheric parameters.

such clump in the HB. The first irrefutable evidence of the presence of Red Clump stars in the local neighborhood was made by Hipparcos ESA mission, Perryman (1997). Hipparcos showed the presence of a clump in the horizontal branch of the color- absolute magnitude diagrams (V-I/M_{Hp}) of the Solar Neighborhood (see 1.

Hipparcos (acronym of High Precision Parallax Collecting Satellite) was the first space mission completely dedited to astrometry. The satellite was launched in 1989 and ended his mission in 1993, accomplishing one of the most important projects of space astrophysics.

The aim of the project was to measure stellar parallaxes, useful for measuring distance and proper motions of a star. Hipparcos measured distances of $2.5x10^6$ stars, reaching distances of ~ 150 pc . The mission was composed by two projects:

- The Hipparcos Experiment, which aim was to measure astrometric parameters of $\sim$ 120000 stars, with a precision of $2 \div 4$ milli-arcsecs.

- The Tycho Experiment, which aim was to measure, less accurately than Hipparcos, astrometry and 2-color photometry of $\sim$ 1000000 of stars.

The final Hipparcos Catalog and the Tycho Catalog were finished in Agoust 1996, and published by ESA in June 1997 (Perryman

et al., 1997), Høg (1997).
This PhD thesis uses data from Hipparcos Catalog (Perryman et al., 1997) and Tycho-2 catalog (Hog et al., 2000).

Hipparcos Red Clump Stars

The Hipparcos ESA catalog contains $\sim$ 1500 clump stars with parallax error lower than 10%, and an error in absolute magnitude lower than 12 mag. This accuracy limit corresponds to a distance of $\sim$ 125 pc within the sample of clump stars is complete. Moreover, accurate BV photometry is available and interstellar absorption is small enough to be neglected. It is important to remark that the sample of red clump stars with $\sigma/\pi_{Hp} < 10\%$ are always at least 0.5 mag brighter than the V$\simeq$ 0.85 completeness limit of the Hipparcos catalog.
ESA(1997) catalog contains $\sim$ 600 clump stars with parallax error lower than 10% , Girardi (1999). Thus the calibration of the absolute magnitude for RC stars of the solar neighbourhood is possible with high accuracy, and hence the use of the Red Clump as standard candle. The same accuracy is not feasible with other distance indicators: for example *Hipparcos* parallaxes of the closest Cepheids and RR-Lyrae has larger errors and the calibration of their absolute magnitude provided questionable results (Feast & Catchpole, 1997 ; Luri et al. 1998).
The main characteristics of RC stars, as derived from Hipparcos sample, are:

- High intrinsic luminosity, characterized by a low dispersion:
  M_V= 0.18 ± 0.29 this work
  M_I= -0.81 ± 0.23 Udalski (1998)
  M_K= -1.60 ± 0.29 Alves (2000)
- High spatial density. 15% of the stars observed by Hipparcos with $\pi/\sigma_\pi < 5\%$, are RC stars.
- Spectral types G8III - K2III.

Therefore Hipparcos provided a big sample of Red Clump stars that allowed a deeper investigation of this type of stars and pointed out their utility in issues as distance scales in Local Group of galaxies and Milky Way structure.

1.6 RED CLUMP STARS AS STANDARD CANDLES: THE CALIBRATION OF $M_{RedClump}$

The idea of using the Red Clump as distance indicator is relatively old (Hat, 1989).
Then Paczínski & Stanek (1998) were the first to use Red Clump stars in the I band as distance indicators, thanks to the fact that this phase of stellar evolution is usually well populated and thanks to the presence of precise parallaxes and magnitudes in the Hipparcos catalog (Perryman et al., 1997). They noticed that the RC M_I magnitude was independent of metallicity both in the HIPPARCOS and in the Bulge OGLE CMDs. In their paper they argued that the dependence of the RC brightness from population effects might be negligible. So they used the $|M_I|$ of RC stars in the solar neighborhood in order to obtain the absolute distance modulus to the center of Milky Way, using M_{IRC}= -0.279 ± 0.088. The same procedure was repeated for stars in M31 (Stanek et al.,1998; Bersier et al., 2000), SMC (Udalski et al., 1998), LMC (Stanek et al., 1998), Carina (Kim, 2002).
While distances for Carina and Andromeda were coherent with distances given in literature, for LMC Stanek et al. (1998) obtained $m_I - M_{ILMC}$=$18.06 \pm 0.03_r \pm 0.09_s$, a distance 15% shorter than the distance of $m - M = 18.50 \pm 0.15$ obtained with other methods (for example the Hubble Space Telescope key project team gives $m - M$ 18.50 ± 0.10, Freedman, 2001).
The discrepancy is partly due to the uncertainty in the extinction of ∼0.2 mag and mainly to metallicity and age effects on the magnitude of Red Clump Stars.
As a matter of fact, taking in account that in the interval $0.8 < V - I < 1.25$ LMC stars have mean metallicity below those of the solar neighborhood, the bulge and M31; and taking in account that theoretical models show a weak dependence of M_{bol} and M_I of RC stars on either age and metallicity, it was clear that metallicity and population effects may be the first cause of the discrepancy in LMC distance.
Thus a complicated dependence of RC magnitude on the stellar population (age, metallicity and age- metallicity relation) exist theoretically. It was demonstrated and quantified by Cole (1998), Girardi (1999), and Girardi (2001).
Other authors have explored the possibility that the K magnitude of the RC might be less sensitive to population effects and reddening uncertainties, with no clear consensus (Alves, 2000; Grocholski, 2002; Salaris, 2002; Pietrzinsky ,2003.). Cole (1998) proposed a revision of the RC distance to the LMC, based on the mean age and metallicity differences between LMC and local stars. Making

use of the theoretical dependence of clump magnitude on age and metallicity, it showed that the LMC Red Clump should be 0.32 mag brighter than the local disk one, and obtained a distance modulus of 18.36 ± 0.17. At the same time Beaulieu (1998) obtained a distance modulus for LMC of 18.3 mag by isochrone fitting a model for the LMC clump.

Udalski et al. (2000) used the McWillam catalog (McWilliam, 1990) obtained metallicities of 673 nearby G and K giants) to determine the metallicity effects on the properties of red clump giants. He found that M_I is weakly correlated to the [Fe/H] (see FIg 9), and that the correlation is expressed by:

$$M_I{=}(0.13 \pm 0.07)\ ([Fe/H] + 0.25\text{-}(0.26 \pm 0.02) \quad (1.1)$$

Using his calibration Udalski (2000) obtained a new distance

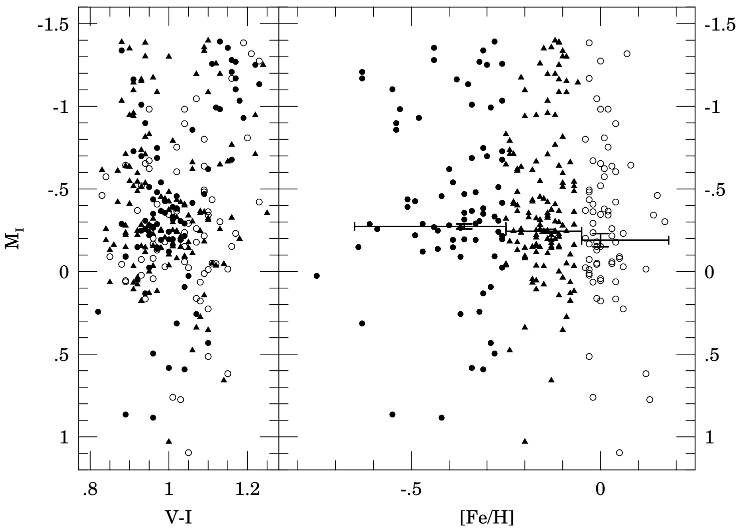

Figure 7: M_I of 284 nearby red giants with precise photometry and spectroscopy plotted as a function of $V - I$ color (left panel) and metallicity [Fe/H] (right panel). Stars of low, medium and high metallicity are marked by filled circles, filled triangles and open circles, respectively. Metallicities come from McWilliam (1990) catalog. (From Udalski, 2000)

modulus for LMC of $m - M_{LMC}$ 18.24 ± 0.08, a 'short' distance again.

Alves (2000) considers the K-band, since this wavelenght range is less sensitive to extinction. They finds:

$$M_K{=}(0.57 \pm 0.36)\ ([Fe/H] + 0.25\text{-}(1.64 \pm 0.07) \quad (1.2)$$

Later on Zhao et al. (2001), in order to detect the empirical dependence of M_I on metallicity, made a high resolution spectroscopic survey on 39 local RC stars. They obtained the [Fe/H] by comparing the measured FWHM of lines with synthetic ones. At the end they found a linear relationship between magnitudes and metallicity:

$$M_I{=}(0.12 \pm 0.11)\ ([Fe/H] + 0.25\text{-}(0.18 \pm 0.04) \tag{1.3}$$

The weak correlation between M_I and [Fe/H] exist as well, with the same slope of the eq. 1.1 derived by Udalski.

Keenan & Barnbaum (1999) calibrate the clump absolute lumi-

Object	**Dist. RC** (Kpc)	σ_D (Kpc)	**Dist. Ceph.** (Kpc)	σ_D (Kpc)
Milky Way				
Bulge	8.4	0.4	8.0	0.5
SMC	58.89	2	61.37	3
LMC	51.29	2	50	2
M31	784	30	760	50
Fornax	136	7	153	18
M33	916	17	912	20
Carina	98.2	4	110	-

Table 2: Distances in Kpc of Milky Way bulge,LMC, SMC, M31, Fornax and Carina as obtained using Red Clump stars method. Values came from $m - M_I$ obtained with RC are taken from: Udalski et al. (1998) for MW bulge, LMC and SMC, Bersier (2000) for M31, Kim (2002) for M33 and Carina. Distances taken with Cepheids came from the Hubble Space Telescope key project Freedman et al. (2001). Distances are in agreement, but it is necessary to use RC method carefully.

nosities in the V band for stars brighter than V=6.5. The luminosity class of Red Clump giants is denoted as IIIb and a new calibration of their visual magnitude has been made. They give the mean M_V as a function of the spectral type: from M_V= 0.70 for class G8 IIIb to M_V=1.00 for class K2 IIIb.

Because of the revised Hipparcos parallaxes (F. Van Leeuwen, 2007), Groenewegen(2008) investigates again the absolute calibration of the RC in the I and K bands, modeling the RC population of the Solar Neighborhood. He finds:

M_{IRC} -0.22 ± 0.03

M_{KRC} -1.54 ± 0.04

with no or very weak dependences on metallicity (see Fig. **??** and Fig. **??**).

All these calibrations imply that the absolute magnitude of the Red Clump of the solar neighbourhood has a rather small (or none)

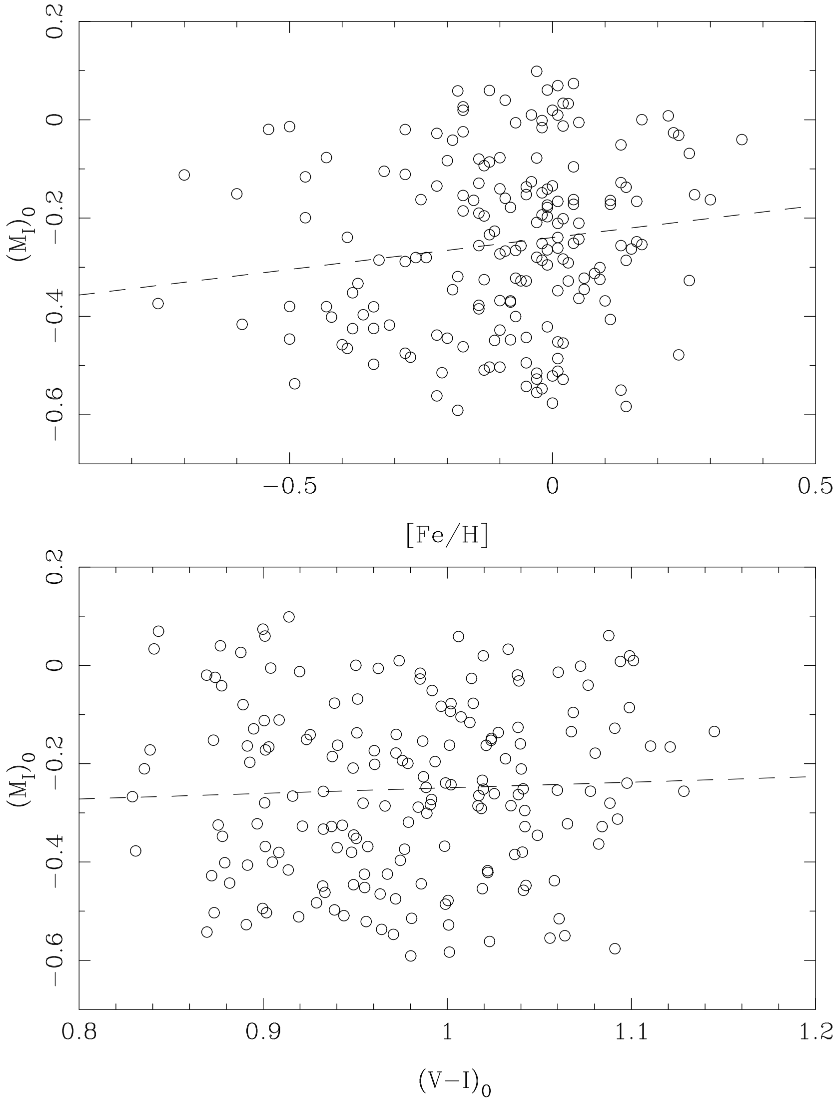

Figure 8: Fit of $M_{\rm I}$ versus metallicity and $V - I$ colour for Groenewegen model of RC stars in the Solar Neighborhood, with best fits indicated by the dashed line. The slope of the fit against colour is not significant.(From Groenewegen, 2008)

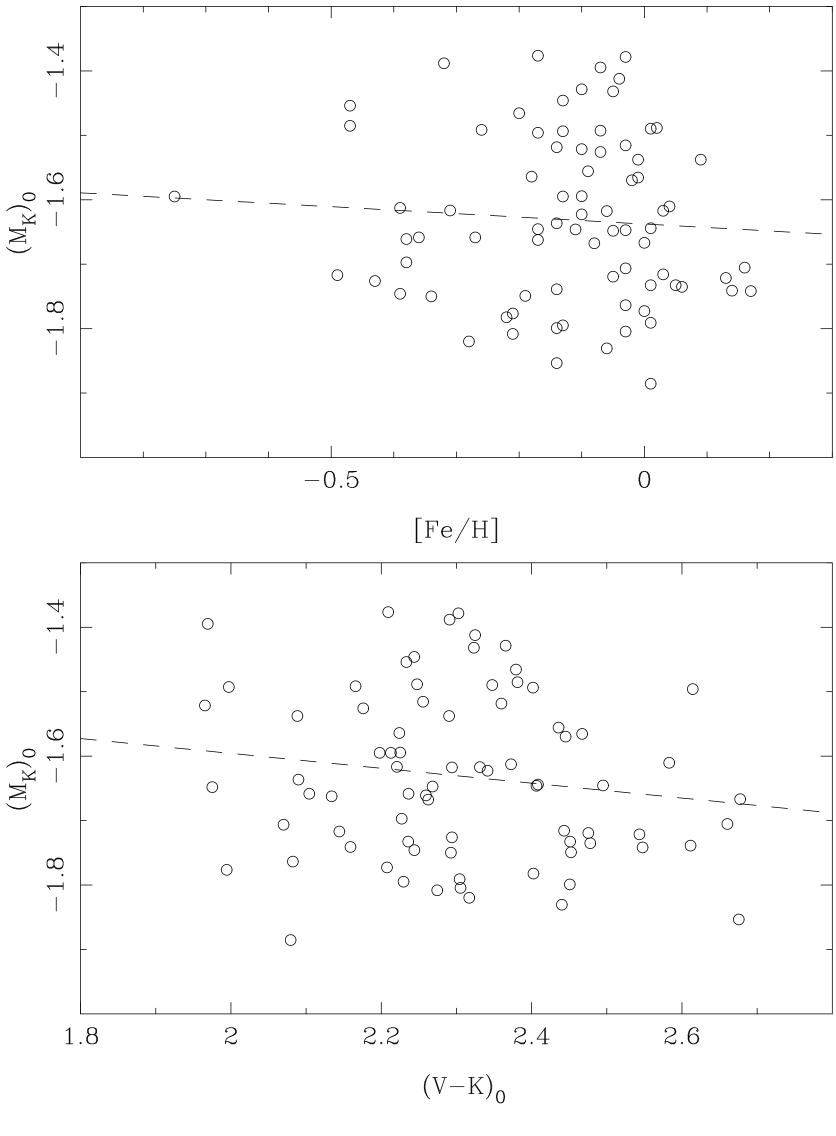

Figure 9: Fit of M_K versus metallicity and $V - K$ colour for Groenewegen model of RC stars in the Solar Neighborhood, with best fits indicated by the dashed line. The slope of the fit against colour is not significant.(From Groenewegen, 2008)

correction for metallicity.
Girardi & Salaris (2001) showed that empirical linear M_I versus [M/H] relations are misleading, since they originated from the particular age and metallicity distributions of the objects included in the calibrating sample, and do not have general validity. Functions 1.1 and 1.3 cannot be used for obtaining distances of objects, as LMC, which metallicity and population is so different from the MW disk one. Girardi & Salaris (2001) were able to reproduce a number of observational features of the RC in nearby galaxy systems, by using an extended set of stellar models, standard population synthesis algorithms and independent data about the distributions of stellar ages and metallicities. In particular they reproduced quite well the RC for the Hipparcos sample (see fig. 6), the Baade's Window clump, LMC and SMC, showing the complex dependence of the red clump magnitude on age, metallicity and star formation history.
Distances to the main objects of the Local Group, obtained by using Red Clump stars as standard candle and paying attention to the metallicity effects, are listed in table 2. There is a good agreement between between distances obtained with RC and the ones obtained with cepheids.
Red Clump stars may be used as distance indicators only if the history and metallicity of the object is well known.
Additionally, taking in account the adequate remarks, clump stars might be a powerful tool for investigating the structure of the Galaxy.

1.7 RED CLUMP STARS AS MILKY WAY STRUCTURE INDICATORS

Red Clump star are used as a tool for investigating the structure of Milky Way, thanks to their abundances in the Galaxy and their high luminosities.
Fux (2001), Mao et al. (2002) and Sumi et al. (2003) used Red Clump stars in order to detect the presence of the Galactic Bar. They analyzed kinematics and distances of RC stars situated in the Milky Way Bulge from data collected by Optical Gravitational Lensing Experiment (OGLE-II), see Udalski (1998). From OGLE-II they selected two groups of clump stars, a faint and a bright one, that were supposed to belong to the further and the nearest part of the Galactic Bar respectively. The result was the detection of a Galactic Bar that moves in the same direction of the Sun with a velocity of v_{Bar}= 100 Km s−1.
Soubiran et al. (2003) made a characterization of the thick disk

using clump stars. They took and analyzed high resolution spectra of 284 local clump stars selected from Hipparcos catalog for investigating the Thick Disk. They obtained proper motions by combining selected radial velocities measured from spectra and proper motion taken from Tycho catalog and metallicities with the method of minimum distance by using a template of spectra with well known atmospheric parameters. The main result was the discovery of a rotational lag of -51±5 km s^{-1} with respect to the Sun, a velocity ellipsoid of $\sigma_U, \sigma_V, \sigma_W$=$63 \pm 6, 39 \pm 4, 39 \pm 4$ km s^{-1}, a mead metallicity of [Fe/H]= -0.48 ± 0.05 and a high local normalization of 15±7%.

Siebert (2003) used the same sample of stars and data of Soubiran et al. (2003). They determined the gravitational force perpendicular to the Galactic plane and the mass density in the Galactic plane Σ 67 $M_\odot pc^{-1}$. They also measured the thickness of the disk: 390^{330}_{-120}pc. They did not found any vertex deviation for old stars, consistent with an axisymmetric Galaxy.

Bienayme et al. (2005) userd Red Clump stars in order to derive the total surface mass density of the Galactic plane. They observed two samples of clump stars: the one used by Soubiran et al. (2003) (a local sample) and a sample of 523 stars up to z=1 kpc (a distant sample). The atmospheric parameters of the distant sample were determined by Kovtyuk et al. (2006) using line-depht ratios. Bienayme et al. (2005) apply two-parameter models to the combination of the two samples and derived the value of the total surface mass density within 0.8 kpc and 1.1 kpc from the Galactic plane: $\Sigma_{0.8kpc}$ = 59-67 $M_\odot pc^{-2}$ and $\Sigma_{1.1kpc}$ = 59-77 $M_\odot pc^{-3}$.

Red Clump stars are also useful tracers of the recent discovered stellar systems as Canis Mayor, Sagittarius Stream, Monoceros Ring, etc. A further knowledge of the shape and the orbit of these relics of accretion events is very important in the light of the current cosmological models in which the growth of large galaxies is driven by the process of hierarchical merger of sub-units White (1978) and White (1991). The tidal disruption of dwarf galaxies within the Galactic potential may lead to the production of stellar streams (as Sagittarius Stream, see Ibata et al. (1998). The study of these relics may reveal fundamental informations about the processes of tidal disruption, the mass distribution within the Galactic Halo of Dark Matter, its degree of clumpiness, etc. (see Ibata et al., 2001; Helmi et al., 2004; Johnston et al., 2005; Law et al., 2005). An example of this type of investigation is the study of the Canis Major overdensity.

The Canis Major/Monoceros Ring is a recent discovery: it was detected as a strong elliptical shaped overdensity nearly coplanar

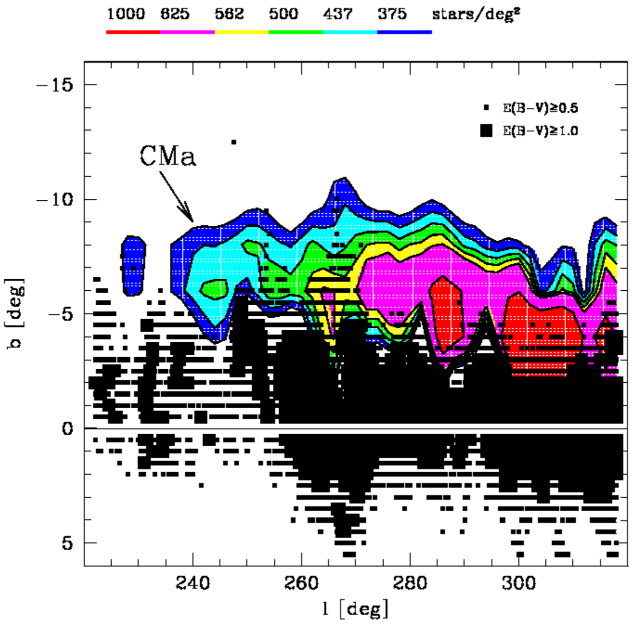

Figure 10: Subtracted map (South-North) in terms of surface density in the sky for RC stars in the range $11.5 \leq K \leq 14.0$. The surface density has been computed on a grid of $4^\circ \times 4^\circ$ pixels spaced by 2° both in latitude and longitude. In this case stars with $|b| < 5.0^\circ$ have also been included in the sample. The position of CMa is indicated by a labeled arrow. Small squares mark positions where the reddening is $0.5 \leq EB - V < 1.0$, large squares correspond to reddening in excess of 1.0 mag.

with the Galactic disk (Newberg et al. 2002; Majewski et al., 2003; Cutri et al., 2003). Its nature cannot yet ruled out definitely: it was identified as the stellar component of the southern Galactic Warp (Momany et al., 2004) or as the relic of an accretion event(Bellazzini et al., 2004). Recently Bellazzini et al. (2006) used Red Clump stars selected from 2MASS Point Source Catalog for tracing the core of the Canis Major. They found that the main body of the system has a central surface brightness of $\mu_{V,0} \simeq 24.0 \pm 6$ mag/arcsec^2 and a line of sight profile peaked at $D_{\odot}$ 7.2 ± 1.0kpc with a FWHM of ~ 2.0 kpc.

1.8 THE RED CLUMP AS STAR FORMATION HISTORY TRACERS

The study of the Horizontal Branch can offer the opportunity of probing the star formation history of an object.
For example the presence of the blue part of the HB in a galaxy is usually interpreted as clear evidence of an old component, even if its absence dos not necessarily exclude old ages.
On the other hand the clear presence of the Red Clump traces both the old and the intermediate-age populations. That's because the core He-burning stars with ages between 1 and 13 Gyr in almost the whole range of metallicity (except the oldest and most metal poor) present in a composite stellar system are concentrated in a small and well defined area of the Color Magnitude Diagram. This implies that only limited information on the Star Formation History may be interfered from the RC, after taking into account theoretical uncertainties and observational errors. In addiction, as pointed out by Girardi & Salaris (2001) (see fig. ??), the age distribution in the clump is strongly biased toward 'young' (1-3 Gyrs) ages toward the higher metallicities, because metallicity usually increases with time.
Girardi et al. (1998) and Piatti (1999), however, pointed out a particular feature, the *secondary clump*, that can provide specific information on a particular range of ages. This feature is a classic prediction of stellar evolution theory. Piatti (1999) noted the presence of the secondary red clump in the CMDs of several fields in the Large Magellanic Cloud. Girardi et al. (1998) deeply discussed the characteristics of this feature in the CMDs of stellar populations containing metal rich ($Z \geq 0.004$), ~ 1 Gyr old stars. These two papers described the evolutionary origin of the complex RC morphology, demonstrating that the secondary clump is made of stars with mass in a narrow range ($0.3 M_{\odot}$) above the limit for non-degenerate He ignition. It is the faint extremity of a vertical structure in the CMD, formed by core He-burning stars

of increasing mass, as show in fig. 6 form Girardi et al. (1998) for Hipparcos RC stars.
By simulating CMDs for different populations, as done by Girardi & Salaris (2001), it is possible to see how the mean color of the RC gets redder, and the RC color range gets larger as metallicity increases.
This illustrates the potential use of RC as tracer of the age- metallicity relation in a composite stellar population in the presence of a secondary clump. The disadvantage of using RC as SFH tracer is that its morphology is dependent on the unknown age- relation and the range of ages. However, with reasonable assumptions about the local SFH, Girardi et al. (1998) found an agreement between the observed and predicted morphologies of RC. Finally, an age indicator introduced by Hatz (1991) is the color difference between the median color of the RC and the RGB at the level of the HB. The conclusion, obtained by comparing their result to Girardi et al. (1998)'s one, is that the empirical trend is clearly present in the models, except maybe for the solar metallicity models, which may underestimate the color difference.
Soubiran et al. (2008) determined an age- metallicity relation (AMR) and an age-velocity relation (AVR) for Galactic Disk stars using Red Clump stars. They used the same data of the sample of stars used in Bienayme et al. (2005) (two samples of clump giants: a local sample of 387 stars and a distant sample of 523 stars). The AMR that they obtained exhibits a very low dispersion, increases smoothly from 10 to 4 Gyr with a steeper increase for younger stars. The AVR presented in the paper is characterized by the saturation of the V and W dispersions at 5 Gyr, and a continuous heating in U.

1.9 CATALOGS OF RED CLUMP IN LITERATURE

Because of the wide spread interest, a great effort have been carried out in better defining the properties of RC stars. McWilliam (1990), Mishenina (2006), Hekker and Mendelez (2007) and Takeda (2008) realized massive surveys aiming to derive T_{eff} , $logg$, [M/H] and chemical abundances of giant stars.
McWilliam (1990) computed an extensive catalog of 671 G-K giants, mostly RC giants. He derived T_{eff} from broad-band Johnson colours, $logg$ using the relation between T_{eff}, M, L and $logg$, and [Fe/H] from direct line by line analysis.
Mishenina and collaborators provided fundamental parameters and abundances for a sample of nearby RC stars ($\sim$ 177 stars with $\pi_{Hip} > 10$ mas) . They derived T_{eff}, [M/H] and elemental abundances with the classic line by line analysis, while $logg$ is de-

termined by combining two methods: one based on the ionization balance of iron and the other based on fitting of the wings of the CaI 6162.17 Å line .
Hekker and Mendelez (1997) provided radial velocities and atmospheric parameters of 380 G and K giant stars with V magnitude brighter than 6. They obtained T_{eff}, *logg* and [Fe/H] from the equivalent width of FeI and FeII lines, by imposing excitation and ionization equilibrium through stellar atmosphere models.
The same method based on FeI and FeII line was adopted by Takeda et al. (2008): they provided atmospheric parameters for 322 intermediate-mass late-G giants, with $V \leq 6$, many of which are red-clump giants.
Femay et al.(2005) carried out a survey on giant stars with CORAVEL, deriving precise radial velocities for all the K stars with $M_{Hip} < 2$ and M stars with $M_{Hip} < 4$ present in the Hipparcos catalog: their survey gives radial velocities for a sample of $\sim$ 6600 K giants, mostly RC stars.

1.9.1 *This thesis and the ARCS survey*

ARCSs (the Asiago Red Clump Spectroscopic survey) derives from high resolution optical spectra, accurate multi-epoch radial velocities and atmospheric parameters for a well selected sample of 500 equatorial Red Clump stars ($|b| < 6\circ$), belonging to the solar neighborhood. Spectra are obtained with the Asiago 1.82m + Echelle spectrograph, they cover a wide spectral interval (3700-7300 Å) with a high resolution (R = 20,000) .
Radial velocity measurements are performed by cross-correlating spectra against synthetic templates; atmospheric parameters are derived via $\chi 2$ fitting with a synthetic database of spectra. The synthetic spectra are taken from the library of Munari et al. (2005) , based on Kurucz's codes. The red clump may be an useful distance indicator only if we know the distribution of ages and metallicities inside the galaxy object we are observing.
The Hipparcos catalog provides us an extremely interesting sample of clump stars, complete up to 125 pc, and it represents a well-understood evolutionary stage. Thanks to the finding of the fine structure in the local red clump sample, Girardi et al. (1998) able to provide interesting checks to the theory of stellar population and population synthesis.
The perspective of using the clump data for probing the chemical evolution of the Galactic disc are very promising. With accurate and reliable data on chemical abundance determinations, the sample of RC stars in the local neighborhood may help the computa-

tion of chemical evolutionary models of the Solar Neighborhood and disk SFR.

The aims of this PhD thesis are to create a exhaustive catalog of Red clump stars of the local neighborhood, to investigate the possible existence of a relation between RC magnitudes and their atmospheric parameters and to use this type of stars as a tool to investigate Milky Way structure.

2

TARGET SELECTION AND ASSEMBLING OF THE IMPUT CATALOGUE

Contents

2.1 ARCS SELECTION CRITERIA

We applied selection criteria aiming to obtain an highly pruned sample of RC stars candidates. We tried to minimize the reddening and to avoid as much as possible the contamination from binaries.
The program stars for ARCS were selected according to the following criteria:

1. *Accurate spectral classification between G8III and K2III*: we took the identification from the Michigan Spectral Catalog (Houk, 1982) (see Fig 11. Objects must have MK classification quality index better than 2.

2. *Observability from Asiago*: since the Michigan Spectral Catalog contains stars with $\delta \leq 6°$, we selected stars whose declinations are not too low. Selected stars lay within 6° from the celestial equator. The distribution of ARCS targets in the celestial sphere is plotted in Fig 12.

3. *High galactic latitude* $|b| \geq 25°$. Thanks to this selection criteria we minimized the reddening and we aimed to observe stars at high distance from the Galactic plane (see Fig. 13).

4. *Absolute magnitude*: $6.8 \leq \mathrm{V}_{T}ycho-2 \leq 8.1$. We observe RC stars at fainter magnitude intervals respect most of the previous works. Thus our stars are located at higher distances and higher z.

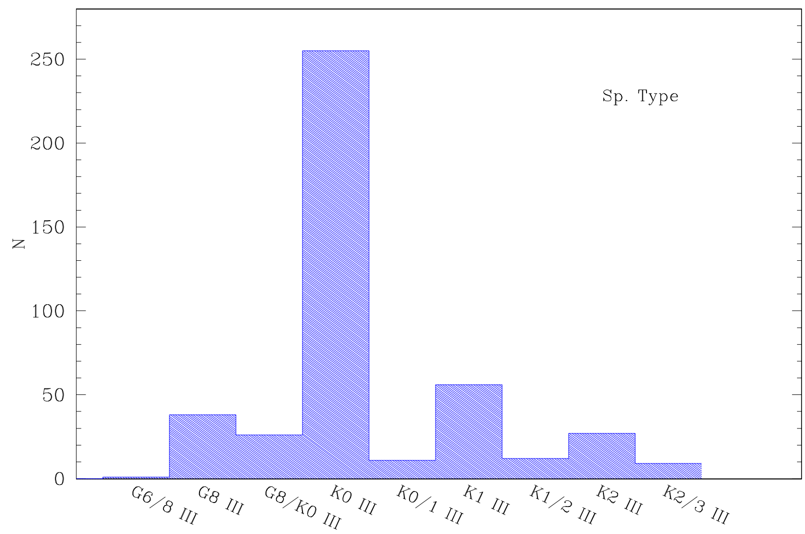

Figure 11: Distribution of the objects of ARCS in spectral type. Spectral classification comes from Houk (1982).

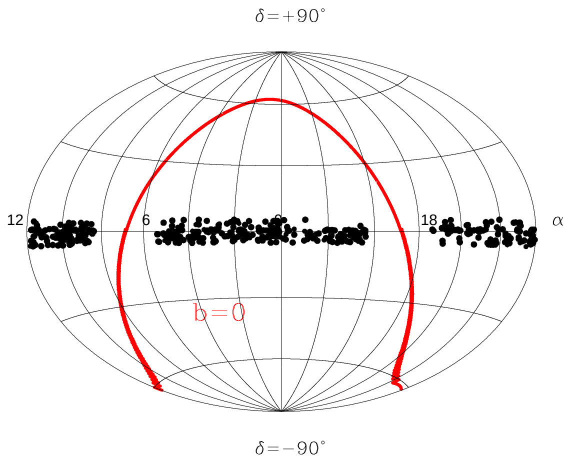

Figure 12: Aitoff equatorial projection of ARCS targets. Is clearly evidenced our choice of observing stars within 6° on the celestial equator.

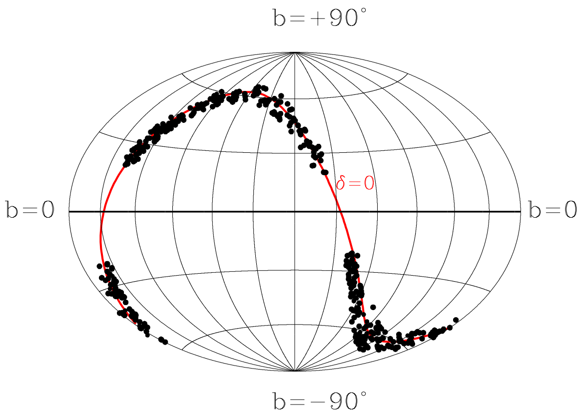

Figure 13: Aitoff projection in galactic coordinates of ARCS targets. Is clearly evidenced our choice of observing stars with high declination from the Galactic plane.

5. *Accurate Hipparcos and Tycho-2 proper motions.* By implementing our spectroscopic data with astrometric measurements, we can obtain Galactic velocities (U, V, W). Proper motions were taken from the Tycho-2 catalog (Høg et al. 2000).

6. *No hint of binarity or variability*: this selection criterion minimize the presence of binary stars in the target sample. Selected stars have blank duplicity index in Michigan catalog, blank variability, blank duplicity flag in Hipparcos catalog and no other HIP or TYCHO-2 star closer than 10 arcsec.

7. *2MASS, DENIS, UBVRI, ubvy photometry available.* In order to characterize as better as possible our stars, we selected those stars which posses the largest and the most accurate photometric data in literature.

426 stars match these selection criteria.
The selection criteria at points 3 and 4 minimize the overlap of ARCS catalog and other catalogs present in literature: we selected stars at fainter magnitude intervals and with more restrictive criteria than previous spectroscopic surveys.
Within the selection criteria we adopted our highly pruned sample can be considered as complete.

2.2 THE PROBLEM OF CONTAMINATION

2.2.1 *Binaries*

We adopted such selection criteria in order to minimize as much as possible the contamination of the target sample from binaries or non-Red Clump stars.
The binaries that contamines the ARCS catalog must have $6.8 < V_{Tyc} < 8.1$ and $0.7 \leq (B - V)J \leq 1.5$, and no hint of binarity or variability in Hipparcos, Tycho and Michigan catalogs. That imply two possible scenarios for our contaminating binaries: a system composed by a RC and a less luminous star at very high distance or a system composed by two RC stars. Both cases are extremely rare.
The first case, a system composed by a RC and a less luminous star at very high distance, imply that the less luminous star is a low-mass main sequence star or a evolved star, as a white dwarf. In this case the secundary star can be detected only spectroscopically. But the low luminosity of the secundary stars and the low resolution of the spectrograph will not help us in detecting this type of binaries from the spectrum: the lines will appear blended or thicker. Having said this, the only way for detecting such type of binary stars will be in a detection of a difference in the radial velocity.
The second case, the contamination by RC-RC binaries, is quite rare. A theoretical argument against an high contamination by RC-RC binaries rests on the fine evolutionary timing required to get two stars in the RC phase at the same time. The timing requirement can be converted into a statement about the relative masses of the progenitor stars. The bulk of RC stars have progenitors with main sequence lifetimes in the 1 to 4 Gyr range (in order to match the increase in the star formation efficiency in the last few Gyr inferred by several previous investigators for the LMC, cf. Gallagher et al., 1996)). If two stars are going to reach the red clump phase at the same time, then their main sequence lifetimes must differ by less than the red clump phase lifetime. Therefore, the maximum allowed percentage difference in their main sequence ages, $\sim 5\%$, is given by the ratio of the red clump lifetime, 10^8 years (Castellani, Chieffi, Pulone 1991), to the main sequence lifetime, t_{ms}. Using the relationship that $t_{ms} \propto M/M_{\odot}{}^{-3}$ for stars somewhat more massive than the Sun (Mihalas and Binney 1981), the upper limit on the mass difference of the two progenitor stars is 2% (Zaritsky e Lin (1997).
In order to clean ARCS sample from the few possible binaries we adopted a particular observational strategy. We planned to ob-

serve our stars twice, with a time interval of minimum 45 days. This observational strategy was suggested by the work of Udry et al. (1997): their Monte-Carlo simulations shows that with this method binaries are detected with an efficiency better than 50%.

2.2.2 *AGB*

While investigating the clump giants, many works in literature faced the problem of their selection , since this region of the CMD is also occupied by the stars of the ascending giant branch. All the works in literature based on Red Clump stars adopted only photometric criteria. According to that, the differentiation between the first-ascending RGB stars and the “clump" stars is rather complicated. Even for open cluster stars, it is very difficult to establish with the good level of certainty, which stars from the group under investigation are the real clump ones (Pasquini et al., 2004).
A tool for discriminating ascending giant branch stars from RC stars is to investigate the chemical abundances. This method is adopted, for example, in the work of Mishenina et al. (2006). When the star moves towards the RGB, the superficial convection zone deepens and the nuclearly processed material penetrates into the atmosphere changing of its chemical composition. During this so-called first dredge-up phase, the surface abundances of Li, C, N, and Na, together with the $^{12}C/^{13}C$ ratio, are being altered. The effect depends both on the stellar mass and metallicity (see Charbonnel 1994). Typically, the surface abundance of carbon decreases by $\sim$ 0.1-0.2 dex and that of nitrogen increases by 0.3 dex or more (Iben, 1991).
We are the first who used an accurate spectral classification ad selection criteria. Thanks to that, contamination of ARCS from AGB stars is rather small, and it could be mainly due to a misleading classification by Hawk (1982). This error in the spectral classification, if present, will be easily detected by our analisys. AGB stars will have rather lower gravities than RC stars, $logg \leq$ 2 dex, while RC stars have $2 \leq logg \leq 3.5$ dex.

2.3 COMPARISON OF ARCS WITH OTHER CATALOGS IN LITERATURE

In literature are present some catalogs on giant stars, which contains a large number of RC stars. Among all we cite the works of Famaey (2005), McWilliam (1990), Hekker & Mendelez (1997),

Mishenina et al. (2006) and Takeda et al. (2008).
McWilliam (1990) computed an extensive catalog of 671 G-K giants, mostly RC giants. He derived T_{eff} from broad-band Johnson colours, *logg* using the relation between T_{eff}, M, L and *logg*, and [Fe/H] from direct line by line analysis.
Mishenina and collaborators provided fundamental parameters and abundances for a sample of nearby RC stars ($\sim$ 177 stars with $\pi_{Hip} > 10$ mas) . They derived T_{eff}, [M/H] and elemental abundances with the classic line by line analysis, while *logg* is determined by combining two methods: one based on the ionization balance of iron and the other based on fitting of the wings of the CaI 6162.17 Å line .
Hekker and Mendelez (1997) provided radial velocities and atmospheric parameters of 380 G and K giant stars with V magnitude brighter than 6. They obtained T_{eff}, *logg* and [Fe/H] from the equivalent width of FeI and FeII lines, by imposing excitation and ionization equilibrium through stellar atmosphere models.
The same method based on FeI and FeII line was adopted by Takeda et al. (2008): they provided atmospheric parameters for 322 intermediate-mass late-G giants, with $V \leq 6$, many of which are red-clump giants.
Femay et al.(2005) carried out a survey on giant stars with CORAVEL, deriving precise radial velocities for all the K stars with $M_{Hip} < 2$ and M stars with $M_{Hip} < 4$ present in the Hipparcos catalog: their survey gives radial velocities for a sample of $\sim$ 6600 K giants, mostly RC stars.
Fig. 26 shows the distribution in V and K magnitudes and in spectral types of ARCS target stars and the stars of Famaey (2005), Hekker & Mendelez (1997), Takeda (2008) catalogs. We have no star in common with the Famaey (2005) catalog, 3 stars in common with the Mishenina (2006) catalog, 9 star in common with the catalog of Hekker and Mendelez (2007) and 1 with Takeda (2008) catalog.
Our survey observed stars fainter and at higher z than those present in the Hekker, Mishenina and Takeda catalogs: our sample has $6 \leq V_{Tyc} \leq 8$ and $d \geq 50$ pc (see Fig. 1) .
Unlike the catalogs present in literature, we derived atmospheric parameters by a χ^2 fitting of our spectra with a grid of synthetic spectra built with the library of synthetic spectra of Munari et al. (2005). With this method we performed the analysis of a large number of spectra with high accuracy in short computational time: the χ^2 technique stands as an excellent tool for large spectroscopic surveys.

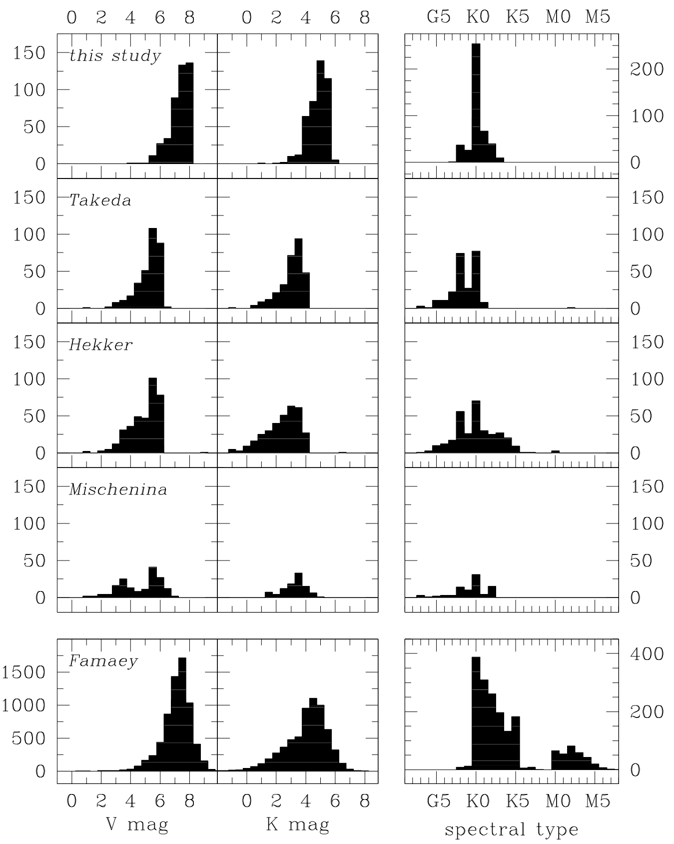

Figure 14: Distribution of the objects of ARCS, Takeda (2008), Hekker & Mendelez (2007), Mishenina (2006) and Famaey (2005) catalogs in V and K magnitudes and spectral type. From left to right: $V_{Johnson}$ magnitude, K_{2MASS} magnitude and spectral types (in ARCS catalog spectral type comes from Michigan Classification (Houk, 1982); in the case of literature catalogs spectral classification is given by the authors).

3 DATA ACQUISITION AND REDUCTION

Contents

3.1 INSTRUMENT AND PERFORMANCES

The program stars were observed with the REOSC Echelle spectrograph + CCD attached to Cassegrain focus of the Asiago 1.82m telescope. The telescope is a classic Cassegrain reflector with a primary mirror of 182cm. It is the main observing facility at the observing site of Cima Ekar (1350m). The spectra have a resolving power close to 20,000 and cover the wavelength range from 3700 to 7300 Å in 30 orders.

3.1.1 *Spectrograph characteristics*

The ECHELLE spectrograph basically consists of a collimator, an Echelle grating, a set of cross disperser gratings mounted on an orientable support, a calibration arm and a slit viewer intesified camera. The mechanical stability is well suited for the measurement of accurate radial velocity, with flexure in the spectrograph focal plane and in the wavelength dispersion direction not exceeding 7 μm (about 2.7 km/sec at H_{alpha}) for +/- 2 hours telescope slewing in HA from the meridian at any declination.
The slit, placed at the focal plane of the telescope, is 30 mm long (380 arcsec): we adopted an aperture of 200 μm and a projected on the sky lenght of 12.6 arcsecs.

3.2 MODUS OPERANDI AT THE TELESCOPE

For each targets we obtained three identical consecutive exposures, 120 sec each, that were median combined in order to increase the S/N and automatically reject the cosmic rays. The spectrograph slit was kept fixed to a projected width of 1.9 arcsec and to a East-West orientation throughout the whole observing campaign.

3.3 DATA REDUCTION

3.3.1 *Data Modeling with IRAF*

The spectra were reduced and calibrated with IRAF, using standard Dark, Bias and dome Flats calibration exposures. Special care was devoted to the 2D modeling and subtraction of the scattered light. Deep exposures of Moon light scattered by the night sky were obtained and later cross-correlated to the calibrated stellar spectra. The results confirmed that the sky subtraction procedure accurately removed, from extracted stellar spectra, scattered moon-light. The spectra were finally normalized.
Exposures of the thorium calibration lamp were obtained both immediately before and also immediately after the three exposures of the star, with the telescope tracking it. These exposures on the thorium lamp were combined before extraction, so that to compensate for spectrograph flexures. From the start of the first thorium exposure to the end of the last one, the whole observing cycle on a program star took about 10 minutes. According to the detailed investigation and 2D modeling by Munari and Lattanzi (1992) of the flexure pattern of the REOSC Echelle spectrograph mounted at the Asiago 1.82m telescope, and considering that we preferentially observed our targets when they were crossing the meridian, the impact of spectrograph flexures on our observations is less than 0.1 km/sec, thus completely negligible. This is fully confirmed by (1) the measurement via cross-correlation of the radial velocity of the rich telluric absorption spectrum in the red portion of all our spectra, and (2) the measurement of all night sky lines we detected on our spectra, taken from the compilations by Meinel et al. (1968), Osterbrock and Martel (1992), Osterbrock et al. (1996).
Given the red color of Red Clump stars and instrument response, the S/N of recorded spectra was steeply increasing with increasing wavelengths. Consequently we restricted our analysis to the wavelength range 4700-6600 Å. The blue cut-off was imposed by the requirement that the S/N should always be larger than 50,

and the red one by the necessity to avoid stronger concentrations of telluric absorption lines (starting with the *B*-band at 6860 by O_2) and the appearance of fringing (not detectable below 6650 Å). The S/N of the reddest orders was always larger than 120.
a tipycal spectrum of ARCS target is showed in Figures [**?**],[**?**][**?**][**?**][**?**].

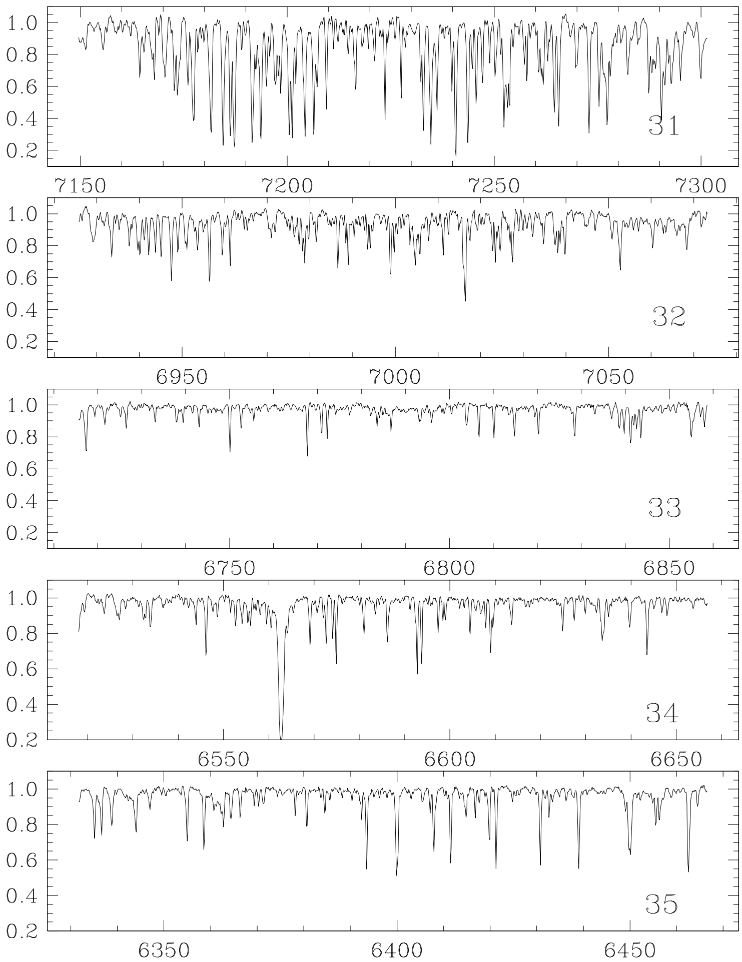

Figure 15: Echelle orders 32-36 of ARCS 203222. These orders cover a wavelenght interval from 6331 Å to 7308 Å. In Echelle order 31 the telluric absorption lines are clearly visible. In the Echelle order 34 there is the H_α line at $\sim$ 6562 Å.

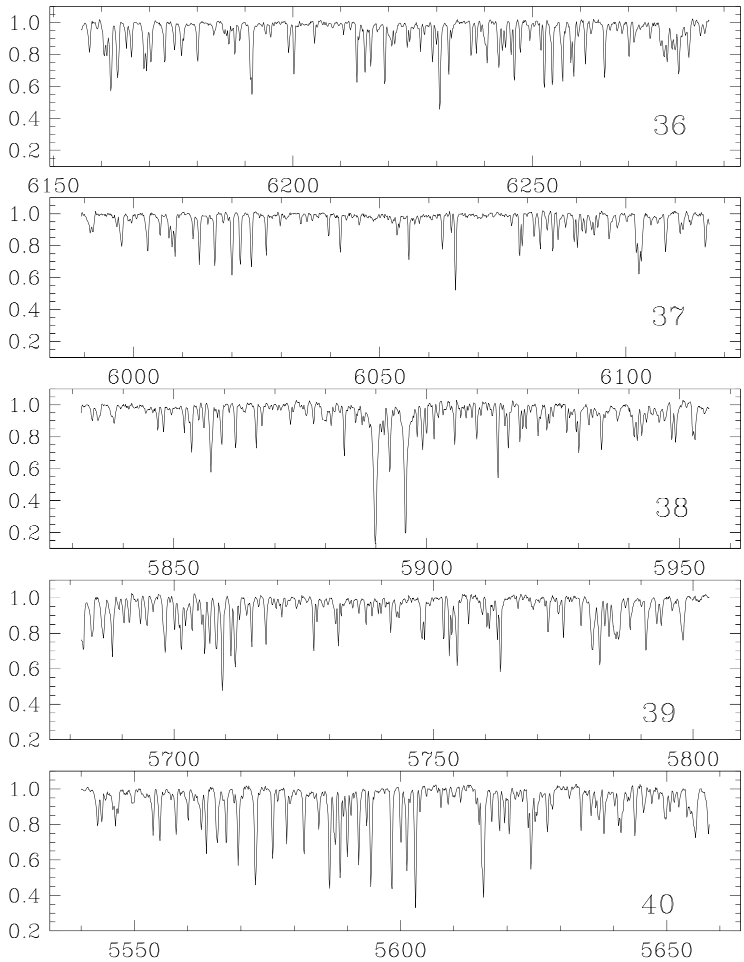

Figure 16: Echelle orders 36-40 of ARCS 203222. These orders cover a wavelenght interval from 5539 Å to 6296 Å. in the Echelle order 36 the O_2 telluric band at 6276 $\sim$ 6287 is visible. In the order 38 is clearly visible the NaI doublet.

3.3.2 *Scattered Light Evaluation and Correction*

Echelle spectrograph are affected by scatterd light contamination. In the spectrum some of the light entering in the spectrograph may appear away from the proper position of focus. These scattered photons may have been deflected by optical imperfections in the gratings and in the mirror, dust in the air and so on. The presence of this scattered light results in a systematic error in line strenght and shape measurements, because the scattered light fills

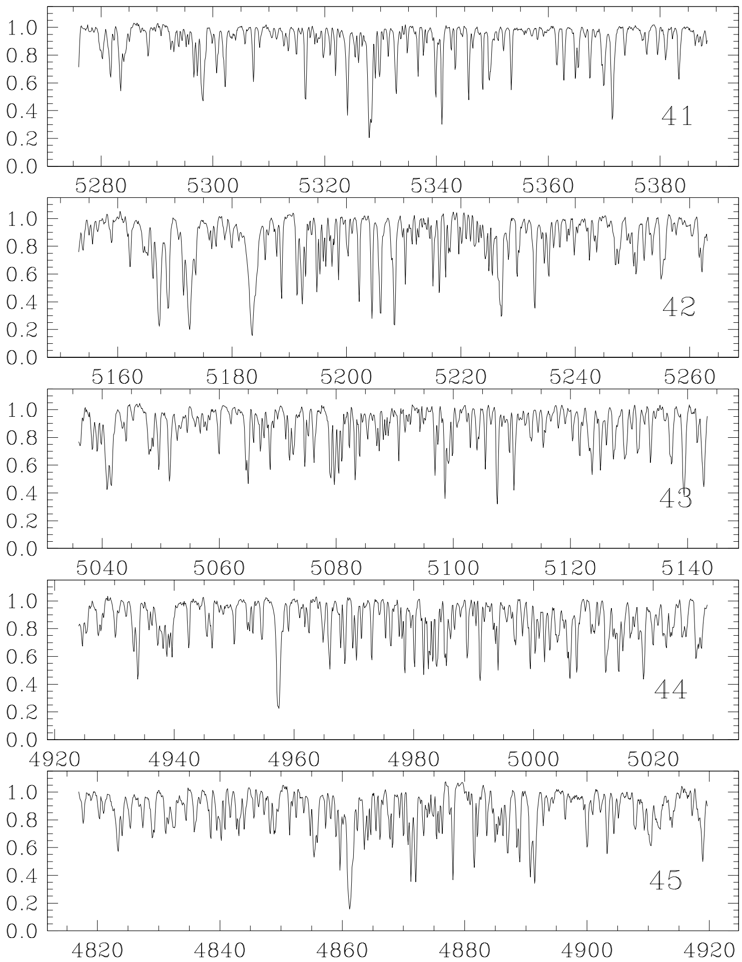

Figure 17: Echelle orders 41-45 of star ARCS 203222. These orders cover a wavelenght interval from4923 Å to 5522 Å. In the Echelle order 42 the Mg triplet at ∼ 5184 -5173 Åis clearly visible.

the absorption lines.
The scattered light is usually 5-10% and it can be measured and corrected by measuring the light in the obsured portion of the spectrum. In the case of Echelle spectra it means to measure the light in between the Echelle orders.
For correcting our spectra for scattered light we used the task APSCATTER of IRAF ECHELLE package. This tasks smooths creates an image by smoothing light in between the orders. Then it subtracts this 'scattering-image' from the original image.

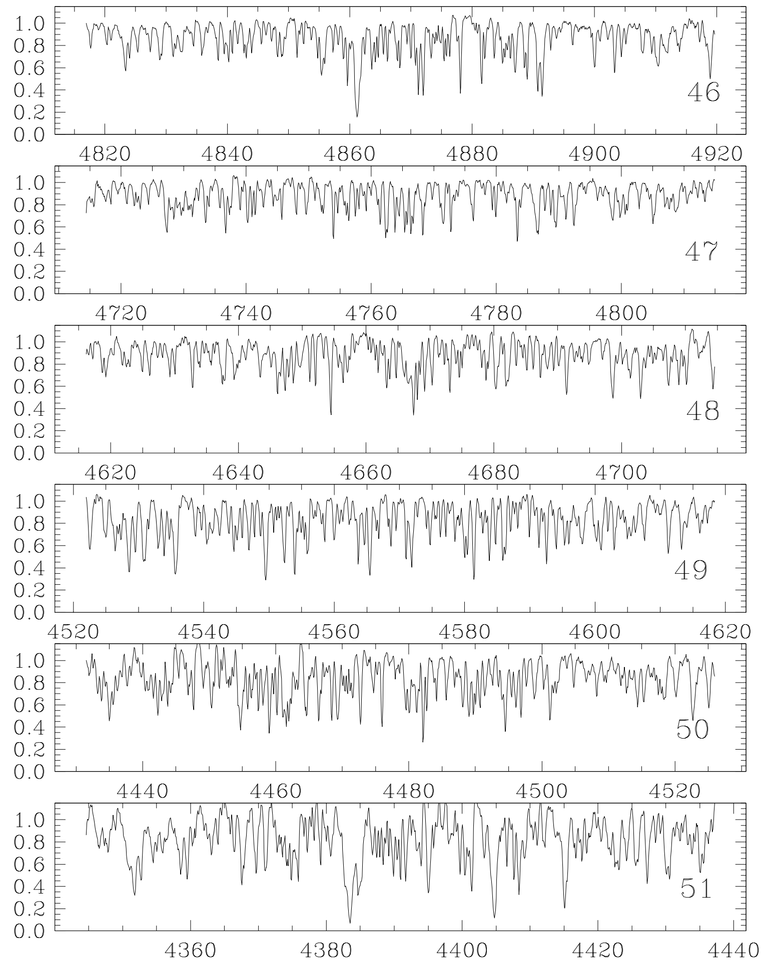

Figure 18: Echelle orders 49-54 of star ARCS 203222 . These orders cover a wavelenght interval from 4343 Å to 4922 Å. In the Echelle order 46 is visible the H_β line at ∼4861 Å.

In the spectra of ARCS targets the scattered light never exceed 2-3%, Fig. 20 shows how scattered light fulfills absorpion lines. With scatterd light the line depht changes are stricly proportional to the line depht at each point, reducing the contrast.

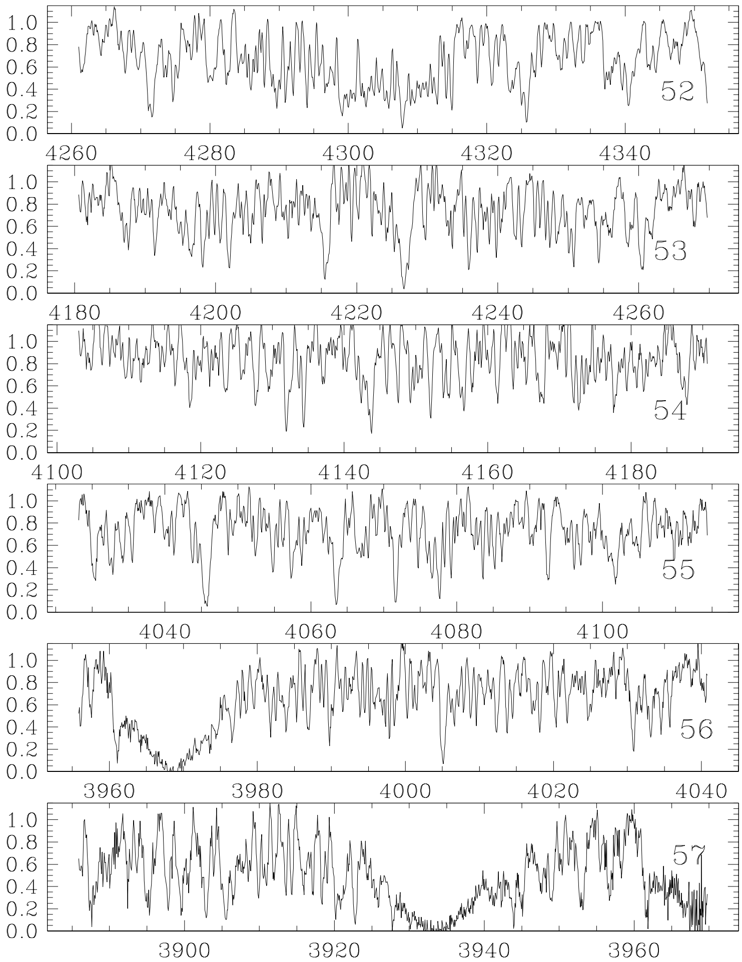

Figure 19: Echelle orders 55-56 of star ARCS 203222. These orders cover a wavelenght interval from 2937 Å to 4357 Å. In Echelle order 52 H_γ at ∼4340 Åis clearly visible. Echelle order 53 contains Ca ∼4227 Åand the CN absorption band at ∼4215 Å. Echelle prder 54 contains H_δ (4101 Å). In the Echelle order 56 there is the CaI ∼ 3968 feature. In the Echelle order 56 there is the Ca ∼3934 Åabsorption line.

Order Echelle	$\Delta\lambda$ in Å	**Disp.** Å/pix	**Ordine Echelle**	$\Delta\lambda$ in Å	**Disp.** Å/pix	**Ordine Echelle**	$\Delta\lambda$ in Å	**Disp.** Å/pix
57	3885-3969	0.082	48	4625 - 4717	0.099	39	5681 - 5807	0.123
56	3967-4048	0.108	47	4713 - 4817	0.102	38	5831 - 5965	0.131
55	4018-4121	0.100	46	4816 - 4922	0.103	37	5988 - 6196	0.203
54	4088-4197	0.106	45	4923 - 5030	0.104	36	6155 - 6296	0.137
53	4178-4275	0.094	44	5035 - 5144	0.104	35	6331 - 6478	0.143
52	4260-4357	0.095	43	5152 - 5264	0.109	34	6517 - 6669	0.148
51	4343-4441	0.096	42	5275 - 5389	0.111	33	6714 - 6870	0.152
50	4430-4530	0.097	41	5404 - 5522	0.115	32	6925 - 7083	0.154
49	4520-4622	0.100	40	5539 - 5661	0.119	31	7148 - 7308	0.156

Table 3: Wavelenght intervals covered by Echelle Orders.Orders start form the redder order 56 to the bluer 31. They covers a wavelenght interval from 3937 Åto 7308 Å.

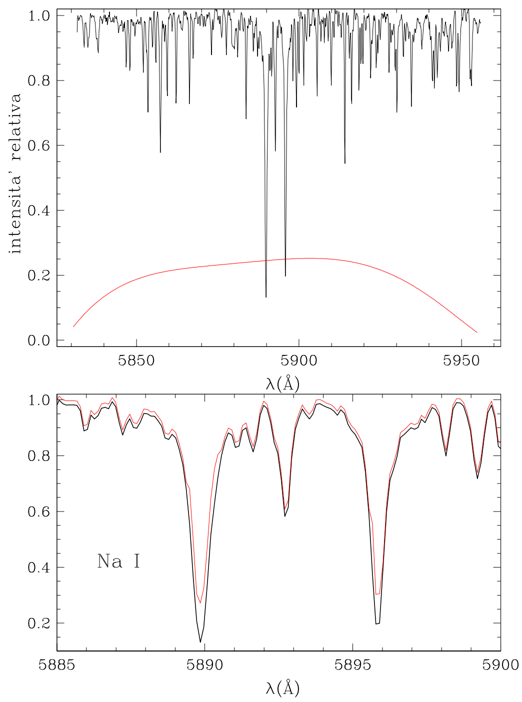

Figure 20: This image shows how much scattered light fills the lines profils, making the line more shallow everywhere. The spectrum of the star ARCS 199442 is the black line, in the wavelenght interval of 5831 - 5965 Å(Echelle order 38), the deep absorption lines of NaI are clearly visible. The red line (grey) is the scattered light.

4 RADIAL VELOCITY AND ATMOSPHERIC PARAMETER DETERMINATION

Contents

4.1 INTRODUCTION

For determining Vrad and atmospheric parameters we performed a cross-correlation analysis and a $\chi 2$ fitting against the synthetic library of Munari et al. (2005).

4.2 THE SYNTHETIC LIBRARY

The library of sinthetic spectra of Munari et al. (2005) is based on Kurucz's atmospheres, line-lists and computing software. The library is provided at different resolutions and rotational velocities, it covers a wide wavelength range. the library also adopt the improved model atmospheres based on the new opacity distribution functions (ODFs) by Castelli and Kurucz (2003), the use of the TiO line list of Schwenke (1998), the inclusion of α-element enhancement and different micro-turbulent velocities.
The whole grid of spectra in our library was computed using the SYNTHE code by Kurucz (Kurucz and Avrett 1981, Kurucz 1993), running under VMS operating system on a Digital Alpha workstation in Asiago. They adopted as input model atmospheres the ODFNEW models (http://wwwuser.oat.ts.astro.it/castelli/grids/; Castelli and Kurucz 2003). They differ from the NOVER models (http://kurucz.harvard.edu/grids.html; Castelli et al. 1997) for the adoption of new ODFs, replacement of the solar abundances from Anders and Grevesse (1989) with those from Grevesse and Sauval (1998), and improvements in the molecular opacities among which the adoption of the molecular line-lists of TiO by Schwenke (1998, as distributed by Kurucz 1999a) and of H_2O by Partridge and Schwenke (1997, as distributed by Kurucz 1999b).

For the combination of atmospheric parameters for which no ODFNEW models were available at the time of writing, we adopted the corresponding NOVER input model atmospheres. Both the NOVER and the ODFNEW models were computed with the overshooting option for the mixing-length convection switched off, while Kurucz (K) atmospheric models (also available from http://kurucz.harvard.edu/grids.html) were computed with the overshooting option switched on. Several papers have demonstrated that for stars with active convection ($T_{\rm eff}$<9000 K) the no-overshooting convection treatment provides better agreement with the observations than the overshooting case does (Castelli et al. 1997, Smalley and Kupka 1997, Gardiner et al. 1999, Smalley et al. 2002). The no-overshooting models used by us were computed for the mixing-length parameter to the scale height of 1.25. This value allows to fit the observed solar irradiance, while a lower value, like that of 0.5 suggested by Smalley et al., 2002, does it not. On the contrary, 0.5 seems to better fit the wings of Hβ, provided that the position of the continuum is known with an uncertainty smaller than 1%. In fact, a difference of 1% in the position of the solar continuum corresponds to the difference between 0.5 and 1.25 of the mixing-length parameter (Castelli et al., 1997). Generally, it's very difficult to state the location of the continuum across the wings of the Balmer lines, especially in Echelle spectra which are notoriously severely affected by the blaze function.
The range of atmospheric parameters explored by the adopted synthetic spectral library of Munari et al. (2005) is showed in Tab. 4.

The spectra in the adopted library covers from 2500 to 10500 Å and were calculated at a resolving power $R_P=\lambda/\Delta\lambda$=500 000 and then degraded by Gaussian convolution to lower resolving powers and properly re-sampled to Nyquist criterion (the FWHM of the PSF being 2 pixels), to limit the data volume and therefore facilitate the distribution.
All spectra in the library can be directly accessed and retrieved through the dedicated web page http://archives.pd.astro.it/2500-10500/. The version of the library at 1 Å/pix is accessible also via ESA's web site http://gaia.esa.int/spectralib/, where browsing facilities based on Virtual Observatory tools are provided. A distribution via DVDs will be possible in special cases (to be arranged directly at munari@pd.astro.it).
We selected the library of Munari et al. (2005) for the high range of stellar parameters covered, for its demonstred reliability with test on binaries (see Munari et al.,2005 paper), the absence of predicted lines and its avaiability at our resolution power.
For the construction of the grid we started from the fluxed library with no predicted lines. For reducing computational time we took

Table 4: Range of atmospheric parameters explored by the adopted synthetic spectral library of Munari et al. (2005).

temperature (K)	$3500 \leq T_{\rm eff} \leq 47\,500$	steps of 250 K for $T_{\rm eff} \leq 10\,000$ K; proportionally larger for higher $T_{\rm eff}$	
gravity (cgs units)	$0.0 \leq \log g \leq 5.0$		
metallicity	$-2.5 \leq$ [M/H] $\leq +0.5$		
rotation velocity (km $\rm sec^{-1}$)	$0 \leq V_{\rm rot} \leq 500$	0,2,5,10,15,20,30,40,50,75,100	for $T_{\rm eff} \leq 6000$ K
		0,10,20,30,40,50,75,100,150,200,250,300,400,500	for $T_{\rm eff} > 6000$ K
enhancement	$[\alpha/{\rm Fe}] = 0.0, +0.4$	$[\alpha/{\rm Fe}]=+0.4$ for [M/H]=-0.5, -1.0, -1.5	
micro-turbulent velocity (km $\rm sec^{-1}$)	$\xi = 1, 2, 4$	1 and 4 km $\rm sec^{-1}$ for $[\alpha/{\rm Fe}]=+0.4$	
ODFs	new	old where new ones not yet available	
predicted lines	excluded		

only the syntetic spectra computed with no α-enhancement: our stars are located in the solar neighbourhood, then a small portion of our stars could be α-enhanced. We are further investigating this aspect with a new observation campaign at higher resolution. We also considered only spectra with ξ=2 km s^{-1}: from the works of Hekker & Mendelez (1997), Mishenina (2005) and Takeda (2007) this value is a good compromise for red clump stars. We adopted the fluxed version of the library and therefore we normalized it. First we cut the spectra in intervals of the same wavelenght interval as the Echelle orders of the spectrograph of Asiago telescope. Then we normalized the spectra by adopting the same function we used for ARCS target spectra: a Legendre function of order 6.

4.3 CROSS CORRELATION ON SYNTETIC SPECTRA

Radial velocities are obtained with an automatic pipeline that uses a standard cross-correlation technique (Tonry & Davis, 1979). We rejected orders with low counts, high S/N, difficult normalization (due to stron absorption lines) and huge contamination by telluric lines. At the end we computed radial velocities measurements on the normalized spectra of 9 Echelle orders separately, from order 38 (5830-5965 Å) to order 46 (4815-4921 Å).
The grid of synthetic templates comes from the cut and the normalization of the library of synthetic spectra of Munari et al. (2005). The pipeline chooses the appropriate template and it calculates the radial velocity for each order. The internal accuracy of v_{rad} within orders is 0.5 km s^{-1} in average.
Cross correlation of a synthetic telluric spectrum against telluric absorptions in the reddest Echelle order 31 (7145-7300 Å) allows us to control the zero point of the wavelength scale at the 0.3 Km $^{-1}$ level.
In order to clean our sample from binaries we tried to re-observe targets at two separate epochs (typically 45 days apart). This observational strategy was suggested by the work of Udry et al. (1997): their Monte-Carlo simulations shows that with this method binaries are detected with an efficiency better than 50%. Fig.3 shows an histogram of the Δv_{rad} of the 150 stars with multi-epoch observations: the majority of stars has radial velocities that differs less than 10 Km s^{-1}. We considered as 'binary candidates' those stars with $\Delta v_{rad} \geq$ 10 Km s^{-1}.
At the moment we detected 10 binary candidates among the 150 observed Red Clump giants, corresponding to an observed frequency of spectroscopic binaries of 0,15%. We are now investigating the properties of these objects, trought more spectroscopic and photometric measurements.

4.4 χ^2 TEST

4.4.1 *The χ^2 method*

Measurement of T_{eff}, $logg$,[M/H], $V_{rot}sini$ is performed via $\chi 2$ fitting to a grid of synthetic spectra.
We built the grid of synthetic spectra from the library of Munari et al. (2005). The Munari's library is computed for a wide range of parameters, spanning the ranges $3500 \leq T_{eff} \leq 47500$ K, 0.00 $< logg <$ 5.0, -2.5 $\leq$ [M/H] $\leq$ 0.5, [α/Fe]=0.0, +0.4, ξ=1,2,4 Km s^{-1} and $0 \leq V_{rot} \leq 500$ Km s^{-1}. The library was computed using the SYNTHE code by Kurucz (Kurucz & Avrett, 1981; Kurucz, 1993) using the ODFNEW model atmospheres (Castelli & Kurucz, 2003). The solar partitions adopted by Munari et al. (2005) are the ones from Grevesse and Sauval (1998).
For the construction of the grid we started from the fluxed library with no predicted lines. For reducing computational time we took only the syntetic spectra computed with no α-enhancement: our stars are located in the solar neighbourhood, then a small portion of our stars could be α-enhanced. We are further investigating this aspect with a new observation campaign at higher resolution. We also considered only spectra with ξ=2 km s^{-1}: from the works of Hekker & Mendelez (1997), Mishenina (2005) and Takeda (2007) this value is a good compromise for red clump stars.
We prepared the grid by cutting the Munari's library in the same wavelength intervals as the Echelle orders, and then we normalized these intervals by using the same function and the same rejection threshold adopted in IRAF for stellar spectra: a Legendre function of order 6, with lower rejection of 0.5 and higher rejection of 1.5.
The adopted χ^2 technique is a simple χ^2 test of the stellar spectrum over the synthetic grid of stellar spectra. The χ^2 explores the space of the T_{eff}, *log*, [M/H] and $V_{rot}sini$ parameters, looking for the deepest minimum and determining its lowest point. This technique is adopted for each order separately. For each parameter we selected the best performing orders in order to obtain the correct value of T_{eff}, *log*, [M/H] and $V_{rot}sini$: at this first step the selected orders were orders from 38 to 46 (wavelength range 4816 - 5965 Å).
We obtained an internal error consistency between orders of 50 K in T_{eff}, 0.11 dex in *log*, 0.10 dex in [M/H] and 1 Km s^{-1} in $V_{rot}sini$. For the 150 stars that possess multi-epoch observations, we find an rms between the 2 observations of 57 K in T_{eff}, 0.10 dex in *log*, 0.09 dex in [M/H] and 1 Km s^{-1} in $V_{rot}sini$.
The quality of our results were deeply tested by observing and

analisyng with the same technique adopted for ARCS some samples of stars which parameter are well determined in literature. Thanks to these tests we may say that the χ^2 technique and the selected Echelle orders perform very well, with no evident dependence of atmospheric parameters on S/N (see Fig. 4) and with no dependences or degenerancies between parameters (see Fig. 5) .
We took as final result for T_{eff}, *logg* and [M/H] the mean of all the 9 orders, with a correction in T_{eff} and [M/H] in order to be in the same system of reference of the catalogs present in literature (Hekker & Mendelez (1997), Mishenina (2000), Soubiran et al. (2005) and Takeda et al. (2008)). The adopted correction is a rigid shift:

$$T_{eff ARCS \chi^2} = T_{eff\ \chi^2} + 40\ \mathrm{(K)}$$
$$[M/H]_{ARCS\chi^2} = [M/H]_{\chi^2} + 0.27\ \mathrm{(dex)}$$

where $T_{eff\chi^2}$ and $[M/H]_{\chi^2}$ are the values of temperature and metallicity as come from the χ^2.
The external consistency of our measurements and the way we found the rigid shift are described in Section 7.

5 TESTING THE METHOD

Contents

5.1 INTRODUCTION

In order to check the reliability of the method adopted in ARCS we made a series of test on both radial velocity and atmospheric parameters determinations.
We selected and observed a large number of stars taken from different sources in literature. We then observed these stars with the same telescope setup as ARCS, we reduced and analyzed spectra in the same way as ARCS spectra.
We may argue that ARCS radial velocity determinations are reliable: we did not detected any shifts in both IAU Velocity Standard stars and RAVE DR2 stars.
The test on atmospheric parameters based on the spectroscopic catalogs of McWilliams (1995), Soubiran(2005) and Takeda (2008) revealed that corrections of 0.27 dex on [M/H] and 40 K in Teff are needed. With this correction we found a good agreement of atmospheric parameters derived with ARCS $\chi 2$ with stars with atmospheric parameters well determined in literature and with stars belonging to Coma and Praesepe Open Clusters.
The $\chi 2$ analysis of spectra against a sinthetic library revealed to be a powerful and reliable tool for analysing big amount of data.

Table 5: Comparison between literature velocities and velocity measured with the ARCS's method of cross-correlation for 7 IAU standard velocity stars. All the values are in km s^{-1} .

Star	Literature		Asiago		Δv_{rad}
	v_{rad}	$\sigma_{v_{rad}}$	v_{rad}	$\sigma_{v_{rad}}$	(As.-Lit.)
HD 003712	−3.9	0.1	−4.1	0.3	−0.2
HD 012929	−14.3	0.2	−13.8	0.4	−0.5
HD 062509	3.3	0.1	3.3	0.6	0.0
HD 065934	35.0	0.3	34.6	0.5	0.4
HD 090861	36.3	0.4	36.7	0.4	−0.4
HD 212943	54.3	0.3	54.2	0.4	−0.1
HD 213014	−39.7	0.0	−40.0	0.5	−0.3

5.2 TESTS ON RADIAL VELOCITY MEASUREMENTS

5.2.1 *IAU Velocity Standards*

With the Asiago 1.82m + Echelle, with the same set-up as for ARCS, we observed 7 IAU standard radial velocity stars. By adopting the same method of ARCS we derived radial velocities. The mean difference between ARCS measurement and literature differs of ΔV_{rad}= -0.15 Km s^{-1} with an rms of 0.71 Km s^{-1} . There is an excellent agreement between IAU velocities and Asiago ones (results are labeled in Tab. 1, electronic only), confirming the reliability of our radial velocity measurements.

5.2.2 *RAVE*

In the work of Valentini and Munari(2007) we presented an external test of the accuracy of RAVE results, by deriving radial velocities for a sample of 25 RAVE targets. We went for targets with I band listed in DR2 as brighter than 10.0 mag and we tried to cover the widest range in atmopheric parameters T_{eff}, *logg* and [M/H] and we observed them with the same telescope set-up used for ARCS's targets. We derived radial velocities with the same cross-correlation method adopted for ARCS survey (results labeled in Tab.2, electronic only).

Table 6: Comparison between velocities given by RAVE DR2 (Zwitter et al., 2008) and velocity measured with the ARCS's method of cross-correlation for stars. All the values are in km s^{-1}

Star TYC	RAVE-DR2		Asiago		Δv_{rad}
	v_{rad}	$\sigma_{v_{rad}}$	v_{rad}	$\sigma_{v_{rad}}$	(As-RAVE)
T4678-00087-1	−2.6	2.4	0.8	0.2	3.4
T4679-00388-1	13.1	1.0	18.4	0.7	5.3
T4701-00802-1	−42.6	0.5	−41.2	0.3	1.4
T4702-00944-1	26.4	0.5	29.1	0.4	2.5
T4704-00341-1	−20.9	1.6	−19.6	0.6	0.7
T4749-00016-1	−29.8	0.6	−27.9	0.3	0.9
T4749-00085-1	61.8	0.7	62.8	0.9	1.0
T4749-00143-1	18.2	1.2	18.3	0.6	0.1
T4763-01210-1	−0.4	0.6	1.2	0.3	1.6
T5178-01006-1	−36.1	0.6	−37.4	0.3	−1.3
T5186-01028-1	−7.9	1.0	−7.7	0.5	0.2
T5198-00021-1	−32.9	0.6	−33.3	0.8	−0.5
T5198-00784-1	−54.7	1.6	−54.0	0.7	0.7
T5199-00143-1	−26.9	2.4	−26.7	0.9	0.2
T5201-01410-1	−1.7	1.0	0.0	0.9	−1.7
T5207-00294-1	25.7	0.9	24.6	0.6	−1.1
T5225-01299-1	−8.6	0.8	−9.6	0.3	−1.0
T5227-00846-1	−11.3	0.7	−10.2	0.8	1.1
T5228-01074-1	−8.6	1.0	−7.5	0.3	1.1
T5231-00546-1	−29.4	2.7	−28.2	0.7	1.2
T5232-00783 1	−21.0	0.8	−20.1	0.4	0.9
T5242-00324 1	−10.9	3.4	−11.9	0.8	−1.0
T5244-00102 1	−7.5	0.9	−5.8	0.5	1.7
T5246-00361 1	11.8	0.7	11.5	0.5	−0.3
T5323-01037 1	20.5	0.7	22.4	0.7	1.9

The mean differences between Asiago and RAVE velocities is Vrad$ASIAGO-$ Vrad$_{RAVE}$ 0.96 Km s^{-1} ($\sigma = 1.30$ Km s^{-1}). There is a very good agreement between RAVE and Asiago radial velocities.

5.3 TEST ON ATMOSPHERIC PARAMETERS :SOUBIRAN, HEKKER, TAKEDA CATALOGS

In order to further investigate the external consistancy of our atmospheric parameters measurements we observed a set of stars which atmospherical parameters were spectroscopically determined in literature. We considered the catalogs of Hekker and Mendelez (1997), Soubiran et al.(2005) and Takeda et al.(2008). In this works the authors determined atmospherical parameters with the classical spectroscopic method based on the FeI and FeII lines.
We selected $\sim$ 12 object per catalog, in all we selected 35 stars uniformely distributed in the same spectral type of the ARCS objects (G8III-K2III). We observed the literature targets with the same telescope set-up and the same technique adopted for ARCS targets. We also managed in order to have the same <S/N> of ARCS's spectra and we obtained atmospherical parameters with the same χ^2 technique against the same synthetic grid adopted for ARCS. The list of target stars, the parameters present in literature and the parameters obtained with ARCS technique are listed in Table 1 (Hekker Catalog), Table 2 (Soubiran Catalog) and Table 3 (Takeda Catalog).

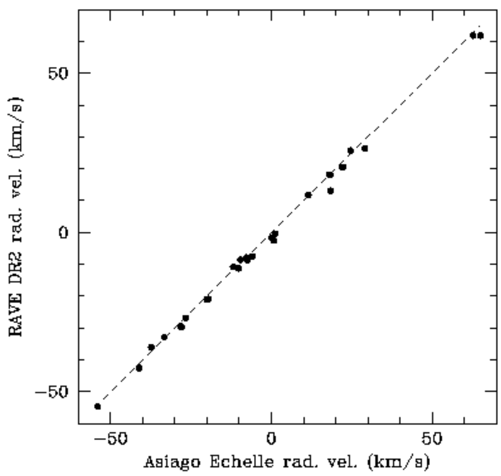

Figure 21: Comparison between radial velocities in Rave DR2 and those derived with the ARCS cross-correlation method. The diagonal gives the 1:1 relation.

It is relevant to notice that systematic differences in atmospheric parameters are present in between the catalogs we considered, even if the authors adopted the same method. For example, Takeda's spectroscopically determined *logg* values appear to be sistematically lower of 0.2 - 0.3 dex than the values in Hekker and Mendelez (2007) for the 147 stars in common. Differences of 0.7 - 0.8 Km s^{-1} are also present in the v_t values and the Takeda T_{eff} values are sistematically ∼50 K lower than Hekker's. These differences are partly due to differences in the sets of lines adopted (Takeda et al. 2008).
With this test we also refined the selection of the most performing orders starteded at the beginning of our work. At the end we considered the same six orders for the determination of the T_{eff} and *logg* (Echelle orders 41-45, corresponding to wavelenghts 4920 - 5530 Å) and we considered 4 orders for the [M/H].
The rms of ARCS results - literature results are 80 K in T_{eff}, 0.15 dex in *logg* and 0.15 dex in [M/H], as visible in Fig. 5. We may state that our results are in agreement with the values present in literature, without any significant systematic difference.
With these external test we demonstrated the reliability of the χ^2 technique and of the adopted library. The quality of the measurements and the short computational time needed for analysing large amount of data put forward the χ^2 technique as one of the most promising tool for large spectroscopical surveys (as the present survey RAVE and the forthcoming LAMOS).

5.3.1 *The importance of the S/N*

5.4 TEST ON ATMOSPHERIC PARAMETERS: STARS FROM LITERATURE

We observed with the Asiago Echelle spectrograph a set of 16 stars with atmospheric parameters well known in literature.
We selected the target stars from SIMBAD and asked for the list of stars with published atmospheric parameters. We restricted our attention to those stars with F-G-K spectral type and focused to the brightest onesin order to maximize the S/N. Among them we selected a random sample that tried to cover the widest range in metallicity. The spectra of these targets from literature were treated in the same way as we did for ARCS targets and analized them in the same way.
In Tab. 11 the selected stars are listed with the literature atmospheric parameters and parameters derived with our χ^2 analysis. The two data sets are compared in Fig. 25.
Atmospheric parameters derived with ARCS's χ^2 analysis and lit-

Table 7: Average and errors of the difference between the values of the atmospheric parameters of the 34 stars present in literature catalogs and the ones obtained with the χ^2 method for Echelle orders from 38 (5830-5966 Å) to 46 (4815-4922 Å).

ord	T_{eff}		$logg$		[M/H]	
	Δ	σ	Δ	σ	Δ	σ
	(K)	(K)	(dex)	(dex)	(dex)	(dex)
38	−67	119	−0.03	0.55	−0.19	0.11
39	17	80	0.14	0.24	−0.15	0.10
40	−89	159	−0.06	0.38	−0.35	0.15
41	−118	107	−0.87	0.32	−0.45	0.13
42	−115	83	−0.37	0.29	−0.49	0.10
43	114	108	0.17	0.30	−0.28	0.17
44	253	107	0.48	0.31	−0.23	0.18
45	108	137	0.18	0.48	−0.24	0.13
46	263	96	0.34	0.52	−0.07	0.13
mean	40		0.00		0.27	
	±50		±0.13		±0.05	

Table 8: Comparison between the atmospheric parameters obtained with ARCS's χ^2 method and values present in Soubiran catalog (Soubiran et al. 2005) for 14 stars. Soubiran's objects were observed with the same set-up and S/N of ARCS sample, and atmospheric parameters were derived by using the same method and synthetic grid as ARCS.

HD	T. Sp.	Soubiran			ARCSχ^2		
		T_{eff} (K)	$logg$ (dex)	[M/H] (dex)	T_{eff} (K)	$logg$ (dex)	[M/H] (dex)
124897	K2IIIp	4208	1.59	−0.75	4273	1.60	−0.51
161074	K4III	3951	1.62	−0.49	4004	1.62	−0.27
180711	G9III	4751	2.57	−0.46	4848	2.55	−0.19
212943	K0III	4550	2.51	−0.60	4663	2.53	−0.29
213119	K5III	3845	1.12	−0.52	3922	1.15	−0.31
216174	K1III	4342	1.84	−0.73	4403	1.71	−0.49
219615	G9III	4795	2.33	−0.79	4909	2.27	−0.48
005234	K2III	4447	2.10	−0.07	4473	2.29	0.10
006833	G8III	4587	1.55	−0.79	4251	1.36	−0.85
009927	K3III	4343	2.27	0.19	4361	2.15	0.08
010380	K3III	4199	1.79	−0.07	4114	1.63	−0.16
019476	K0III	4852	2.93	0.14	4934	3.18	0.13
039003	K0III	4618	2.32	0.03	4657	2.42	0.00

Table 9: Comparison between the atmospheric parameters obtained with ARCS's χ^2 method and values present in Hekker catalog (Hekker & Mendelez, 1997) for 11 stars. Hekkers's objects were observed with the same set-up and S/N of ARCS sample, and atmospheric parameters were derived by using the same method and synthetic grid as ARCS.

HD	T. Sp.	Hekker & Mendelez			ARCSχ^2		
		T_{eff} (K)	*logg* (dex)	[M/H] (dex)	T_{eff} (K)	*logg* (dex)	[M/H] (dex)
192944	G8III	5000	2.70	−0.10	4988	2.81	−0.06
203644	K0III	4740	2.75	0.04	4748	2.82	−0.03
210762	K0III	4185	1.65	0.00	4251	1.58	0.03
214995	K0III	4880	2.85	−0.04	4743	2.69	−0.02
199253	K0III	4625	2.35	−0.19	4644	2.27	−0.16
213119	K5III	4090	1.65	−0.48	4101	1.63	−0.45
214868	K3III	4445	2.50	−0.17	4329	1.86	−0.17
215373	K0III	4950	2.87	0.01	5059	3.21	0.11
216646	K0III	4600	2.65	0.07	4644	2.71	0.08
219945	K0III	4880	2.85	−0.09	4840	2.74	−0.14

Table 10: Comparison between the atmospheric parameters obtained with ARCS's χ^2 method and values present in Takeda catalog (Takeda et al., 2008) for 10 stars. Takeda's objects were observed with the same set-up and S/N of ARCS sample, and atmospheric parameters were derived by using the same method and synthetic grid as ARCS.

HD	T. Sp.	Takeda			ARCSχ^2		
		T_{eff} (K)	*logg* (dex)	[M/H] (dex)	T_{eff} (K)	*logg* (dex)	[M/H] (dex)
006186	K0III	4829	2.30	−0.31	4930	2.48	−0.23
007087	K0III	4908	2.39	−0.04	4972	2.63	−0.03
009057	K0III	4883	2.49	0.04	4986	2.87	0.03
009408	K0III	4746	2.21	−0.34	4834	2.40	−0.31
010761	K0III	4952	2.43	−0.05	5031	2.64	−0.04
019476	K0III	4933	2.82	0.14	5041	2.27	0.12
204771	K0III	4967	2.93	0.09	4992	3.24	0.04
215373	K0III	5007	2.69	0.10	5107	3.31	0.14
219945	K0III	4874	2.61	−0.10	4909	2.75	−0.11
221345	K0III	4813	2.63	−0.24	4719	2.44	−0.29

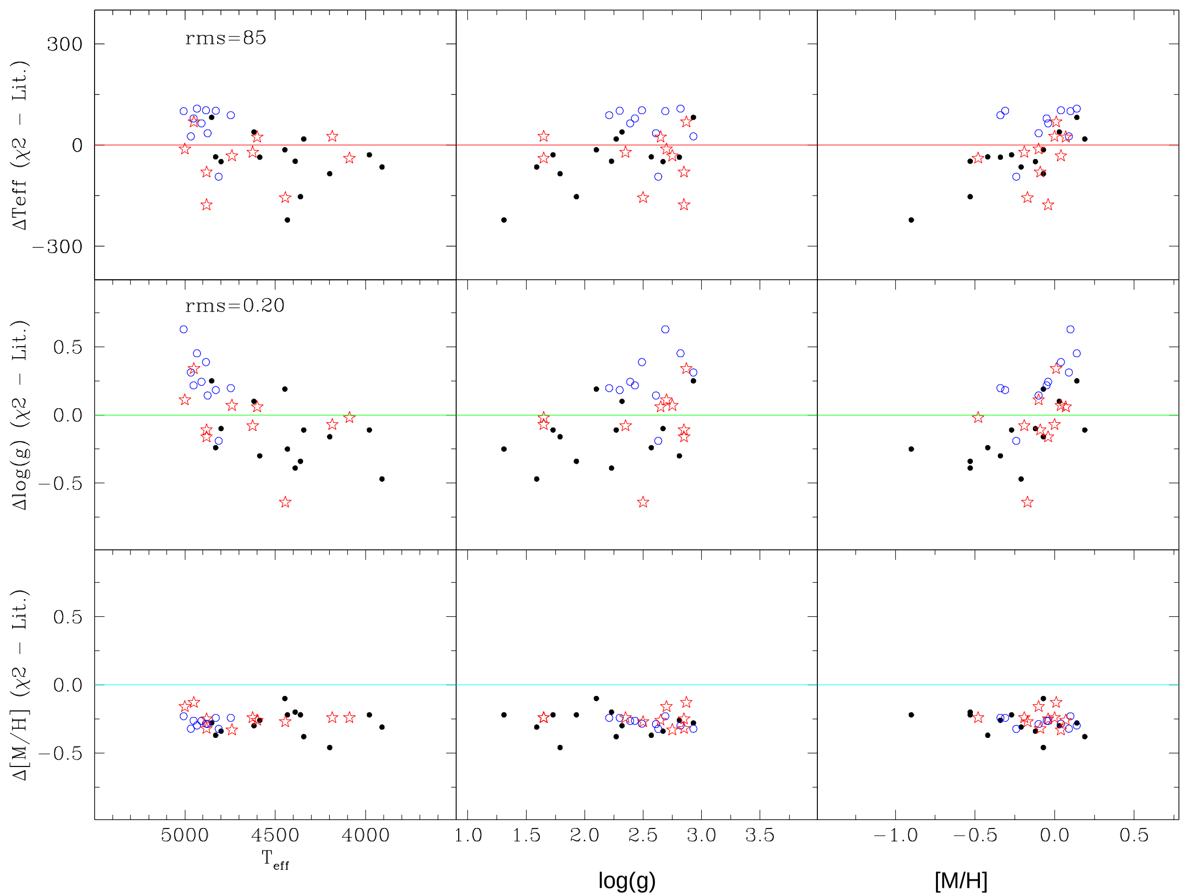

Figure 22: Differences between atmospheric parameters obtained with ARCS χ^2 technique and literature values. Full circles are objects from Hekker & Mendelez (1997), empty cyrcles are Soubiran (2005) objects and stars are Takeda et al. (2008) objects. We may argue that there is no evident shift ore dependence for atmospheric parameters for data obtained with ARCS χ^2.

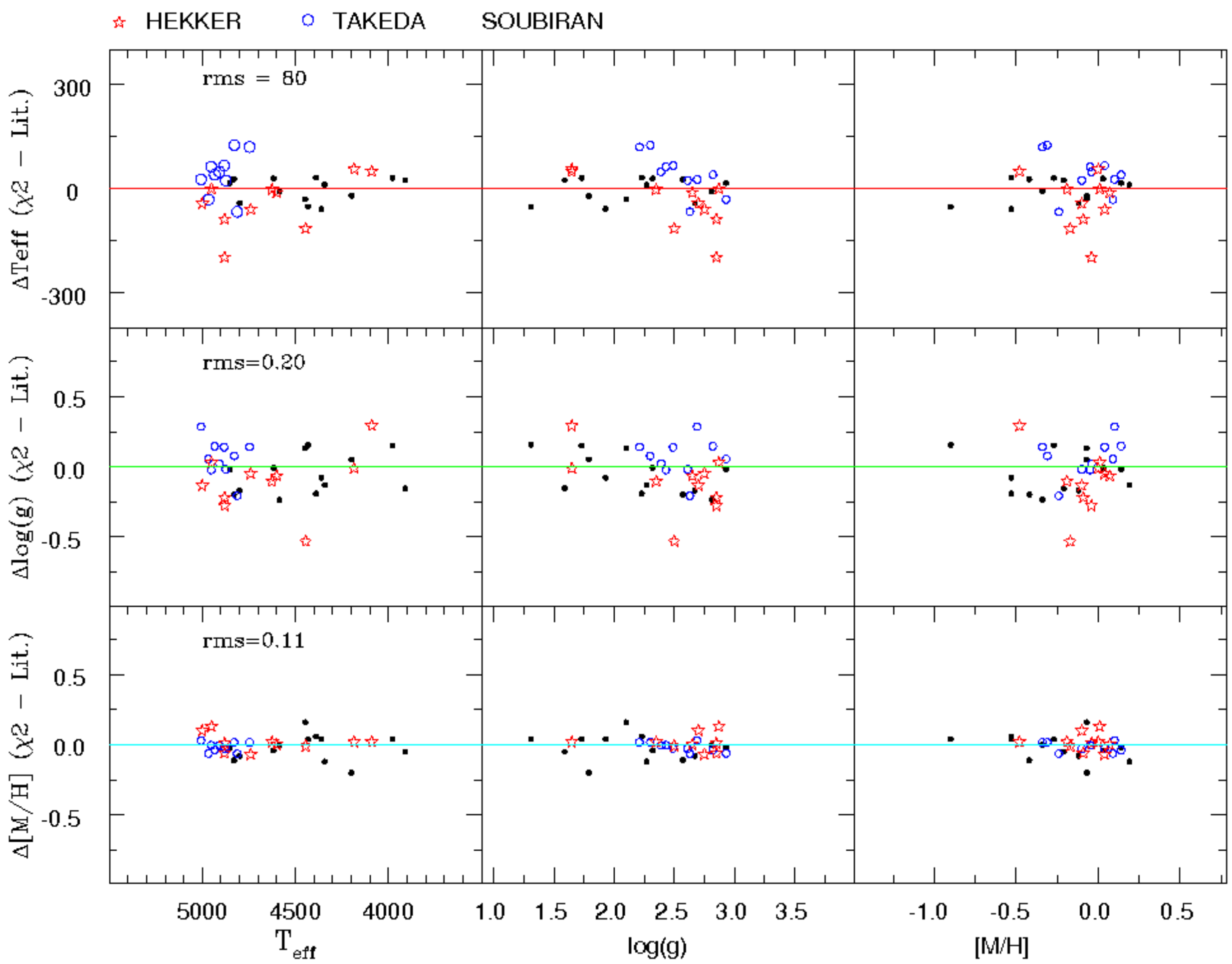

Figure 23: Differences between atmospheric parameters obtained with ARCS χ^2 technique and literature values. Full circles are objects from Hekker & Mendelez (1997), empty cyrcles are Soubiran (2005) objects and stars are Takeda et al. (2008) objects. We may argue that there is no evident shift ore dependence for atmospheric parameters for data obtained with ARCS χ^2.

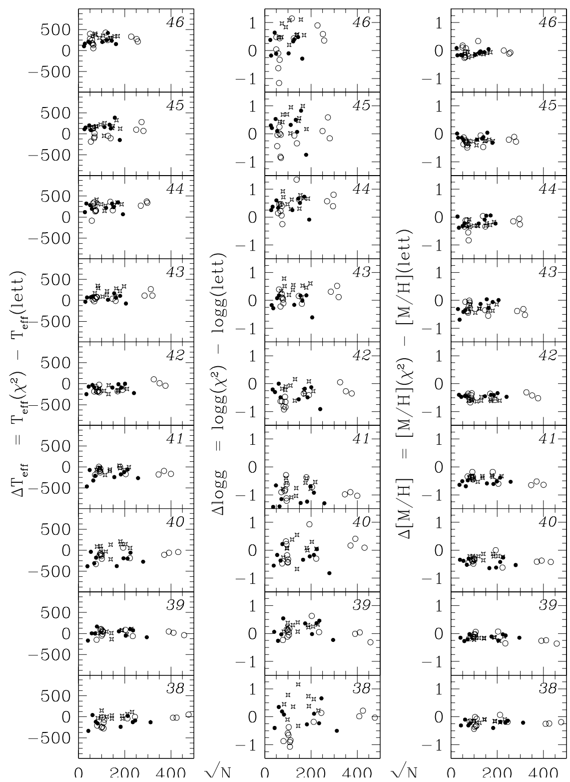

Figure 24: Comparison between atmospheric parameters present in literature and those derived with the ARCS $\chi 2$ for 16 stars. The diagonal gives the 1:1 relation.

erature parameters do not show offsets. The mean differences for the atmospheric parameters are:
$\langle Teff_{lit} - Teff_{\chi 2} \rangle$ 57±72
$\langle logg_{lit} - logg_{\chi 2} \rangle$ 0.21±0.18
$\langle M/H_{lit} - M/H_{\chi 2} \rangle$=+0.029±0.028

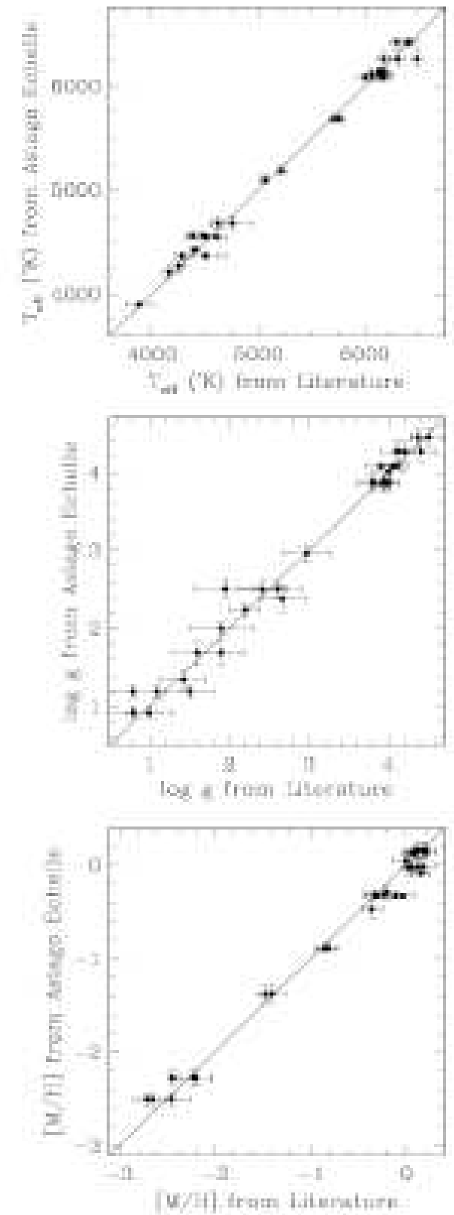

Figure 25: Comparison between atmospheric parameters present in literature and those derived with the ARCS $\chi 2$ for 16 stars. The diagonal gives the 1:1 relation.

Table 11: Comparison between published atmmospheric parameters of F, G, K field stars of luminosity class from I to V, and those derived from ARCS $\chi 2$. The 'ref' column identifies the listed source paper for the literature atmospheric parameters.

HD	Literature							ARCS χ_2				
	T_{eff} (K)	err (K)	*logg* (dex)	err (dex)	[M/H] (dex)	err (dex)	ref	T_{eff} (K)	err (K)	*logg* (dex)	err (dex)	[M/H] (dex)
91752	6488	50	3.92	0.10	−0.23	0.05	1	6262	71	3.85	0.08	−0.32
	6310	80	3.99	0.12	−0.32	0.10	3					
	6180		3.80		−0.33		2					
101606	6000		4.00		−0.82		2	6090	33	4.01	0.08	−0.88
87141	6403	50	4.05	0.10	0.04	0.05	1	6420	36	4.08	0.03	0.13
	6417	80	4.11	0.12	0.21	0.10	3					
	6300		3.9		0.07							
124850	6177	50	3.94	0.10	−0.11	0.05	1	6139	38	3.88	0.12	−0.33
	6136	80	4.00	0.12	−0.31	0.10	3					
	6146		3.8		−0.03		2					
102870	6176	50	4.14	0.10	0.13	0.05	1	6097	47	4.27	0.12	0.16
	6190	80	4.20	0.12	0.10	0.10	3					
	6146	100	4.4	0.2	0.20	0.05	5					
	6072		4.1		0.18		2					
74462	4620	50	1.60	0.3	−1.47	0.05	6	4682	70	1.69	0.15	−1.38
	4744	200	1.9	0.3	−1.40	0.15	7					
76151	5763	50	4.37	0.10	0.01	0.05	1	5686	31	4.45	0.11	−0.03
71369	5220	50	2.67	0.30	−0.21	0.11	9	5189	43	2.38	0.18	−0.29
88609	4600	50	1.50	0.3	−2.81	0.04	10	4552	23	1.19	0.08	−2.50
	4500	100	1.1	0.3	−2.50	0.20	11					
	4500	200	0.8	0.3	−2.70	0.15	7					
110184	4275	50	0.80	0.3	−2.44	0.04	1	4367	36	0.92	0.08	−2.27
	4500	100	1.0	0.3	−2.23	0.20	11					
	4500	200	0.8	0.3	−2.20	0.17	7					
79452	4165		2.20		−0.85	0.15	12	4209	62	2.24	0.09	−0.89
113226	5060	50	2.97	0.30	0.15	0.10	9	5101	43	2.96	0.11	−0.09
85503	4480	50	2.61	0.30	0.17	0.12	9	4560	33	2.51	0.12	−0.02
	4375	50	1.95	0.40	0.12	0.08	13					
102328	4250	50	1.90	0.40	0.09	0.08	13	4274	47	2.00	0.09	0.14
125560	4400	50	2.42	0.30	0.00	0.14	9	4429	32	2.50	0.12	0.05
17709	3880	130	1.42	0.30	−0.36	0.11	9	3903	26	1.34	0.11	−0.47

5.5 TEST ON ATMOSPHERIC PARAMETERS: OPEN CLUSTERS

In order to check the external consistency of our atmospheric parameters measurements we observed a set of stars belonging to open clusters which atmospherical parameters were determined in literature.
We observed 9 objects in the Coma Berenices open cluster, these objects covers a spectral type range from F0V to F2III. Results are labeled in Table 2 (electronic only).

We also observed 4 stars in the Praesepe open cluster, these objects covers a spectral type range from G8III to K0III. Results are labeled in Table 3 (electronic only).

No relevant shifts are present in the ARCS χ^2 values for T_{eff}, *logg* and [M/H] with the values present in the literature.

5.6 DISCUSSION

The large number of test illustrated in this chapter tested the reliability of ARCS radial velocities and atmospheric parameters determination.
Radial velocity measurement with the automatic cross correlation method demonstred to be accurate.
Amospheric parameters detemination need a correction for metallicity of 0.27 dex and 40 K in temperature.

Table 12: Atmospheric parameters of Coma Open Cluster's selected stars as present in literature and as derived with ARCS χ^2 technique. The objects were observed and reduced in the same way as ARCS targets. The number in column 6 indicates the literature reference: (1) Wallerstein & Conti (1964);(2-3) Cayrel de Strobel et al. (2001); (4) Gustafsson et al. (1974); (5) Claria et al. (1996); (6) Boesgaard (1987); (7) Frill & Boesgaard (1992); (8,*) Cayrel et al. (1988); (9, *) Gebran et al. (2008,).

COMA CLUSTER		Age: $\approx$ 400 Myrs [Fe/H]=-0.052 (*)						
Star	S.Type	From Literature				ARCSχ^2		
		T_{eff} (K)	*logg* (dex)	[M/H] (dex)	Ref	T_{eff} (K)	*logg* (dex)	[M/H] (dex)
HD 109069	F0V	6864	4.06		9	7082±52	4.5±0.10	−0.05±0.05
HD 106946	F2V			−0.03	2	6982±46	4.46±0.11	−0.04±0.05
		6890		−0.031	6			
		6892	4.30		9			
HD 107611	F6V	6425		−0.090	6	6583±47	4.50±0.11	−0.10±0.05
				−0.09	2			
		6425		−0.056	7			
		6491	4.57		9			
HD 107793	F8V	6095		−0.113	6	6199±72	4.53±0.21	−0.09±0.05
				−0.11	2			
				−0.06	2			
		6095		−0.059	7			
HD 107583	G0V			−0.06	2	5627±59	3.6±0.12	−0.07±0.08
		5960		−0.057	7			
		5850	4.20	−0.06	8			
HD 105863	G0V	5808			3	5504±47	3.7±0.22	−0.09±0.07
HD 108283	F0III					4979±57	2.43±0.20	−0.08±0.08
HD 111812	G0III	4883		−0.256		5045±42	3.49±0.21	−0.19±0.11
				−0.20	4			
HD 107700	F2III			−0.10	2	6180±47	3.42±0.21	−0.12±0.11
				−0.15	2			
		6210		−0.101	6			
		6210		−0.148	7			

Table 13: Atmospheric parameters for Prasepe Cluster's selected stars as present in literature and as derived by ARCS's χ^2 method. The objects were observed and reduced in the same way as ARCS targets. The number in column 5 indicates the literature reference: (1) Cayrel de Strobel et al, 1997; (2) Taylor (1999); (3) Pasquini (2000);(*) Boedsgaard et al. (2000); (**) Pace et al. (2008).

PRAESEPE CLUSTER Age: ≈ 600 Myrs [Fe/H]=0.13 (*) [Fe/H]=0.27 (**)

Star	S.Type	From Literature			ARCSχ^2		
		T_{eff} (K)	[M/H] (dex)	Ref	T_{eff} (K)	*logg* (dex)	[M/H] (dex)
HD 73665	G8III	4990	−0.04	1	4945±52	2.77±0.10	−0.06±0.10
			0.047	2			
HD 73710	G9III	4893	−0.17	1	4860±53	2.67±0.10	0.08±0.10
			0.245	2			
		4634		3			
HD 73598	K0III		0.014	2	4916±53	2.78±0.10	0.14±0.10
		4799		3			
HD 73974	K0III		0.064	2	4948±61	2.91±0.10	0.14±0.10

6 CONSTRUCTING ARCS HIGH RESOLUTION CATALOG

Contents

6.1 INTRODUCTION

In constructin the ARCS catalog we put great care in the deermination of the distances and in computing UVW velocities.

6.2 DISTANCES

ARCS survey (ARCS stays for Asiago Red clump Spectroscopic) produced a catalog of 300 Red Clump stars of the Solar Neighborhood. It provides spectroscopically derived atmospheric parameters (T_{eff}, $logg$, [M/H], $V_{rot} sini$) and radial velocities . All the stars of ARCS catalog have non-negative Hipparcos parallaxes, good Michigan spectral classification, proper motions from Tycho-2 catalog, 2MASS and I-DENIS photometry.
ARCSs may be an useful tool for investigating the kinematics of the Milky Way disk in the Solar Neighborhood, because it gives us accurate radial velocities, distances and proper motions. The uncertainty on the distance gives the largest error on the calculation of U,V,W , since ARCS V_{rad} has an accuracy of 0.5 Km s^{-1} and Tycho-2 proper motions have an accuracy of μ_α 0.88 mas/yr and μ_δ 0.74 mas/yr, whereas the error on distance from Hipparcos parallaxes can exceed 80% .
In this section we compare distances for ARCSs objects obtained with Hipparcos parallaxes, distances obtained from K-2MASS photometry and with the Keenan & Barnbaum (2000) calibration.

6.2.1 *Hipparcos distances*

We simply adopted a non-negative Hipparcos parallax as selection criteria. Therefore distances for ARCS objects derived from Hipparcos parallaxes can be meaningful or with acceptable error bars only for a small fraction of the target stars.
As a matter of fact only 43 of the 427 target stars has $\sigma_\pi/\pi \leq 0.10$ from Hipparcos parallaxes. With the recent revised Hipparcos parallaxes (F. Van Leeuwen, 2007) we also noticed a rigid shift in the absolute magnitude of the RC stars in the V_J band. As is clearly visible in Fig. 26 there is a shift of 0.1 mag in the absolute magnitude of our 43 RC stars with more precise parallaxes between old and new parallaxes. One of the most useful proper-

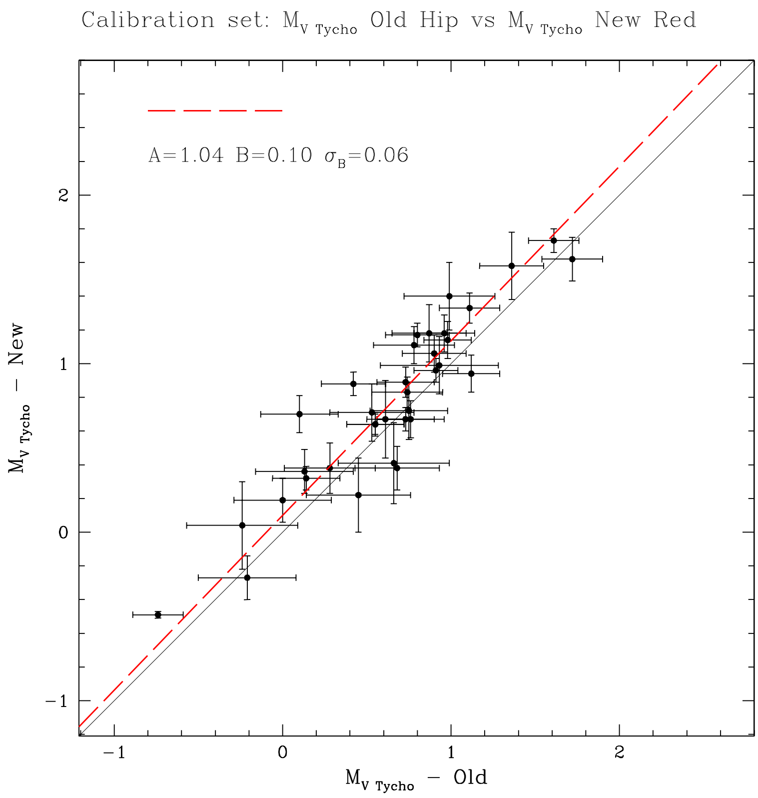

Figure 26: Distances from Hipparcos New Reduction of Raw Data (2007) compared with distances taken from the old Hipparcos catalog (Perryman, 1997) for the 43 stars with $\sigma_\pi/\pi \leq 0.10$. The diagonal line represents the 1:1 relation.

ties of RC stars is their their near-constant luminosity, that has a negligible dependence on metallicity for stars in the Solar Neighborhood . Thus we preferred to derive distances from photometry.

6.2.2 *K-band*

We chose K band because it is the band less sensitive to the metallicity (see Alves, 2000 and Groenewegen, 2008) and because it is less affected by reddening. We used the Hipparcos parallaxes taken from the New Reduction of Hipparcos Raw Data (Van-Leeuwen, 2007). We used the $\langle M_K \rangle$ computed by Groenewegen: $\langle M_K \rangle$=-1.54± 0.04 (Groenewegen, 2008).
Groenewegen obtained this value by using a numerical model that takes in to account several selection criteria and properties of Hipparcos catalog. In this work no relevant dependence on metallicity was found, and the dependence on colour is weak: (-0.15± 0.07)((V-K)$_o$-2.32).
In the Fig. 27 the comparison between distances from Hipparcos New Reduction of Raw Data (2007) catalog and photometric distance from K-2MASS is showed. Each panel sohw stars with different error on Hipparcos parallaxes, lowest error on top and highest error at bottom. As is clearly visible from the figure there is a shift for K2 III stars for stars with larger error on parallaxes: the photometric distances for K2 III stars appears to be shorter than the Hipparcos distances.

6.2.3 *Spectrophotometric distances*

Keenan & Barnbaum (2000) applied a modification to the MK luminosity standards so that luminosity class IIIb denotes members of the clump. They made a new calibration of MK luminosity classes III and IIIb in terms of visual absolute magnitudes. Keenan calibrations are showed in Tab. 28 Fig. 29).
We decided to use the Keenan & Barnbaum calibrations:in Fig. 30 it appear that their calibrations are the most consistant with Hipparcos distances by looking the spectral type.

6.3 GALACTIC VELOCITIES

To derive reliable space velocities the distance must be known with appropriate accuracy. Only 46 of the 426 target stars have Hipparcos parallaxes with $\sigma_\pi/\pi \leq 10\%$, the remaining stars have relevant error on distance. For that reason a photometric parallax is used. Fig. 31 shows the comparison between distances obtained with revised Hipparcos parallaxes (Van Leeuwen , 2007) and those

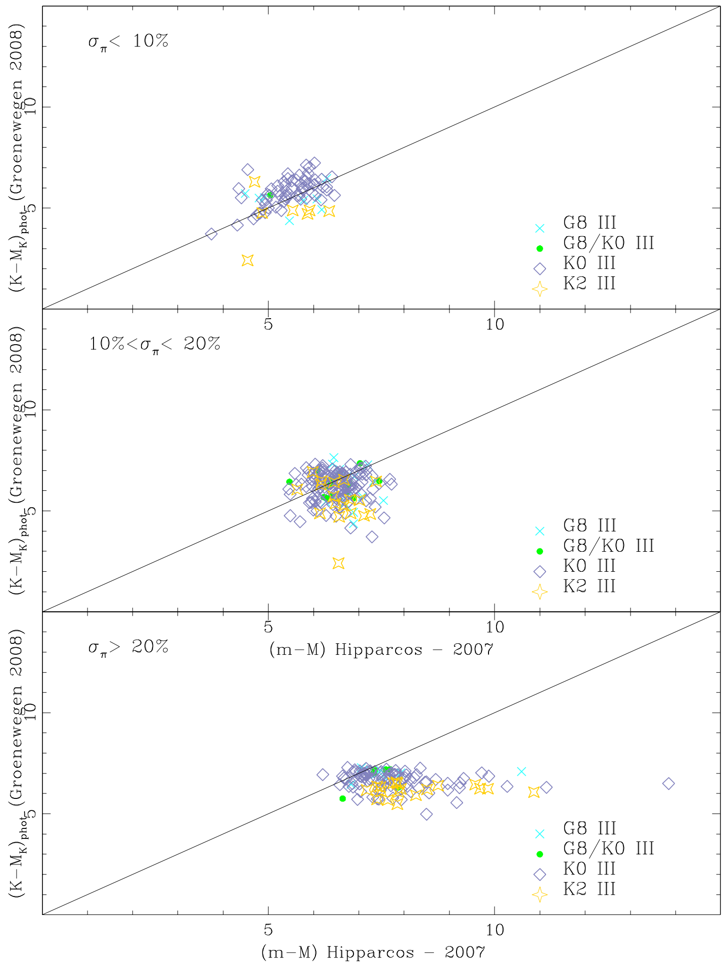

Figure 27: Distances from Hipparcos New Reduction of Raw Data (2007) catalog plotted against photometric distance from K-2MASS. Each panel sohw stars with different error on Hipparcos parallaxes, lowest error on top and highest error at bottom. Different symbol represents different spectral type. The diagonal line represents the 1:1 relation.

MEAN M_v AS A FUNCTION OF SPECTRAL TYPE

Mean Type (1)	Unweighted $\langle\pi'\rangle$ (2)	Weighted $\langle\pi'_w\rangle$ (3)	Mean $\langle\pi'\rangle$ (4)	ΔM (5)	Correction M_v (6)	Correction M_v (7)	Adopted M_v (8)
G7	0.00808	0.00820	0.00814	−0.41	0.24	−0.17	−0.17
G9	0.00791	0.00813	0.00802	−0.48	0.24	−0.24	−0.21
K0.5	0.00816	0.00800	0.00808	−0.46	0.24	−0.22	−0.26
K2	0.00802	0.00793	0.00798	−0.55	0.24	−0.31	−0.29
G4	0.00771	0.00764	0.00768	−0.57	0.24	−0.33	−0.45
M0	0.00648	0.00647	0.00647	−0.95	0.24	−0.71	−0.60
M2.5	0.00666	0.00636	0.00651	−0.99	0.24	−0.75	−0.75
G8+	0.01360	0.01368	0.01364	0.67	0.03	0.07	0.07
G9−	0.01499	0.01494	0.01497	0.88	0.03	0.91	0.83
K0+	0.01463	0.01492	0.01478	0.85	0.03	0.88	0.93
K2−	0.01446	0.01425	0.01436	0.78	−0.12	1.00	1.00

Figure 28

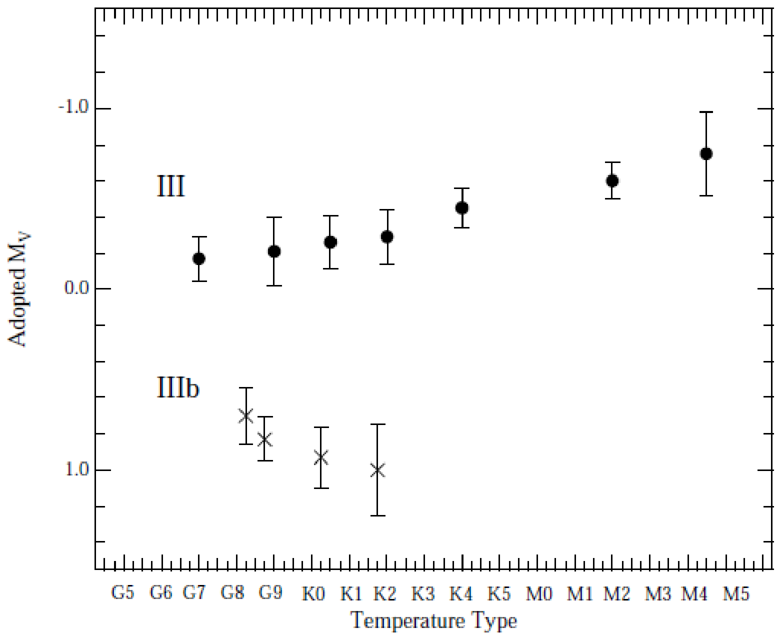

Figure 29: Calibration of revised luminosity classes of cool giants by Hipparcos parallaxes. The values of mean MV have been reduced to constant volume by the Malmquist correction.Figure taken from the Keenan & Barnbaum (1999) article.

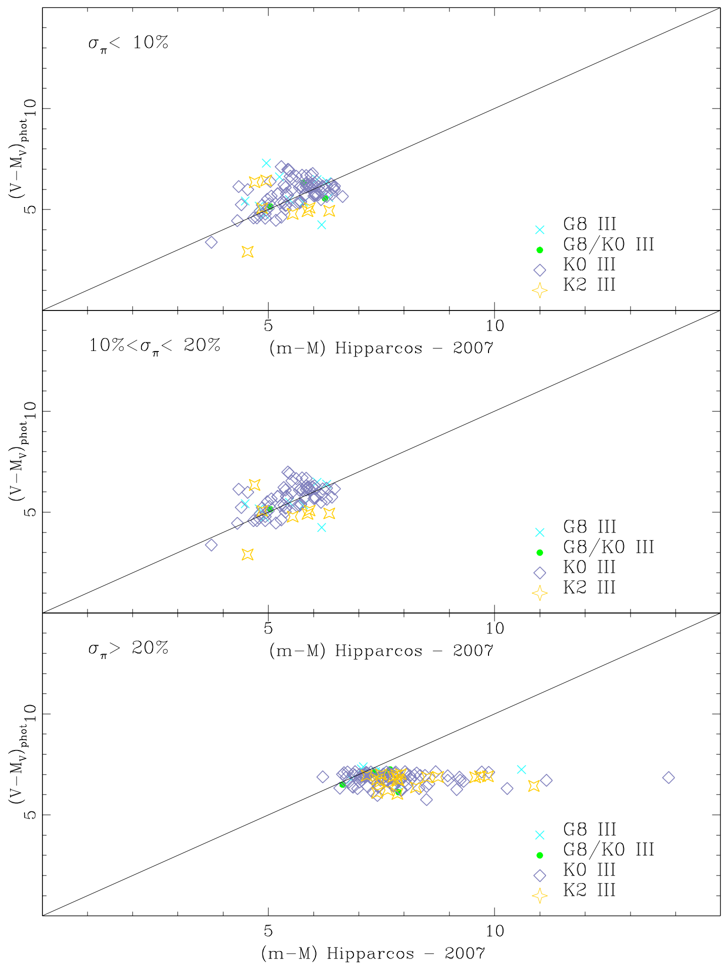

Figure 30: Distances from Hipparcos New Reduction of Raw Data (2007) catalog plotted against photometric distance from V Keenan & Barnbaum (1999) calibrations. Each panel sohw stars with different error on Hipparcos parallaxes, lowest error on top and highest error at bottom. Different symbol represents different spectral type. The diagonal line represents the 1:1 relation.

derived from V calibration of Red Clump (Keenan & Barnbaum, 2000).

Since there is no relevant dependence of M_V on atmospheric parameters (see Fig. 32 and Fig. 33), we have adopted the distance calibrations of Keenan & Barnbaum (1999) for cool giants. We checked the photometric distances against the distances from Hipparcos parallaxes for the subset of the stars with $\sigma_\pi/\pi \leq 10\%$: the photometric and the trigonometric distances agree very well (Fig. 30). Reddening is not an issue at the high galactic latitude of ARCS targets, and following Arenou et al. (1992) the corrections are negligible ($E_{B-V} \leq 0.02$).

A conversion of the space velocity to the usual (U, V, W) system by using the input data of (α, δ, p, μ_α, μ_δ, $V_{\rm r}^{\rm hel}$) was carried out with the help of the formula described in Johnson and Soderblom (1987). We used a left-handed system with U positive outward the Galactic Center.

The analysis of the combined information of the kinematics and the atmospheric properties of ARCS sample is discussed in paper 2, Valentini et al. in preparation.

6.4 REDDENING

Reddening is not an issue at the high galactic longitudes of ARCS targets. We calculated the reddening following Arenou et al. (1992): the corrections are negligible ($E_{B-V} \leq 0.02$) (see Tab. 14).

6.5 DETECTED BINARIES

The internal accuracy of v_{rad} within orders is 0.5 km s^{-1} in average.

Cross correlation of a synthetic telluric spectrum against telluric absorptions in the reddest Echelle order 31 (7145-7300 Å) allows us to control the zero point of the wavelength scale at the 0.3 Km $^{-1}$ level.

In order to clean our sample from binaries we tried to re-observe targets at two separate epochs (typically 45 days apart). This observational strategy was suggested by the work of Udry et al. (1997): their Monte-Carlo simulations shows that with this method binaries are detected with an efficiency better than 50%. Fig.3 shows an histogram of the Δv_{rad} of the 150 stars with multi-epoch observations: the majority of stars has radial velocities that differs less than 10 Km s^{-1}. We considered as 'binary candidates' those stars with $\Delta v_{rad} \geq$ 10 Km s^{-1}.

At the moment we detected 10 binary candidates among the

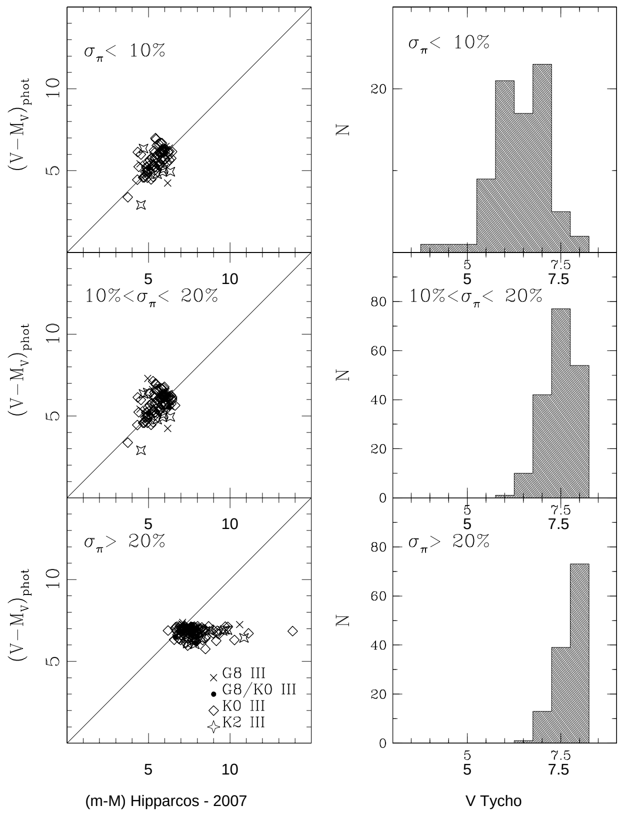

Figure 31: Left column :Comparison between the distance modulus obtained with the photometric parallaxes from Keenan and Barnbaum (2000) calibrations and distance modulus obtained with new Hipparcos parallaxes (Van Leeuwen, 2008). The line represents the 1:1 corrispondence. Each different spectral type is represented with a different symbol. Each panel rehepresents different error bins in the Hipparcos parallaxes. Right column: histograms of the ARCS stars distribution in V_{Tycho} magnitude. Each panel is the distribution in different error bins in the Hipparcos parallaxes.

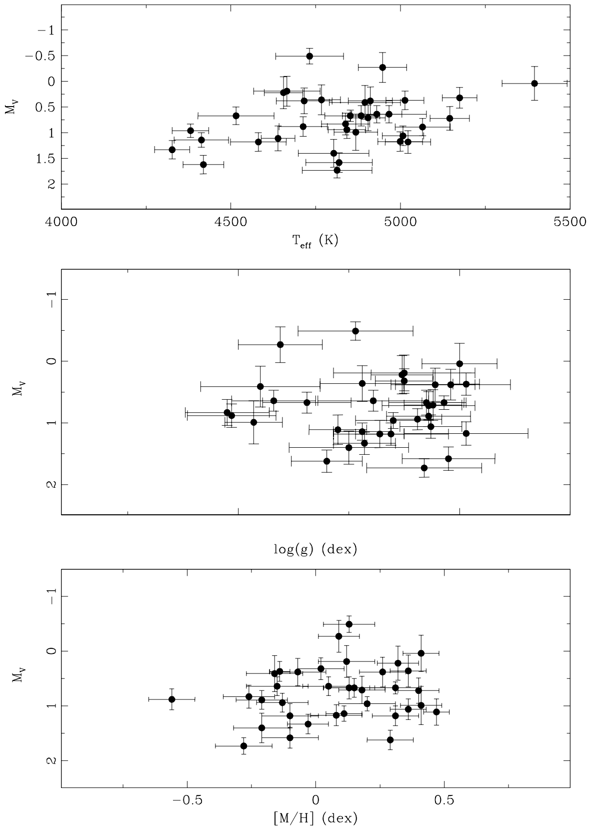

Figure 32: ARCS's V absolute magnitude vs [M/H] for the 46 ARCS targets which parallax has $\sigma_\pi\ \pi \leq 15\%$ (from revised Hipparcos parallaxes, van Leeuwen, 2007). From top to bottom: M_V vs T_{eff}, M_V vs *logg* and M_V vs [M/H]. There is no relevant dependence of M_V from [M/H].

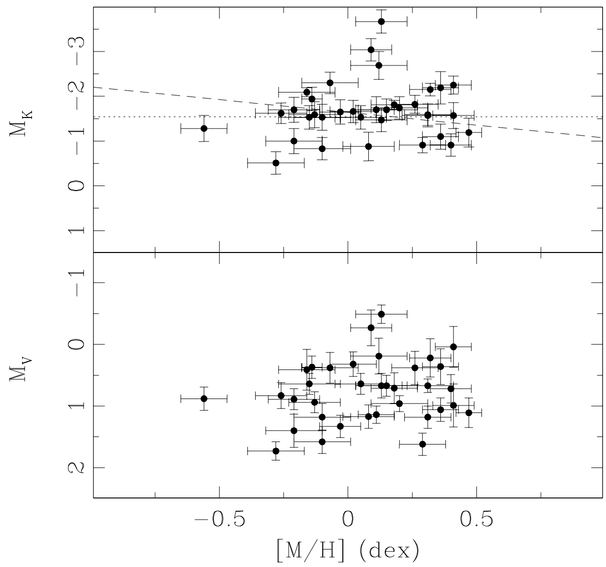

Figure 33: V and K absolute magnitude vs [M/H] for the 46 ARCS targets which parallax has $\sigma_\pi \ \pi \leq 15\%$ (from revised Hipparcos parallaxes, van Leeuwen, 2007). Top panel: M_K vs [M/H]. Dashed line is the dependence of M_K on [M/H] of Alves (2000): $M_{KRC} \quad 0.57 \pm 0.36 Fe/H \ 0.25 \ -1.64 \pm 0.07$. Dotted line is the mean M_K for the Red Clump found by Groenewegen (2008), M_{KRC} = -1.54. Bottom panel: M_V vs [M/H]. There is no relevant dependence of M_V from [M/H].

Table 14: Reddening following Arenou et al. (1992).

ARCS	E_{B-V}	A_V
6	0.02727	0.09860
2023	0.02727	0.09860
8120	0.02724	0.09851
8599	0.02724	0.09851
11037	0.03250	0.11744
12923	0.03250	0.11744
13468	0.03250	0.11744
16467	0.03250	0.11744
18145	0.03250	0.11744
22798	0.10873	0.38875
22796	0.10873	0.38875
22819	0.10873	0.38875
23887	0.10873	0.38875
28322	0.10873	0.38875
32393	0.08040	0.28860
75217	0.04740	0.17093
83618	0.00867	0.03144
85505	0.00867	0.03144
87095	0.00867	0.03144
94363	0.00523	0.01896
94402	0.00523	0.01896
95849	0.00523	0.01896
99055	0.00523	0.01896
99648	0.00523	0.01896
99651	0.00523	0.01896
100920	0.00523	0.01896
101154	0.00523	0.01896
102928	0.00523	0.01896
105089	0.00523	0.01896
109014	0.04835	0.17432
112048	0.04835	0.17432
112992	0.04835	0.17432
118219	0.04835	0.17432
132132	0.07593	0.27271
136514	0.01462	0.05296
138562	0.09304	0.33336
148287	0.09304	0.33336
199442	0.09415	0.33730
203222	0.04141	0.14947
205423	0.04141	0.14947
210434	0.04754	0.17144
213428	0.01944	0.07037

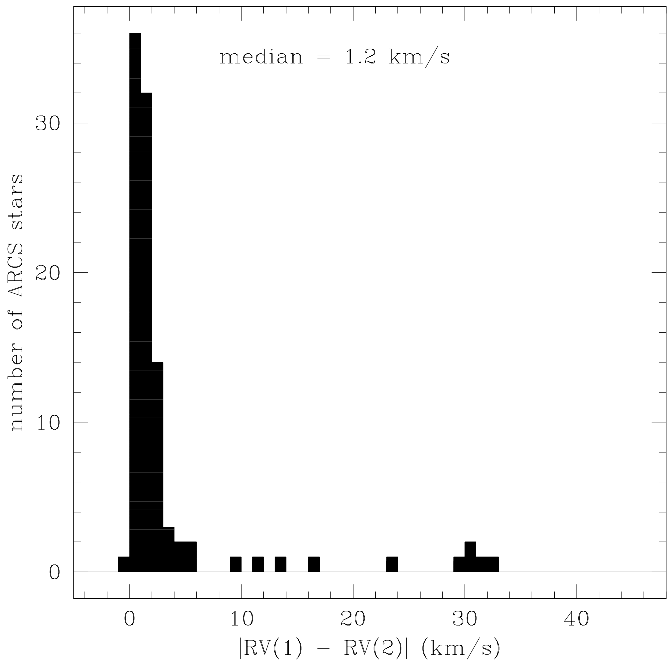

Figure 34: Distribution of the difference in velocity between two observations. The time span between two epochs is minimum 45 days. In the catalog 150 objects with multi epoch velocity measurement are present.

150 observed Red Clump giants, corresponding to an observed frequency of spectroscopic binaries of 0,15%. We are now investigating the properties of these objects, trought more spectroscopic and photometric measurements.

7 ARCS OUTPUT CATALOGUE

Contents

7.1 INTRODUCTION

The ARCS survey at 1.82m telescope resulted in a catalog containing radial velocities and atmospheric parameters for 300 stars, mostly Red Clump stars, located in the $6.8 \leq V_{T}ycho - 2 \leq 8.1$ interval. Data are obtained from Echelle spectra in the 4816 - 5965 Åwavelenght interval, at R=20,000. The adopted techniques are a standard cross-correlation for deriving v_{rad} and a simple χ^2 fitting for atmospheric parameterd. The adopted grid of stellar templates comes from the library of synthetic spectra of Munari et al. (2005).
We obtained accurate radial velocities, $\sigma_{Vrad} \leq 0.5$ Km s^{-1}, and precise atmospheric parameters $\sigma_{T_{eff}} \leq 50$ K, $\sigma_{logg} \leq 0.12$ dex, $\sigma_{M/H} \leq 0.11$ dex.
A grat effort has been done in testing and refining the χ^2 method. This resulted in the quality of the data presented in the catalog and in the consinstancy of our data with other catalogs present in literature.
The full catalog is available online. In Tab. 9 there is the description of the catalog: it contains the photometric data available in literature, in addiction to all the data obaided with ARCS (V_{rad}, T_{eff}, *logg*, distance, U, V, W).
Red Clump stars are of great interest in investigating different properties of the Milky Way and ARCS catalog is providing a large number of high quality data on this type of stars.

7.2 THE CATALOG

Table 15: ARCS CATALOG

ARCS	dist (pc)	err (pc)	Vrad (km/s)	err (km/s)	met (dex)	err (dex)	Teff (K)	err (K)	logg (dex)	err (dex)	U (km/s)	V (km/s)	W (km/s)
6	118.9	5.5	15.9	0.5	0.15	0.20	4743	53	2.57	0.17	1.987	-0.011	-52.224
966	219.1	10.2	-23.0	0.5	0.04	0.21	4882	54	3.31	0.17	21.441	-36.600	12.690
2023	103.5	9.5	15.8	0.9	0.19	0.15	5105	53	2.64	0.23	-30.889	10.587	-13.766
2344	196.2	9.1	0.0	0.5	0.03	0.14	4957	50	3.15	0.19	-18.616	13.122	5.586
2624	242.2	11.3	14.0	0.5	0.15	0.17	4875	49	2.69	0.13	42.448	14.377	1.950
3512	139.0	6.5	-55.0	0.5	0.01	0.18	5108	46	3.47	0.13	-46.704	-1.482	54.493
3819	224.2	10.4	-11.7	0.9	-0.04	0.20	5095	54	3.04	0.23	-28.043	12.833	-27.673
4352	262.8	12.2	-44.2	0.8	0.10	0.15	4989	53	3.07	0.19	97.472	-41.402	23.852
4593	261.2	12.2	3.2	0.3	0.19	0.17	4843	52	3.18	0.18	-112.511	19.027	36.427
4621	237.0	21.9	-29.0	0.5	-0.12	0.14	4636	47	2.47	0.23	12.354	-9.367	0.301
5362	219.0	10.2	-14.0	0.5	0.06	0.15	4931	47	3.22	0.17	-51.012	-33.927	7.910
5544	135.3	6.3	-27.4	0.5	0.15	0.20	4875	47	3.08	0.17	-21.421	3.417	15.364
5720	224.3	10.4	-16.5	0.5	0.01	0.16	5030	47	3.02	0.13	-39.866	-36.973	13.935
5822	192.8	9.0	11.5	0.6	-0.19	0.11	4798	52	2.43	0.19	-21.920	2.885	18.511
7736	116.0	5.4	-1.2	0.5	-0.13	0.14	4834	48	2.58	0.16	-2.797	21.343	0.021
8120	153.8	7.1	1.5	0.5	0.07	0.12	4877	48	2.90	0.12	-9.614	13.299	10.471
8333	218.3	10.2	0.0	0.5	0.10	0.14	5102	45	3.41	0.20	-33.528	15.895	-4.713
8337	111.7	5.2	-27.1	0.5	0.11	0.20	4620	49	2.45	0.18	51.341	-38.489	14.473
8599	167.6	7.8	18.0	0.5	-0.20	0.13	4799	52	2.48	0.22	-20.934	-9.837	26.159
9261	237.9	22.0	-3.8	0.5	-0.06	0.18	4918	53	2.73	0.17	25.262	12.294	0.304
9649	234.4	10.9	22.0	0.5	-0.21	0.12	4329	47	1.82	0.18	-66.212	-83.781	-45.481

Table 16: ARCS CATALOG

ARCS	dist (pc)	err (pc)	Vrad (km/s)	err (km/s)	met (dex)	err (dex)	Teff (K)	err (K)	logg (dex)	err (dex)	U (km/s)	V (km/s)	W (km/s)
9959	248.5	11.6	13.7	0.7	-0.29	0.11	4683	52	2.51	0.20	-16.640	33.114	-15.554
10642	237.4	11.1	18.5	0.7	0.19	0.18	4957	53	3.49	0.15	-4.687	-15.305	-15.039
10955	99.1	4.6	5.4	0.6	0.16	0.15	5067	50	3.11	0.14	-4.770	17.422	-10.754
11037	255.4	12.0	17.7	0.6	-0.18	0.12	4874	52	2.60	0.24	-6.267	21.506	8.695
11455	179.7	8.3	16.9	0.3	-0.48	0.19	4556	51	2.44	0.17	-5.861	14.149	-11.966
12252	242.9	11.3	51.0	0.5	0.17	0.15	4920	49	2.79	0.14	0.733	19.066	-5.286
12254	284.2	13.3	18.6	0.5	0.06	0.11	4643	45	2.58	0.23	40.295	28.471	-23.052
12343	211.8	9.9	15.2	0.6	0.03	0.21	5030	49	3.33	0.22	3.964	12.707	-7.355
12513	100.5	4.7	31.6	0.5	0.01	0.20	5103	48	2.86	0.13	25.375	-1.933	6.031
13468	156.0	7.2	2.9	0.4	0.40	0.21	4924	53	2.85	0.13	-4.679	8.356	-28.242
15005	115.6	5.4	-12.2	0.6	-0.18	0.13	4610	45	2.23	0.21	-34.069	-21.455	-15.371
16467	219.5	10.2	-24.8	0.6	-0.16	0.22	4787	53	2.51	0.19	5.925	2.842	14.411
16672	170.5	7.9	70.8	0.8	-0.08	0.18	4854	49	2.39	0.24	-48.444	29.513	10.023
16708	142.8	6.6	-11.4	0.4	-0.32	0.17	4746	47	2.52	0.15	65.059	2.110	-19.036
17616	243.6	11.3	-20.7	0.6	0.17	0.20	5011	54	2.57	0.20	-36.439	-16.028	38.769
17806	182.1	8.5	19.2	0.7	-0.21	0.13	4623	48	2.45	0.17	28.331	21.606	3.487
18145	157.6	7.3	-44.0	0.5	0.11	0.15	4895	46	2.10	0.23	9.558	23.463	15.622
18175	223.0	10.4	10.9	0.8	0.17	0.16	5080	52	3.25	0.13	-50.685	-20.693	13.206
18682	138.3	6.4	5.9	0.5	-0.26	0.14	4605	52	2.69	0.21	-85.757	-93.275	23.138
18739	166.3	7.7	-33.5	0.5	-0.15	0.17	5016	51	2.98	0.24	48.668	-14.675	16.381
19847	235.2	11.0	-73.0	0.9	-0.18	0.13	5092	49	2.89	0.16	1.412	10.529	-18.368

Table 17: ARCS CATALOG

ARCS	dist (pc)	err (pc)	Vrad (km/s)	err (km/s)	met (dex)	err (dex)	Teff (K)	err (K)	logg (dex)	err (dex)	U (km/s)	V (km/s)	W (km/s)
20792	270.9	12.7	43.2	0.5	0.18	0.18	4963	50	3.33	0.14	71.660	-0.018	4.072
21838	276.1	12.8	24.9	0.9	-0.24	0.14	4755	53	2.46	0.14	-5.955	-8.143	14.516
21887	170.1	7.9	-16.6	0.6	0.03	0.21	4875	53	2.89	0.16	9.642	9.053	5.916
21976	165.1	7.7	-5.3	0.6	0.23	0.13	4466	50	2.62	0.20	28.806	-7.909	1.953
22149	221.6	10.3	-3.2	0.5	0.05	0.14	4705	48	2.91	0.22	-38.752	-11.127	-2.665
22796	247.5	11.5	57.7	0.8	-0.14	0.17	4933	49	1.79	0.19	2.103	23.210	-13.613
22797	181.8	8.4	34.0	0.4	0.13	0.16	4486	51	2.43	0.23	3.443	-22.663	-38.146
22798	163.7	7.6	12.4	0.6	0.04	0.16	4928	50	2.84	0.15	-45.078	-7.939	-0.529
22819	265.6	12.4	-0.8	0.5	-0.08	0.12	4876	48	2.62	0.23	16.406	-4.407	-1.075
22853	177.8	8.2	14.1	0.5	0.10	0.14	4489	50	2.28	0.13	6.582	-1.790	1.440
23223	230.9	21.3	32.3	0.6	-0.04	0.19	4532	47	2.29	0.22	-17.385	-27.534	-34.401
23887	190.5	8.8	9.2	0.6	0.39	0.21	4665	52	2.75	0.18	52.866	-15.872	-17.992
24107	207.6	9.6	-16.0	0.6	0.05	0.11	5043	51	2.94	0.15	14.954	-18.972	-17.894
24120	84.5	3.9	25.0	0.9	-0.25	0.13	4425	50	1.95	0.24	-25.937	-54.897	-35.699
25041	205.6	9.6	43.0	0.3	-0.28	0.14	4692	49	2.48	0.14	-20.527	34.819	-25.940
26606	114.6	5.3	-18.6	0.8	-0.05	0.13	5030	50	2.59	0.21	-9.870	11.653	5.297
26662	109.6	5.1	23.5	0.6	0.02	0.21	4989	54	3.06	0.14	21.180	-1.122	-12.758
27008	185.9	8.6	16.6	0.7	0.20	0.16	4896	54	2.65	0.18	3.531	11.834	12.843
27146	174.1	8.1	26.1	0.3	-0.04	0.15	4836	51	2.52	0.17	13.611	1.164	-23.972
27324	95.9	8.8	66.1	0.5	-0.11	0.20	4842	51	2.38	0.20	-56.423	9.333	12.959
27531	209.6	9.8	39.0	0.5	0.01	0.12	5081	47	2.81	0.15	-19.111	6.095	-4.929

Table 18: ARCS CATALOG

ARCS	dist (pc)	err (pc)	Vrad (km/s)	err (km/s)	met (dex)	err (dex)	Teff (K)	err (K)	logg (dex)	err (dex)	U (km/s)	V (km/s)	W (km/s)
27574	231.6	10.8	28.2	0.6	-0.19	0.18	4867	54	2.53	0.15	27.643	0.800	-7.449
27719	256.4	12.0	9.3	0.6	0.04	0.20	4773	47	2.52	0.14	7.408	-11.027	-7.465
28037	169.8	7.9	7.8	0.8	-0.40	0.17	4563	54	2.29	0.14	9.527	44.146	-31.062
28054	206.7	9.6	0.2	0.5	0.15	0.12	4439	45	2.65	0.19	-12.155	-63.258	51.722
28088	262.4	12.2	38.0	0.5	0.05	0.22	5052	46	3.44	0.24	11.730	-8.658	2.753
28322	247.2	11.5	7.0	0.6	0.06	0.11	4803	54	2.50	0.23	21.872	0.461	4.183
28959	182.1	8.5	36.6	0.6	-0.41	0.12	4123	52	1.35	0.12	10.542	14.751	35.069
29583	241.0	11.2	-42.1	0.3	-0.31	0.17	4148	47	1.75	0.23	-88.589	-90.105	-74.032
29913	249.7	11.6	-0.3	0.5	-0.02	0.16	4772	48	2.56	0.17	-0.138	-21.636	-4.454
29914	198.4	9.2	39.2	0.7	0.03	0.19	4956	54	3.29	0.17	-16.433	11.115	7.419
30057	187.5	8.7	27.1	0.4	0.09	0.12	4857	51	3.43	0.21	15.176	-8.390	2.663
30812	203.1	9.4	27.0	0.2	0.03	0.21	4848	52	2.67	0.17	-33.666	-24.986	2.911
31693	226.2	20.9	-5.5	0.7	0.13	0.14	5039	47	2.92	0.22	1.297	-23.263	1.395
32393	189.9	8.8	24.2	0.4	0.58	0.14	4581	52	2.69	0.18	25.901	-12.564	5.416
35220	110.5	5.1	29.6	0.5	-0.18	0.15	4452	51	1.95	0.19	-31.352	95.025	-67.380
70435	266.6	12.4	-32.8	0.7	-0.32	0.22	3976	53	1.11	0.18	47.059	-27.804	-22.313
71137	230.7	10.8	30.6	0.5	0.10	0.15	5040	53	3.01	0.19	-38.845	-30.326	-21.071
73412	243.8	22.5	-0.2	0.7	0.02	0.15	4951	46	3.35	0.20	7.143	23.662	-24.626
73413	176.7	16.3	-2.0	0.5	-0.11	0.19	5739	47	2.96	0.18	66.487	-11.534	9.535
74444	258.0	12.0	19.5	0.4	0.02	0.18	4851	54	2.69	0.21	2.114	0.418	27.337

Table 19: ARCS CATALOG

ARCS	dist (pc)	err (pc)	Vrad (km/s)	err (km/s)	met (dex)	err (dex)	Teff (K)	err (K)	logg (dex)	err (dex)	U (km/s)	V (km/s)	W (km/s)
75175	242.9	11.3	-6.4	0.5	-0.28	0.14	6054	47	2.99	0.17	-3.870	-17.768	7.200
75193	249.3	11.6	28.0	0.7	-0.23	0.19	5012	49	2.66	0.16	-0.196	4.844	-8.808
76366	193.6	9.0	-1.9	0.5	0.35	0.20	5958	47	2.86	0.12	14.317	5.708	29.424
77236	186.0	8.6	-9.0	0.5	0.18	0.12	5081	50	3.16	0.20	123.824	-123.394	-49.495
77894	223.4	10.4	23.5	0.5	-0.43	0.16	4268	54	1.48	0.18	69.190	4.398	-57.782
78421	96.8	4.5	38.3	0.5	-0.17	0.21	5114	52	2.98	0.23	-27.860	7.045	-13.408
79218	254.7	11.9	-25.3	0.7	0.02	0.15	5022	50	2.96	0.15	-35.248	-4.784	10.507
79567	233.3	10.9	53.9	0.3	0.32	0.17	4549	47	2.62	0.19	-34.270	-72.802	-68.952
80163	187.8	8.7	-2.0	0.5	0.43	0.20	4887	51	3.41	0.19	-39.870	4.447	-5.404
81490	242.2	11.3	26.5	0.5	-0.03	0.22	5038	51	2.81	0.23	5.714	11.575	-0.596
82268	183.1	8.5	-10.0	0.5	0.14	0.12	4969	50	3.41	0.17	14.246	11.030	35.833
82333	235.2	11.0	64.0	0.4	0.17	0.19	5130	51	2.54	0.14	16.372	5.564	0.519
82888	150.9	13.9	37.9	0.3	0.04	0.20	4844	49	2.78	0.18	1.916	33.628	2.406
82957	266.1	12.4	23.4	0.4	0.10	0.13	4807	52	2.67	0.18	-1.947	5.260	-7.579
82958	194.2	9.0	1.6	0.5	0.06	0.16	4958	54	3.36	0.21	-21.509	-3.917	-30.351
83024	164.4	7.6	44.6	0.7	0.11	0.11	4870	47	3.29	0.24	72.914	11.371	-50.823
83046	157.6	7.3	27.4	0.9	0.02	0.17	4939	49	2.90	0.19	-20.032	-15.678	1.832
83161	207.9	9.7	0.8	0.6	-0.19	0.17	4815	53	2.52	0.18	-14.712	3.323	13.010
83453	182.1	8.5	17.2	0.8	-0.14	0.15	4830	46	2.52	0.15	9.494	17.393	-6.536
83536	165.4	15.3	0.0	0.5	-0.09	0.16	4730	46	2.46	0.17	-65.281	-65.741	32.886
83581	237.2	11.1	12.0	0.9	-0.26	0.15	4805	47	2.39	0.13	5.283	-4.552	11.798

Table 20: ARCS CATALOG

ARCS	dist (pc)	err (pc)	Vrad (km/s)	err (km/s)	met (dex)	err (dex)	Teff (K)	err (K)	logg (dex)	err (dex)	U (km/s)	V (km/s)	W (km/s)
83618	233.2	10.9	-18.1	0.4	-0.12	0.15	4241	53	1.70	0.15	-48.462	-36.309	22.550
84050	216.0	10.0	25.4	0.7	0.17	0.14	4950	54	3.42	0.16	5.065	21.052	9.206
84563	228.5	10.6	3.6	0.3	-0.40	0.13	4722	52	2.49	0.20	14.924	16.377	8.726
85180	152.1	7.0	25.9	0.9	0.02	0.21	4846	46	3.34	0.20	-0.185	1.218	-12.880
85219	254.9	11.9	14.7	0.5	0.02	0.12	4964	52	2.57	0.21	19.262	-10.512	11.805
85379	227.9	10.6	54.6	0.6	0.51	0.17	4628	50	3.24	0.16	-111.107	-42.997	9.891
85505	253.3	11.8	-11.6	0.6	0.67	0.20	5145	51	2.86	0.21	2.715	-13.292	3.347
85990	196.5	9.1	1.4	0.2	0.01	0.14	5138	45	3	0.17	-73.659	-44.201	-10.249
86342	176.8	8.2	-13.8	0.7	-0.16	0.19	4820	54	2.87	0.21	-55.213	18.646	-18.911
87095	249.0	11.6	5.7	0.4	0.04	0.15	4717	50	2.78	0.20	-34.355	-49.343	2.178
87502	235.9	11.0	10.0	0.5	-0.22	0.20	4281	45	2	0.21	53.816	-11.461	54.709
87975	166.0	7.7	6.9	0.5	-0.09	0.14	4784	45	2.61	0.21	3.049	2.979	11.512
88083	227.7	10.6	-3.5	0.5	0.06	0.15	4629	50	2.52	0.22	-45.097	17.067	6.152
89114	212.6	9.9	45.9	0.5	0.16	0.16	4667	54	2.73	0.18	38.108	-15.877	-50.375
89776	189.5	8.8	20.1	0.5	-0.07	0.15	4356	54	1.74	0.16	61.770	-19.718	12.014
90080	37.9	3.5	24.1	0.5	0.01	0.21	4732	54	2.76	0.22	32.300	-27.169	32.770
90594	154.1	7.1	1.6	0.5	0.01	0.18	4726	47	2.45	0.21	-0.690	-19.135	49.333
90969	172.9	8.0	-1.6	0.6	0.05	0.13	4969	53	2.83	0.21	20.327	17.773	9.854
91412	237.1	11.0	29.7	0.6	0.04	0.17	4703	52	2.41	0.13	-110.623	-125.761	46.970
92706	186.8	17.2	-2.0	0.5	0.03	0.14	4901	51	3.02	0.23	17.451	-0.618	12.132

Table 21: ARCS CATALOG

ARCS	dist (pc)	err (pc)	Vrad (km/s)	err (km/s)	met (dex)	err (dex)	Teff (K)	err (K)	logg (dex)	err (dex)	U (km/s)	V (km/s)	W (km/s)
93719	120.6	5.6	24.7	0.7	0.17	0.17	4902	47	3.33	0.21	25.072	-6.228	9.546
94058	258.0	12.0	1.1	0.5	0.05	0.12	4969	48	2.83	0.14	-6.168	16.288	-7.275
94279	232.1	21.4	-38.4	0.8	-0.06	0.19	4683	49	2.47	0.18	-5.755	-17.769	-9.375
94363	143.6	6.7	-4.8	0.5	-0.16	0.17	5037	54	3.26	0.14	35.988	-58.681	-31.410
94402	213.7	10.0	68.1	0.4	0.12	0.22	4930	53	2.16	0.13	26.598	-3.391	6.062
94738	238.8	11.1	13.1	0.5	0.18	0.17	4964	51	2.54	0.12	-10.346	27.208	-16.422
95740	249.5	11.7	-16.3	0.5	0.11	0.21	4941	54	3.09	0.13	11.844	1.282	-5.561
95849	222.6	10.3	-5.3	0.1	0.36	0.18	4947	47	2.19	0.21	13.868	8.267	-10.826
96694	204.1	9.5	44.9	0.2	0.17	0.22	5067	53	3.22	0.14	-11.661	-3.849	20.282
96720	182.4	8.5	55.6	0.4	0.04	0.20	4732	48	2.44	0.14	5.528	-25.967	12.025
97197	206.3	9.6	52.5	0.5	0.19	0.16	4693	48	2.76	0.22	45.933	-19.970	13.875
97443	248.2	22.9	6.0	0.5	-0.09	0.18	4295	50	1.79	0.19	30.422	2.597	-12.893
98399	209.1	9.7	19.0	0.8	0.08	0.13	4947	53	2.64	0.17	39.510	-15.286	-5.643
99055	216.5	10.1	19.8	0.8	-0.15	0.11	5026	48	1.92	0.15	-4.709	15.108	-2.951
99648	175.5	8.1	-12.8	0.6	-0.06	0.14	4939	54	1.99	0.14	-16.294	16.236	-0.334
99651	258.8	12.0	7.8	0.6	0.19	0.20	4862	48	2.75	0.12	7.859	11.165	-6.424
99873	120.5	5.6	23.5	0.4	0.05	0.18	5045	51	3.07	0.21	26.558	13.761	-12.303
10082	88.6	4.1	15.3	0.5	22	-0.40	0.15	4943	46	2.37	0.16	0.859	-35.160
-6.148													
10090	135.5	12.5	-27.6	0.5	20	-0.31	0.20	4852	45	2.93	0.17	-4.600	18.812
12.511													
100975	178.6	8.3	-0.1	0.3	-0.13	0.12	4514	52	2.09	0.21	-0.181	-1.632	21.487
101154	97.0	8.9	-8.3	0.5	0.14	0.21	4626	48	2.71	0.15	13.480	17.938	-7.304

Table 22: ARCS CATALOG

ARCS	dist (pc)	err (pc)	Vrad (km/s)	err (km/s)	met (dex)	err (dex)	Teff (K)	err (K)	logg (dex)	err (dex)	U (km/s)	V (km/s)	W (km/s)
102096	139.9	6.5	19.7	0.4	0.08	0.11	4971	49	2.17	0.17	-27.996	-73.729	-47.995
102274	225.1	10.5	28.8	0.5	0.18	0.22	4952	54	2.90	0.22	52.642	-28.429	4.663
102928	204.4	9.5	31.0	0.4	-0.26	0.13	4712	51	2.35	0.15	-9.564	5.159	16.846
104677	236.8	11.0	-6.0	0.9	0.05	0.16	4499	49	2.69	0.18	6.698	-82.321	-10.463
105089	194.4	9.0	9.9	0.5	0.05	0.14	4909	53	2.95	0.18	-1.254	-13.041	12.110
105900	78.1	3.6	-10.2	0.5	-0.54	0.21	4586	54	2.19	0.14	-43.108	-19.560	-14.888
105911	70.1	3.2	-9.1	0.5	-0.22	0.19	4418	50	1.91	0.24	109.412	11.732	-0.149
105911	116.6	5.4	-9.6	0.5	-0.22	0.12	4418	48	1.91	0.14	23.096	18.032	-6.290
106498	160.4	14.8	-15.0	0.5	0.03	0.17	4799	46	2.66	0.16	24.812	-12.543	10.632
106775	197.3	9.2	12.5	0.5	0.26	0.13	4921	49	2.93	0.15	-6.043	-1.684	-7.075
107036	47.4	2.2	1.0	0.5	0.27	0.20	4908	52	2.91	0.13	-3.410	4.168	-2.860
109014	231.6	10.8	19.8	0.5	-0.26	0.22	4838	47	1.95	0.15	76.691	20.773	36.739
112048	118.3	5.5	-15.0	0.5	-0.02	0.18	4713	48	2.95	0.23	-39.197	-28.975	20.158
112281	216.6	20.0	18.9	0.3	0.12	0.19	5017	48	3.38	0.22	11.416	3.868	-7.894
112992	87.1	4.0	14.8	0.7	0.16	0.19	5109	48	3.48	0.16	3.035	15.140	39.510
113564	205.4	9.6	33.9	0.7	-0.34	0.19	4190	46	1.21	0.16	-11.845	14.420	-28.108
113595	128.3	5.9	16.6	0.5	0.04	0.13	4965	52	3.44	0.23	19.884	-74.562	-68.802
114222	145.6	6.7	1.4	0.5	0.06	0.18	4935	49	2.64	0.24	21.726	-1.993	10.161
116817	218.5	10.1	-17.6	0.6	0.07	0.15	4922	45	3.48	0.16	-20.490	-1.045	27.266
118219	205.0	9.5	10.8	0.4	-0.56	0.14	4713	46	1.97	0.19	4.999	44.366	17.998
119373	264.1	12.3	-5.7	0.4	0.04	0.18	4762	53	2.24	0.23	62.732	-36.109	7.999

Table 23: ARCS CATALOG

ARCS	dist (pc)	err (pc)	Vrad (km/s)	err (km/s)	met (dex)	err (dex)	Teff (K)	err (K)	logg (dex)	err (dex)	U (km/s)	V (km/s)	W (km/s)
119461	256.4	11.9	-5.4	0.2	0.14	0.14	4916	50	3.20	0.15	-0.455	-18.705	6.157
120967	123.5	5.7	2.2	0.5	0.09	0.16	4733	47	2.26	0.23	32.311	11.851	-1.665
123509	126.8	5.9	37.7	0.8	0.15	0.15	4433	53	2.29	0.17	-35.973	-14.398	23.612
128200	148.6	6.9	-15.6	0.2	0.02	0.21	4909	54	3.19	0.19	23.252	-3.052	33.290
129887	106.0	4.9	-8.8	0.4	-0.01	0.20	4853	45	2.76	0.18	-18.998	10.443	8.342
131455	179.9	8.4	-31.0	0.2	-0.09	0.16	4701	45	2.63	0.16	-10.342	235	19.820
132132	170.1	7.9	-46.0	0.6	0.06	0.18	5065	47	2.86	0.20	-40.834	19.545	6.590
136380	169.4	7.9	26.3	0.5	-0.20	0.11	4802	52	2.37	0.18	-43.886	24.707	18.442
136514	90.5	4.2	-8.2	0.5	0.19	0.15	4501	46	2.63	0.22	-26.132	-26.755	4.856
138562	244.0	11.4	-17.7	0.4	0.15	0.19	4770	53	2.78	0.22	-21.974	-3.987	11.174
139308	163.7	15.1	4.7	0.5	0.15	0.22	4871	47	3.17	0.19	18.673	0.210	3.159
140489	268.7	12.5	-26.2	0.6	0.04	0.16	5058	50	2.74	0.16	-5.903	6.889	-6.603
143857	262.7	12.2	33.0	0.4	-0.02	0.14	4377	47	1.72	0.21	-22.342	-40.307	-57.804
143857	206.5	9.6	2.0	0.5	-0.02	0.22	4377	48	1.72	0.18	5.139	-2.606	-20.747
148287	251.3	11.7	7.0	0.2	0	0.12	5047	53	2.98	0.13	-42.697	19.019	121
148684	262.3	12.3	-16.4	0.5	0.18	0.12	4952	54	2.59	0.23	-1.117	-22.664	-15.327
150066	82.8	3.8	20.1	0.5	0.12	0.12	4692	50	2.45	0.23	42.435	-29.260	-4.722
152484	137.3	6.4	33.1	0.6	0.13	0.22	4977	47	3.14	0.21	-97.564	-56.620	-37.498
196346	78.4	3.6	9.1	0.5	-0.16	0.17	4418	53	1.83	0.20	33.489	-19.649	8.932
196346	82.1	3.8	-16.1	0.5	-0.16	0.13	4418	50	1.83	0.19	55.170	2.627	-48.799
197421	225.7	20.8	-24.7	0.5	-0.21	0.20	4494	51	1.96	0.22	27.988	31.806	-128.878

Table 24: ARCS CATALOG

ARCS	dist (pc)	err (pc)	Vrad (km/s)	err (km/s)	met (dex)	err (dex)	Teff (K)	err (K)	logg (dex)	err (dex)	U (km/s)	V (km/s)	W (km/s)
197491	177.3	8.2	-12.0	0.5	-0.21	0.14	4494	45	1.96	0.14	-38.666	38.017	-21.602
199442	156.7	14.4	-28.0	0.4	0.25	0.13	4527	47	2.41	0.24	-20.479	-10.483	-10.941
203222	116.7	5.4	4.0	0.5	-0.02	0.18	5073	51	2.96	0.23	-9.686	16.282	13.190
205423	264.1	12.3	-27.0	1.1	0.63	0.11	4767	47	2.56	0.21	-12.450	9.595	10.383
206660	265.7	12.4	-58.7	0.7	-0.30	0.16	4270	46	1.39	0.22	89.365	-10.932	-89.954
207435	214.7	10.0	45.0	0.5	0.02	0.20	4988	50	3.08	0.20	-48.274	-7.099	17.594
207653	192.8	17.8	-25.4	0.5	0.18	0.18	5035	51	2.53	0.16	23.418	-42.528	-1.570
207920	167.6	7.8	48.1	0.5	0.19	0.18	5110	53	3.02	0.13	4.062	22.113	-3.038
208671	102.6	9.5	-25.0	0.6	0.04	0.19	4923	53	2.77	0.19	2.790	17.638	14.483
209321	106.4	4.9	-0.6	0.7	0.10	0.13	4868	52	3.06	0.23	31.304	-1.013	16.111
210185	90.6	8.3	-1.8	0.5	-0.40	0.20	4414	51	1.73	0.15	-10.260	-44.792	-36.758
210434	166.3	7.7	0.0	0.8	0.03	0.21	5079	54	3.06	0.16	28.135	-3.180	-0.435
212474	139.8	6.5	0.3	0.5	0.19	0.11	5013	53	3.20	0.13	86.265	-4.264	-3.840

Table 25: ARCS CATALOG

ARCS	dist (pc)	err (pc)	Vrad (km/s)	err (km/s)	met (dex)	err (dex)	Teff (K)	err (K)	logg (dex)	err (dex)	U (km/s)	V (km/s)	W (km/s)
212927	212.7	9.9	-44.4	0.9	-0.27	0.16	4828	48	2.64	0.23	179	-13.412	-0.945
215749	139.7	6.5	6.9	0.5	0.03	0.18	4897	47	2.87	0.16	-17.769	14.278	-12.581
216401	254.9	11.9	-5.7	0.8	0.18	0.20	5130	53	2.97	0.24	20.803	1.471	6.627
216540	230.2	21.3	-30.0	0.8	0.10	0.12	4822	48	2.58	0.13	-17.358	16.627	-12.203
217428	232.5	10.8	-7.6	0.7	0.04	0.13	5139	53	2.71	0.15	12.018	20.475	-16.548
217591	107.4	5.0	-18.1	0.5	-0.24	0.21	4966	49	3.12	0.22	-1.934	-310	-11.491
217187	160.3	7.4	-32.0	0.5	-0.22	0.18	4931	47	2.58	0.20	0.143	24.203	-1.449
220858	258.8	12.1	-16.7	0.2	-0.15	0.21	4866	45	2.54	0.23	5.960	-14.821	-4.092
220859	202.3	9.4	18.6	0.5	0.06	0.13	4958	52	3.36	0.16	99.129	-152.550	-42.055
221296	256.1	11.9	-12.3	0.5	-0.59	0.19	4284	51	1.46	0.13	-102.127	-21.685	-1.878
222455	228.8	10.6	13.1	0.4	0.05	0.17	4519	48	2.74	0.22	-82.593	269	20.771
223252	244.9	11.4	-9.8	0.6	0.07	0.18	5063	52	2.88	0.20	24.290	5.819	-15.177
223336	117.0	5.4	-7.6	0.6	0.02	0.16	4939	48	2.90	0.15	-4.325	26.274	4.066
224776	238.7	11.1	-53.4	0.9	-0.36	0.18	4362	50	2.33	0.18	13.985	25.279	3.561
222754	264.4	12.3	0.8	0.3	-0.23	0.20	4868	54	2.61	0.14	-15.602	23.142	-19.099
222936	193.6	17.9	-3.0	0.3	-0.17	0.12	5027	50	2.82	0.12	16.209	0.437	3.584
223870	267.8	12.5	28.2	0.4	-0.21	0.11	4835	54	2.59	0.14	-35.014	25.123	-19.040

8

APPLICATIONS OF ARCS RESULTS ON GALACTIC STRUCTURE AND KINEMATICS

Contents

8.1 INTRODUCTION

ARCS high resolution catalog might help us in the understanding of the kinematics and structrure of the Solar Neighborhood.
Red Clump stars (hereafter RC stars) are excellent tracers of Galactic disc kinematics. Their abundance in the solar neighbourhood, brightness and the nearly constant luminosity make RC stars an useful tool for investigating the three-dimensional kinematics and properties of various Galactic subsystems.
S

8.2 THE MILKY WAY DISK

The Milky Way is a late-type spiral galaxy, as suggested by stellar concentrations, gas and dust. It contains a complex mix of stars, planets, interstellar gas, dust, radiation and dark matter. The Sun is at 7.62 $\pm$ 0.32 kpc from the Galactic center ([**?**]).
The Galaxy can be divided in three main components:

- the central Bulge containing a bar; it extends out to $\sim$3 kpc ([**?**]);
- the nearly spherical Halo, that extends from with the bulge out to $\sim$ 100$kpsandthatisstuddedwithglobularclustersandmainlycomposedbydar$ 15 kpc and that defines the Galactic plane; it is patterned into spiral arms and it is usually decomposed by two components, the Thin and the Thick disks.

The total baryonic mass of the Galaxy is supposed to be $\sim 10^{11}$ $M_{\odot}$. Most of the baryonic mass is in the Galactic disk and in the bulge. A massive black hole (SgrA) is located at the centre of the Galaxy and, adopting the distance of [**?**], it has a mass of $\sim$(3.5$\pm$0.3)$\times$ $M_{\odot}$ ([**?**]).
The dark matter halo is the most massive component of the Galaxy, its mass is thought to be 1-3 $\times$ 10^{12} $M_{\odot}$ ([**?**], [**?**], [**?**]). ([**?**])
Properties of the Galaxy components are summarized in Tab. 26 and Tab. 27.
Since the ARCS survey is a local survey on RC stars located at 50$<$ d $<$ 400 pc and 40$<$z $<$ 300 pc, we may assume that our investigation as limited to the disk.
The disk is the most massive stellar component of the Galaxy, its mass is estimated to be $\sim 5\times 10^{10}$ $M_{\odot}$ and most of the current star formation have place in it. The understanding of the disk formation is one of the challenges of the galaxy formation theory.
The Milky Way disk is composed by a thick disk and a thin disk.

8.3 MOVING GROUPS

Disk kinematics can be examined in detail with a typical analysis of the distribution of stars in the UVW space. This allows to determine its parameters (e.g. U, V and W dispersions) and it permits the study of a variety of different local irregularities. Some of these irregularities come out as concentrations of stars in the U-V velocity space: the moving groups or stellar streams.
Eggen (1996) was the first who determined the spatial and kinematical properties of several stellar streams, and he focused on the

Table 26: Properties of the major components of the Milky Way, from [?].

	Age (Gyr)	[Fe/H] (dex)	$\frac{dFe/H}{dR}$ (dex/kpc)	IMF	SFR
	0–0.15	0.01 ± 0.12			
	0.15–1	0.03 ± 0.12			
	1–2	0.03 ± 0.10		$\frac{dn}{dm} \alpha\ m^{-\alpha}$	
Disk	2–3	0.01 ± 0.11	-0.07	α 1.6 per $m < 1M_\odot$	constant
	3–5	-0.07 ± 0.18		α 3.0 per $m > 1M_\odot$	
	5–7	-0.14 ± 0.17			
	7–10	-0.37 ± 0.20			
Thick disc	11	-0.78 ± 0.30	0.00	$\frac{dn}{dm}\alpha\ m^{-0.5}$	one burst
Stellar halo	14	-1.78 ± 0.50	0.00	$\frac{dn}{dm}\alpha\ m^{-0.5}$	one burst
Bulge	10	0.00 ± 0.40	0.00	$\frac{dn}{dm}\alpha\ m^{-2.35}$ per $m > 0.37M_\odot$	one burst

hypothesis that moving groups are the results of the dispersion of stellar cluster (since these structures share their kinematics with certain open clusters). The advent of Hipparcos (Perryman et al., 2007) astrometric data contributed to better identify these moving groups (Chereul, 1998; Asiain et al. 1999) and it contributed to introduce a new dynamical hypothesis on the origin of some of these moving groups. Using an adaptive kernel and wavelet transform analisys, Skuljan et al. (1999) studied a sample of 4000 Hipparcos stars and found that the the distribution function of in the U-V plane is characterized by a few branches that are diagonal, parallel and roughly equidistant. Skuljan et al. (1999) related the origin of these branches to the Galactic spiral structure, or to some other global characteristics of the Galactic potential. Later Famaey (2005) used a Bayesian approach to divide a sample of giant stars into several kinematic groups. Antoja (2008) deeply investigated the structures in the UV-plane builded with more than 24 000 stars, taken from different catalogs . Nowadays the dynamic or "resonant" mechanism appears to be the most plausible explanation for most of the moving groups.
The first theoretical arguments in favour of different dynamical origin of moving groups were proposed by Mayor (1972) and Kalnajs (1991): these moving groups can be also associated with dynamical resonances related to the Galactic bar or spiral arms. The Hercules group,for example, is believed to be associated with the local resonant kinematic disturbances by the inner bar. Bensby et al. (2007) showed that the chemical properties of the Hercules group cannot be distinguished from those of the field stars at similar [Fe/H], confirming that this group is probably just a dynamical group. Other moving groups are instead debris of star forming aggregates in the disk, as the HR1614 group. De Silva (2007) measured very precise abundances for many chemical elements in HR1614 group and found no significant spread: this suggests that stars in HD1614 group are probably coming from a dispersed relic of an old star forming event. Some moving groups may also be debris of infalling objects, as predicted in ΛCDM simulations (Abadi et al. 2003). The Arcturus group could be an example (Navarro et al. 2004): to test this Williams et al. (2008) investigated the kinematics and detailed chemical abundances for many stars of the Arcturus group. They didn't find a clear chemical homogeneity, leaving, for the moment, unsolved the origin of the group.

8.4 THIN DISK

In this work we use ARCS data also to focus on some properties of the thin disk, such as metallicity distribution, vertical metallicity gradient, age-metallicity gradient (AMR) and age-velocity relation. A big amount of studies have been done, using different tracers and, as result, showing a certain disagreement. Open clusters, planetary nebulae, field dwarf and clump giants have been used. Significant progress in the study of the MW disk needs an increment of data available. A major contribution to the subject come from the recents surveys as the RAVE survey (Steinmetz, 2003) and the Geneva-Copenhagen survey of the Solar Neighborhood (Nordstrom et al., 2004). RAVE aims to provide radial velocities, atmospheric parameters and abundance ratios of 500,000 stars, the Geneva-Copenhagen survey include stellar parameters and radial velocities for 16,682 F and G dwarf stars (but they derived a less reliable metallicity from Stromgren photometry). Another contribution comes from the work of Soubiran et al. (2008): they provides parameters of 891 clump giants and they investigated disk properties as AMR and AVR. ARCS paper I catalog contains accurate radial velocities and atmospheric parameters of 300 Red Clump stars. (I HAVE TO WRITE IT BETTER)

8.5 ARCS SPACE VELOCITIES AND ORBITS

8.5.1 *Distances and space velocities*

In PaperI we transformed radial velocities, Tycho proper motions and photometric distances into the corresponding galactocentric velocities U, V, W. The conversion of the space velocity to the usual (U, V, W) system was carried out with the help of the formula described in Johnson and Soderblom (1987). We used a left-handed system with U positive outward the Galactic Center. We corrected for the solar motion, adopting ($U_\odot$,$V_\odot$,$W_\odot$)=(-10.0,5.25,7.17) km s^{-1} (Denhen & Binney, 1998) to the local standard of rest.
By using a Monte Carlo simulation we calculated the errors on U,V and W velocities. The higher contribution to the errors is given by distances, reaching an error of 8 km s^{-1}. Errors on Tycho-2 proper motion contributes of $\sim$ 1 kms^{-1} and radial velocities of $\sim$ 1.8 kms^{-1}. Fig.1 and Fig. 2 displays U,V,W distributions of ARCS objects.

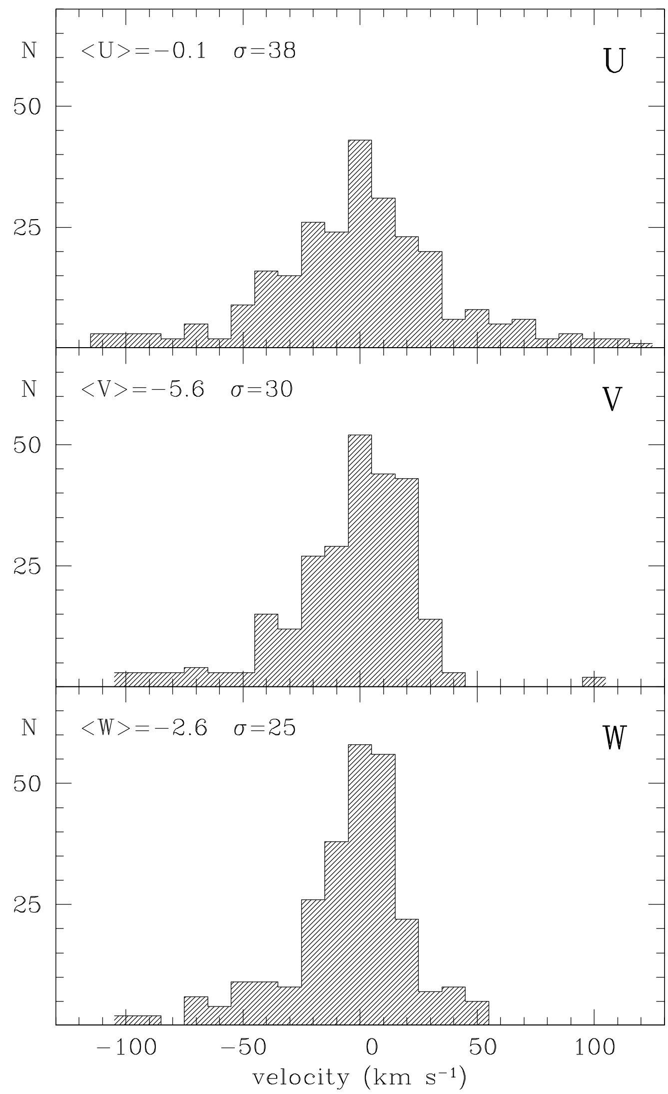

Figure 35: Distribution of the U,V,W velocities of ARCS objects. From top to bottom: U, V and W velocities with respect to the Sun.

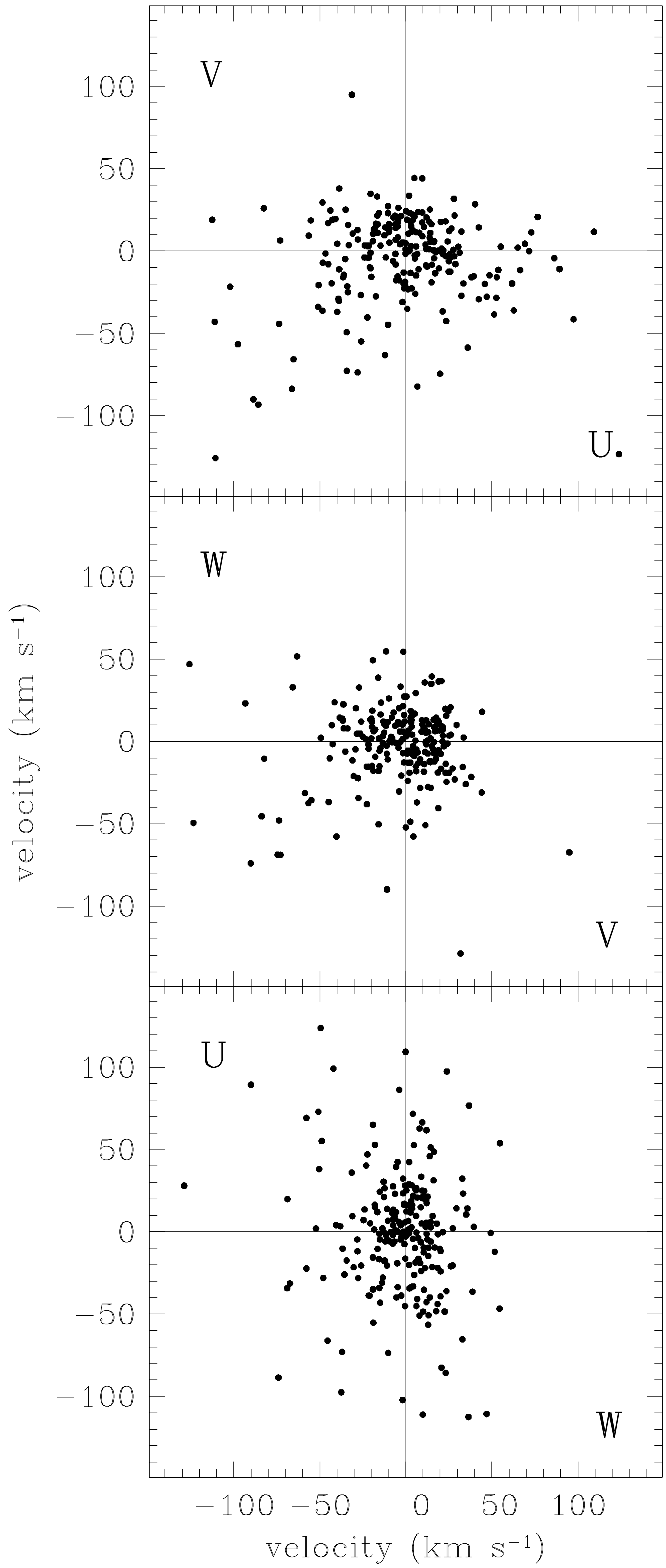

Figure 36: Distribution in the U,V,W velocity space of ARCS objects. From top to bottom: U-V space, V-W space and W-U space with respect to the Sun.

8.5.2 *Galactic model of mass distribution and orbits integration*

For integrating the equation of motion we adopted the model for the Galactic gravitational potential and the corresponding mass distribution of Allen & Santillán (1991), adopting a default value of 2 Gyr as integration time.
In the adopted model the mass distribution of the Galaxy is described as a three component system: a spherical central bulge, a flattened disk described in the Miyamoto-Nagai form and a massive spherical halo. The gravitational potential is fully analytical, continuous everywhere and has continuous derivatives, in order to make the integration faster but with an high numerical precision. The expressions for the potential of the three components are:

$$\phi_B r, z \quad \frac{GM_B}{\sqrt{r^2 \;\; z^2 \;\; b_B^2}} \tag{8.1}$$

$$\phi_D r, z \quad \frac{GM_D}{\sqrt{r^2 \;\; (a_D \;\; \sqrt{z^2 \;\; b_D^2})^2}} \tag{8.2}$$

$$\phi_H r, z \quad \frac{GM_H}{\rho} \cdot \frac{\left(\frac{\rho}{a_H}\right)^{2.02}}{1 \;\; \left(\frac{\rho}{a_H}\right)^{1.02}} - \frac{M_H}{1.02 \cdot a_H}\left[-\frac{1.02}{1 \;\; \left(\frac{\rho}{a_H}\right)^{1.02}} \;\; ln\left(1 \;\; \left(\frac{\rho}{a_H}\right)^{1.02}\right)\right]_R^{100} \tag{8.3}$$ 3

Where $\rho \quad \sqrt{r^2 \;\; z^2}$, G is the constant of gravity, M_B, M_D, M_H, b_B, a_D, b_D and a_H are the masses and scale lenghts for the Bulge, Disk and Halo respectively.Their values are listed in Table 28. The total mass of this model is 9×10^{11} $M_\odot$, and the halo is truncated at 100 kpc. The adopted velocity of the Sun with respect to the LSR is (−10.0,5.25,7.17) km s^{-1} (Denhen & Binney, 1998), the solar galactocentric distance $R_\odot$=8.5 kpc and circular velocity V_{LSR}=220 km s^{-1}. Results are labeled in Table 29.

8.6 ARCS AGES

Ages of ARCS targets have been computed with the code PARAM, developed by L. Girardi, available via interactive web form. The consists in a Bayesian estimation method which uses theoretical isochrones computed by Giradi et al. (2000) taking into account mass loss along red giant branch. Starting from observed T_{eff}, absolute magnitudes, metallicities and related errors, the code estimates the probability that such a star belongs to each small section of a theoretical stellar isochrone of a given age and metallicity. Then, the probabilities are summed over the complete isochrone, and hence over all possible isochrones, by assuming a Gaussian probability of having the observed metallicity and its error, and a constant probability of having stars of all ages. The latter assumption is equivalent to assuming a constant star formation rate in the solar neighbourhood. In this way, at the end, we have the age probability distribution function (PDF) of each observed star. PDFs can also be obtained for any stellar property, such as initial mass, surface gravity, intrinsic colour, etc[1].

Although a full discussion of the PDF method is beyond the scope of this thesis, we note the following. The method, with just some small differences, has already been tested on both main sequence stars (Nordstrom,2004) and on giants and subgiants (da Silva, 2006). Ages of dwarfs turn out to be largely undetermined by this method, due to their very slow evolution while on the main sequence. Ages of giants turn out to be well determined provided that the effective temperature and the parallax (absolute magnitude) are measured with enough accuracy. In fact, da Silva et a. (2006) find that stars with errors of 70 K in T_{eff}, and less than 10% errors in parallaxes, have ages determined with an accuracy of about 20%. These errors become larger on the red clump region, where stars of very different age and metallicity become tightly clumped together, and where in addition there is a superposition of red clump stars and first-ascent RGB ones. Stars of very different age and metallicity become tightly clumped together. In this case PDF of ages can be asymmetric or double peacked. As a conseguences ages are accurate for only a part of our ARCS objects (150 objects), and we used the computed ages only for a statistical investigation.

This method was initially developed by Jørgenson & Lindegren (2005) and slightly modified as described in da Silva et al. (2006). As explained in Biazzo et al. (2007), ages of giants turn out to be well determined when effective temperature and the parallax (absolute magnitude) are measured with enough accuracy. In fact, stars with errors of 70 K in T_{eff}, and less than 10% errors in parallaxes, have ages determined with an accuracy of about 20%.

1 A Web version of this method is available at the URL http://stev.oapd.inaf.it/~lgirardi/cgi-bin/param.

Ages are labeled Table 40.

8.6.1 *Comparison of ARCS gravities with PARAM gravities*

8.7 AGE DISTRIBUTION OF ARCS OBJECTS

The age distribution of ARCS objects seems bimodal, with two prominent peaks at ≈1 Gyr and ≈6 Gyr. Taking into accout that the age estimation of Red Clump stars is not easy, we may compare this result with the literature about star formation in the local disk. The star formation history of the solar neighborhood have been investigated using different objects as white dwarfs (Salaris et al, 2008), M-dwarfs (Juric et al., 2008) and data from different surveys as RAVE (Steinmetz et al. 2006) and Geneva-Copenhagen (Nordstrom, 2005). Tracing the Star Formation Rate (SFR) of the local disk is a challenge due to the large number of factors involved (as radial migration, merging, passage of spiral arms, and so on). Most of the works agree in two major peaks at ≈2 Gyr and ≈6 Gyr ago overimposed on an undelying slow variation (Fuchs et al., 2009; Rocha Pinto et al. (2000); Noh & Scalo, 1990; Soderblom et al., 1991).

The peak at ≈1 Gyr is also present in the Geneva-Copenhagen survey (N'ordstom et al., 2008) on F-K dwarfs, in wich they computed ages by adopting a complex statistical analysis with isochrones, and in Soubiran (2008) sample of red clump stars, in which they computed ages using the same PARAM tool as ARCS . The peack at 1Gyr is also present in the theoretical work of Girardi (2000): he models the age distribution of RC stars of Solar Neighborhood by assuming a constant SFR. It comes out that the distribution of clump stars peaks at 1 Gyr and the decreases monotonically, as result of the continous decrease of the birth rate of post-main sequence stars with age.

The peak we found at at ≈6 Gyr is composed by stars with a large error on age ($(\sigma_{Age}/Age \geq 25\%)$) but is present also in the independent saple of RC stars of (Soubiran et al., 2008).

8.7.1 *Age-Velocity relation - don't know if feasible*

There is a lack of energy at 2-5 Gyr? If we reject the 2 stars with higher energy at age ∼5 and ∼6 the lack of energy is not so evident (see Fig. 3b and Fig. 3c).

Table 45: PARAM ages for 144 ARCS stars.

ARCS	T_{eff}	σ_{Teff}	*logg*	σ_{logg}	[M/H]	$\sigma_{M/H}$	V	σ_V	π	σ_π	Age	σ_{Age}	Mass	σ_{Mass}	*logg*	σ_{logg}	R	σ_R
	K	K	dex	dex	dex	dex	mag	mag	mas	mas	Gyr	Gyr	$M_\odot$	$M_\odot$	dex	dex	$R_\odot$	$R_\odot$
94363	5037	56	3.26	0.11	-0.16	0.16	6.220	0.009	8.30	0.39	[illegible]	1.6	1.12	0.39	2.51	0.17	9.4	0.5
94402	4930	57	2.16	0.10	-0.12	0.16	5.556	0.009	11.29	0.52	[illegible]	0.6	1.40	0.49	2.57	0.17	9.3	0.5
95740	4941	50	3.02	0.13	-0.11	0.09	7.296	0.011	5.60	0.26	[illegible]	0.2	1.83	0.44	2.79	0.14	8.7	0.6
95849	4947	53	2.19	0.09	0.36	0.09	6.065	0.010	10.31	0.95	1.0	0.2	2.07	0.14	2.83	0.06	8.8	0.6
96720	4732	56	2.44	0.08	-0.04	0.14	7.806	0.013	4.44	0.21	4.4	3.1	1.08	0.20	2.43	0.09	10.1	0.5
97197	4693	45	2.76	0.10	-0.19	0.16	7.601	0.012	4.89	0.23	4.1	2.4	1.11	0.23	2.42	0.09	10.4	0.4
97443	4295	51	1.79	0.11	-0.29	0.09	7.936	0.013	1.10	0.01	0.3	0.1	2.20	0.32	1.31	0.09	52.3	2.5
100822	4943	58	2.37	0.14	-0.40	0.17	7.294	0.011	5.07	0.24	4.9	3.8	1.02	0.19	2.45	0.09	9.7	0.5
100920	4852	43	2.93	0.09	-0.31	0.13	4.414	0.009	21.10	0.98	5.6	3.6	1.05	0.14	2.50	0.08	9.2	0.5
100975	4514	44	2.09	0.10	-0.13	0.09	7.873	0.013	4.32	0.20	6.9	2.7	1.00	0.05	2.30	0.05	11.3	0.6
101154	4626	53	2.71	0.10	0.14	0.11	6.418	0.010	8.45	0.39	5.3	2.5	1.08	0.19	2.40	0.08	10.5	0.5
102096	4971	53	2.17	0.09	0.08	0.17	7.409	0.012	4.80	0.22	1.2	0.6	1.42	0.53	2.60	0.18	9.6	0.5
104677	4499	45	2.69	0.11	0.05	0.09	7.616	0.012	4.87	0.23	6.5	2.6	1.06	0.08	2.31	0.06	11.5	0.7
105089	4909	56	2.95	0.07	0.05	0.15	6.475	0.010	7.79	0.36	1.6	1.1	1.22	0.44	2.53	0.18	9.6	0.6
105900	4586	47	2.19	0.08	-0.54	0.09	6.861	0.010	6.87	0.32	8.9	2.2	0.92	0.02	2.29	0.04	11.0	0.5
105911	4418	51	1.91	0.10	-0.22	0.11	7.759	0.011	1.19	0.01	0.3	0.1	2.17	0.39	1.39	0.10	47.1	2.2
105911	4418	48	1.91	0.09	-0.22	0.11	7.759	0.011	1.19	0.01	0.3	0.1	2.17	0.38	1.40	0.10	47.1	2.1

ARCS	T_{eff}	σ_{Teff}	*logg*
	K	K	dex
136514	4501	46	2.63
138562	4770	57	2.78
143857	4377	46	1.72
148287	5047	47	2.98
148684	4952	57	2.59
150066	4692	57	2.45
196346	4418	57	1.83
196346	4418	58	1.83
197421	4494	56	1.96
197491	4494	48	1.96
199442	4527	49	2.41
203222	5073	50	2.96
205423	4767	43	2.56
206660	4270	73	1.39
210185	4414	65	1.73
212927	4828	58	2.64
216540	4822	56	2.58

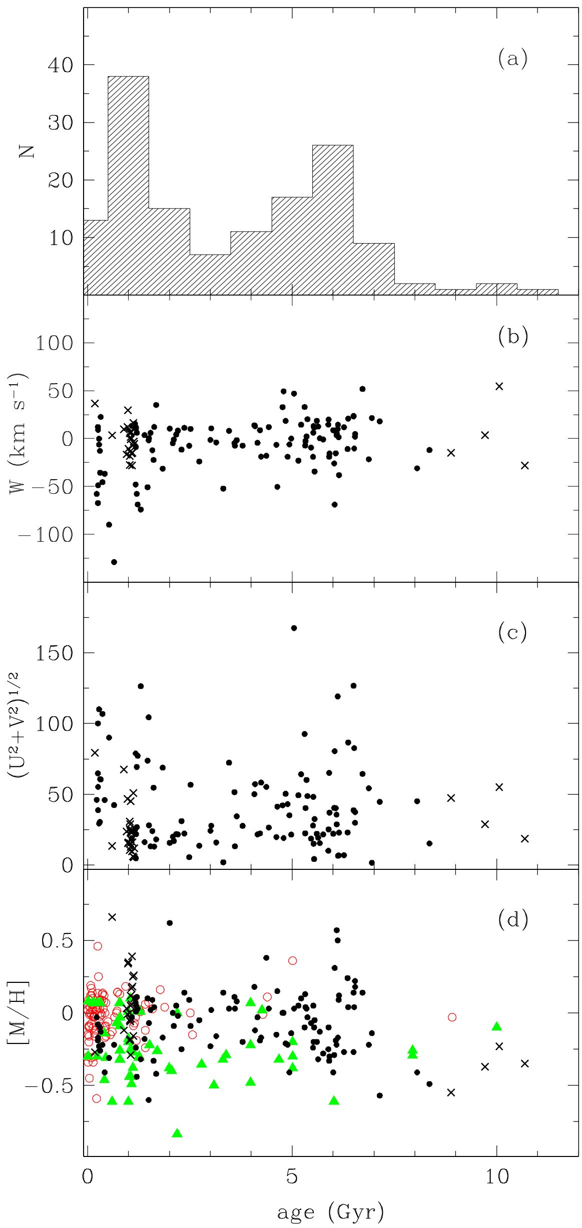

Figure 37: Distribution in age of the ARCS stars with a meaningful age computed by PARAM. Crosses represents stars with an error on age ≤25%, full dots represents stars with an error on age ≥25%. (a) Histogram of age distribution; (b) Age vs W velocity; (c) Age vs $\sqrt{U^2 V^2}$; (d) Age vs [M/H] of ARCS stars (black filled circles and crosses) and OC from Dias et al. (2005), red (or grey) empty dots are OC with 6<R_g<10, full green (or grey) triangles are OC with R_g≥10.

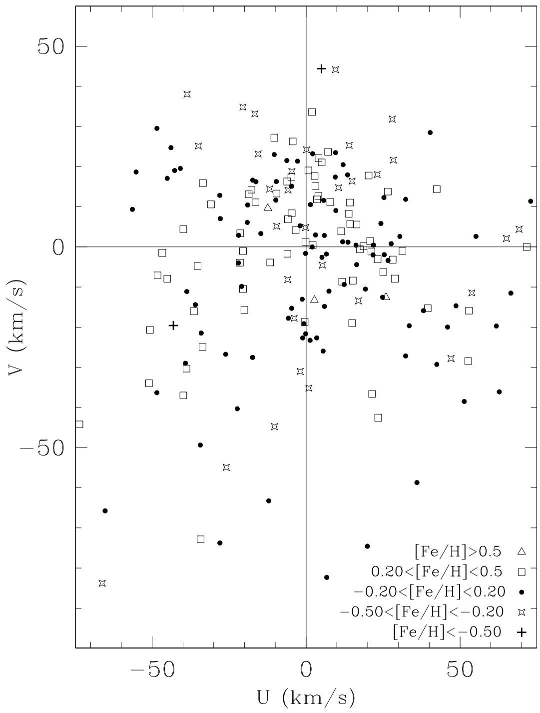

Figure 39: UV distribution of the 300 ARCS objects. Different metallicity is labeled with a different sign.

8.7.2 *Age-Metallicity relation -to check*

ARCS objects seem to show a good agreement with Open Cluster's age and metallicities from the catalog of Dias et al. (2005).

8.7.3 *Vertical metallicity gradient- to check*

Figure of the vertical gradient of metallicity (Zmax vs [M/H]).

8.7.4 *A signature of Radial Mixing?(provvisory title)*

By looking the Age-Metallicity diagram (Fig. 3d), the Age-Energy diagram (Fig.3b) and the Age-W diagram a group of old-metal poor-'cold' stars is evidenced. Does the kinematics, age and metallicity of these stars suggest their different nature respect to the average ARCS stars?
Those old metal poor stars (labeled in Tab. ?) that now are in the solar neighborhood could have formed elsewhere:

- they can be stars belonging to low end of the thin disk;
- these stars could have formed in satellite galaxies that were assimilated later on circular orbit (Abadi et al., 2003);
- they formed in the outer disk and then migrated inward due to the influence of transient spiral arms (Roŝkar et al., 2008).

Informations on [α/Fe] and abundances could provide another tip about the nature of these stars.

8.8 STRUCTURES IN THE U-V VELOCITY SPACE OF ARCS OBJECTS

8.8.1 *Moving Groups*

In the UV-space of ARCS object some overdensities are clearly visible. The low error in the U,V,W velocities excludes that these overdensities are some artifacts. We can identify three overdensities, that we recognized as the Sirius, Coma and Pleiades moving groups.
The Sirius moving group is clearly identified in ARCS sample: it starts from UV=(20,2) km s^{-1} and ends at U,V=(30,-2) km s^{-1}. Its center is not well defined and it appears as a branch-shape feature with a clear extension. The average metallicity of the Sirius moving group is [Fe/H]= +0.12 dex with σ=0.22 dex, while Antoja et al. (2008) finds [Fe/H]=-0.21 dex σ=0.27 dex. Average age is 1Gy with σ=1.2 Gyr .
The Coma Berenices moving group (or middle branch) starts from U,V=(-3,+3) km s^{-1} and it ends at U,V = (5,-5) km s^{-1}. It appear as a long branch-shape feature. The average metallicity of the Coma moving group is [Fe/H]= +0.18 dex with σ=0.29 dex, while Antoja et al. (2008) finds [Fe/H]=-0.16 dex σ=0.21 dex. Ages seems more etherogeneus spanning from 1Gy to 6 Gyr .
The Hyades-Pleiades moving group is not very well defined, we may identify the Pleiades moving group at U,V $\approx$ (0,-22) km s^{-1}. The average metallicity of this moving group is [Fe/H]= +0.02 dex with σ=0.17 dex, while Antoja et al. (2008) finds [Fe/H]=-0.11 dex σ=0.20 dex.. Ages seems more etherogeneus also in this group from 1Gy to 6 Gyr.

8.8.2 *Kinematic branches*

Even if the moving groups are present as overdensities in the UV distribution, they can also be marked as long parallel branches. Skuljan et al. (1999) and Antoja et al. (2008) detected the presence of at least three long, parallel and equidistant branches in the U-V plane: the Sirius branch, the middle (or Coma Berenices) branch and the Pleiades (or Hyades-Pleiades) branch. In order to emphasize the branches, a clockwise rotation through an angle β is applied to the original (U,V) components. Thanks to this rotation in the new coordinates U_{ROT}, V_{ROT} the branches are better aligned with the horizontal axis. Althought Skuljan et al. (1999) adopted a β=25° and Antoja et al. (2008) adopted $\beta \approx$ 16°, a value of β=34.4° is more suitable for ARCS data (see Fig. 4).
This difference in β among these three studies are apparently due to different distance scales to the targets. Skuljan et al. (1999)

Table 27: Kinematic properties (U,V,W dispersions and asymmetric drift) of the major components of the Milky Way, from [?].

	Age (Gyr)	σ_U (km s^{-1})	σ_V (km s^{-1})	σ_W (km s^{-1})	V_{rot} (km s^{-1})	$\frac{d \ln \sigma_U^2}{dR}$
	0–0.15	16.7	10.8		3.5	
	0.15–1	19.8	12.8		3.1	
	1–2	27.2	17.6		5.8	
Disc	2–3	30.2	19.5	220	7.3	-2×10^{-1}
	3–5	36.7	23.7		10.8	
	5–7	43.1	27.8		14.8	
	7–10	43.1	27.8		14.8	
Thick disc		67	51	180	53	0
Halo		131	106	–	226	0
Bulge		113	115	0	79	0

Table 28: Constants for the Galactic model.

distance of the Sun from GC	$R_\odot$	8.5	kpc
local circular velocity	Θ	220	km s6−1
Bulge	M_B	1.41×10^{10}	$M_\odot$
	b_B	0.3873	kpc
Disk	M_D	8.56×10^{10}	$M_\odot$
	a_D	5.3178	kpc
	b_D	0.2500	kpc
Halo	M_H	80.02×10^{10}	$M_\odot$
	b_H	12.0	kpc

Table 29: Orbital parameters of ARCS stars.

ARCS	R_{min} kpc	σR_{min} kpc	R_{max} kpc	σR_{max} kpc	$\lvert Z_{max}\rvert$ kpc	$\sigma\lvert Z_{max}\rvert$ kpc	ecc.	σecc
6	7.124	0.105	8.508	0.002	0.328	0.020	0.089	0.007
966	5.719	0.131	8.643	0.023	0.260	0.015	0.204	0.011
2023	7.917	0.051	9.735	0.074	0.203	0.014	0.103	0.007
2344	8.293	0.021	9.498	0.051	0.193	0.008	0.068	0.003
2624	7.717	0.068	10.424	0.126	0.242	0.013	0.149	0.008
3512	7.307	0.070	9.947	0.073	1.016	0.028	0.153	0.005
4352	4.885	0.200	10.511	0.258	0.465	0.058	0.365	0.021
4593	6.631	0.117	14.341	0.425	0.838	0.050	0.367	0.015
4621	7.391	0.126	8.674	0.033	0.236	0.012	0.080	0.008
5362	5.682	0.074	9.205	0.059	0.237	0.019	0.237	0.007
5544	7.976	0.031	9.122	0.037	0.285	0.012	0.067	0.003
5720	5.596	0.033	8.923	0.008	0.216	0.007	0.229	0.003
5822	7.932	0.049	9.130	0.053	0.330	0.013	0.070	0.004
7736	8.568	0.005	9.955	0.091	0.183	0.009	0.075	0.005
8120	8.454	0.011	9.342	0.047	0.156	0.007	0.050	0.002
8333	8.029	0.034	10.182	0.069	0.155	0.008	0.118	0.004
8337	5.444	0.185	9.181	0.089	0.294	0.021	0.256	0.016
8599	7.286	0.036	8.812	0.010	0.363	0.008	0.095	0.002
9261	8.112	0.046	9.680	0.089	0.163	0.011	0.088	0.005
9649	3.856	0.149	9.471	0.073	1.517	0.073	0.422	0.016
9959	8.531	0.037	11.288	0.164	0.349	0.015	0.139	0.008

Table 30: Orbital parameters of ARCS stars.

ARCS	R_{min} kpc	σR_{min} kpc	R_{max} kpc	σR_{max} kpc	$\|Z_{max}\|$ kpc	$\sigma\|Z_{max}\|$ kpc	ecc.	σecc
10642	7.145	0.107	8.618	0.010	0.285	0.014	0.093	0.007
10955	8.594	0.012	9.675	0.077	0.262	0.013	0.059	0.004
11037	8.534	0.006	10.017	0.047	0.122	0.007	0.080	0.002
12252	8.593	0.007	9.767	0.058	0.171	0.010	0.064	0.003
12254	8.244	0.168	11.467	0.165	0.447	0.038	0.164	0.016
12343	8.619	0.020	9.334	0.108	0.256	0.014	0.040	0.006
12513	7.636	0.094	9.130	0.071	0.198	0.012	0.089	0.006
13468	8.498	0.014	8.937	0.022	0.395	0.010	0.025	0.002
15005	6.468	0.035	9.004	0.022	0.239	0.011	0.164	0.003
16467	8.246	0.065	8.612	0.018	0.347	0.014	0.022	0.004
16672	8.050	0.123	11.898	0.226	0.252	0.017	0.193	0.014
16708	6.945	0.071	10.877	0.125	0.371	0.029	0.221	0.006
16786	7.884	0.028	9.249	0.031	0.162	0.008	0.080	0.002
17122	7.625	0.063	9.124	0.040	0.341	0.015	0.089	0.004
17524	8.500	0.025	9.269	0.082	0.261	0.013	0.043	0.004
17616	6.803	0.064	9.200	0.027	0.619	0.014	0.150	0.004
17806	8.486	0.025	10.210	0.080	0.298	0.019	0.092	0.004
18145	8.551	0.010	10.236	0.046	0.243	0.010	0.090	0.002
18175	6.293	0.038	9.475	0.026	0.214	0.010	0.202	0.003
18682	3.087	0.119	9.745	0.043	0.434	0.035	0.519	0.013
18739	6.554	0.118	9.857	0.103	0.240	0.020	0.201	0.008

Table 31: Orbital parameters of ARCS stars.

ARCS	R_{min} kpc	σR_{min} kpc	R_{max} kpc	σR_{max} kpc	$\lvert Z_{max} \rvert$ kpc	$\sigma \lvert Z_{max} \rvert$ kpc	ecc.	σecc
19847	8.693	0.014	9.199	0.129	0.319	0.018	0.028	0.007
19866	7.588	0.039	10.264	0.070	0.145	0.012	0.150	0.005
19903	8.456	0.015	10.223	0.078	0.161	0.010	0.095	0.004
19928	6.912	0.132	8.656	0.010	0.291	0.015	0.112	0.009
20792	6.861	0.081	10.886	0.132	0.214	0.023	0.227	0.008
21196	7.702	0.145	11.742	0.098	0.431	0.050	0.208	0.011
21215	8.596	0.010	9.084	0.074	0.127	0.007	0.028	0.004
21838	7.662	0.108	8.730	0.017	0.266	0.014	0.065	0.007
21887	8.505	0.026	9.066	0.064	0.149	0.009	0.032	0.003
21976	7.346	0.162	9.127	0.079	0.160	0.017	0.108	0.009
21993	6.848	0.103	8.649	0.008	0.120	0.008	0.116	0.007
22149	6.958	0.055	9.380	0.039	0.144	0.010	0.148	0.004
22796	8.557	0.005	10.118	0.079	0.214	0.012	0.084	0.004
22797	6.802	0.063	8.653	0.008	0.597	0.012	0.120	0.005
22798	6.915	0.024	9.580	0.033	0.085	0.005	0.162	0.003
22819	7.724	0.063	8.745	0.021	0.074	0.004	0.062	0.004
22853	8.058	0.082	8.672	0.014	0.126	0.007	0.037	0.005
23223	6.509	0.129	8.678	0.055	0.517	0.018	0.143	0.008
23887	6.488	0.129	9.546	0.082	0.235	0.029	0.191	0.008
24107	6.892	0.102	8.730	0.014	0.263	0.012	0.118	0.007
24120	5.240	0.211	9.307	0.051	0.971	0.065	0.280	0.019

Table 32: Orbital parameters of ARCS stars.

ARCS	R_{min} kpc	σR_{min} kpc	R_{max} kpc	σR_{max} kpc	$\|Z_{max}\|$ kpc	$\sigma\|Z_{max}\|$ kpc	ecc.	σecc
24604	8.635	0.017	10.070	0.116	0.209	0.013	0.077	0.005
25041	8.484	0.027	11.678	0.207	0.426	0.047	0.158	0.009
26606	8.521	0.025	9.375	0.087	0.130	0.010	0.048	0.004
26662	7.925	0.071	9.065	0.046	0.227	0.013	0.067	0.004
27008	8.697	0.012	9.277	0.099	0.221	0.015	0.032	0.005
27146	8.180	0.044	8.885	0.029	0.324	0.013	0.041	0.003
27324	7.408	0.049	10.908	0.092	0.232	0.019	0.191	0.003
27351	8.166	0.045	9.385	0.061	0.156	0.015	0.069	0.003
27574	7.829	0.042	9.253	0.038	0.145	0.011	0.083	0.003
27719	7.415	0.071	8.679	0.009	0.138	0.008	0.079	0.005
28037	8.644	0.012	12.606	0.311	0.566	0.040	0.186	0.012
28054	4.655	0.407	8.707	0.027	0.900	0.130	0.304	0.040
28088	7.554	0.086	8.711	0.016	0.114	0.010	0.071	0.005
28322	7.850	0.042	9.023	0.031	0.078	0.009	0.070	0.002
28531	8.107	0.117	11.329	0.108	0.276	0.023	0.166	0.008
28624	8.264	0.032	10.148	0.079	0.162	0.015	0.102	0.004
28959	9.259	0.032	10.541	0.386	0.944	0.082	0.064	0.018
29583	3.507	0.147	10.350	0.076	2.208	0.159	0.494	0.015
29913	6.801	0.106	8.729	0.011	0.121	0.011	0.124	0.008
29914	8.374	0.042	9.589	0.103	0.150	0.013	0.068	0.004
30057	7.601	0.084	8.813	0.021	0.129	0.012	0.074	0.005

Table 33: Orbital parameters of ARCS stars.

ARCS	R_{min} kpc	σR_{min} kpc	R_{max} kpc	σR_{max} kpc	$\|Z_{max}\|$ kpc	$\sigma\|Z_{max}\|$ kpc	ecc.	σecc
30781	8.091	0.072	8.855	0.034	0.255	0.015	0.045	0.004
30812	6.303	0.073	9.048	0.086	0.092	0.007	0.179	0.005
31693	6.737	0.138	8.683	0.010	0.104	0.009	0.126	0.010
32393	7.073	0.059	8.868	0.021	0.078	0.010	0.113	0.004
35220	9.147	0.065	24.517	0.881	3.352	0.269	0.456	0.014
70435	6.715	0.200	9.532	0.086	0.498	0.067	0.174	0.014
70435	6.456	0.051	8.929	0.039	0.179	0.014	0.161	0.004
71137	5.931	0.037	9.093	0.084	0.275	0.014	0.210	0.007
71955	7.676	0.077	8.691	0.014	0.158	0.012	0.062	0.005
73412	8.612	0.008	10.295	0.135	0.361	0.031	0.089	0.006
73413	6.608	0.085	10.111	0.095	0.154	0.020	0.210	0.007
74216	6.261	0.036	8.590	0.009	0.170	0.008	0.157	0.003
74444	8.351	0.087	8.697	0.021	0.395	0.022	0.020	0.005
75408	8.220	0.039	9.175	0.050	0.113	0.010	0.055	0.003
76334	5.462	0.050	8.632	0.010	0.285	0.009	0.225	0.004
76366	8.355	0.034	8.980	0.048	0.417	0.015	0.036	0.002
77236	6.991	0.193	9.746	0.240	3.275	0.371	0.165	0.014
77894	7.766	0.152	11.285	0.197	1.426	0.109	0.185	0.011
79218	7.188	0.086	9.426	0.090	0.159	0.009	0.135	0.008
79567	4.212	0.085	8.853	0.030	1.413	0.127	0.355	0.009
80163	7.479	0.064	9.992	0.065	0.149	0.011	0.144	0.005

Table 34: Orbital parameters of ARCS stars.

ARCS	R_{min} kpc	σR_{min} kpc	R_{max} kpc	σR_{max} kpc	$\lvert Z_{max}\rvert$ kpc	$\sigma\lvert Z_{max}\rvert$ kpc	ecc.	σecc
80871	7.539	0.076	8.964	0.046	0.121	0.010	0.086	0.005
81490	8.618	0.011	9.143	0.083	0.137	0.010	0.030	0.005
82268	8.444	0.021	9.331	0.070	0.470	0.138	0.050	0.004
82333	8.278	0.068	8.970	0.074	0.155	0.013	0.040	0.005
82356	6.935	0.061	9.253	0.050	0.484	0.020	0.143	0.005
82888	8.621	0.012	11.219	0.112	0.176	0.013	0.131	0.005
82957	8.369	0.054	8.723	0.045	0.134	0.011	0.021	0.004
82958	7.542	0.049	9.075	0.027	0.435	0.025	0.092	0.002
83024	7.370	0.183	11.668	0.307	1.084	0.115	0.226	0.016
83046	6.895	0.050	8.876	0.025	0.143	0.012	0.126	0.004
83161	8.004	0.039	9.042	0.040	0.188	0.010	0.061	0.003
83453	8.585	0.015	9.648	0.110	0.159	0.013	0.058	0.006
83536	4.143	0.076	9.365	0.083	0.509	0.061	0.387	0.009
83581	7.860	0.056	8.596	0.008	0.186	0.008	0.045	0.003
83618	5.523	0.039	9.212	0.031	0.326	0.011	0.250	0.004
84050	8.568	0.006	9.922	0.068	0.154	0.010	0.073	0.003
85180	8.231	0.074	8.616	0.020	0.187	0.012	0.023	0.004
85219	7.368	0.072	8.730	0.026	0.208	0.013	0.085	0.005
85379	4.597	0.186	11.127	0.406	0.206	0.026	0.415	0.027
85505	6.965	0.057	8.553	0.004	0.110	0.009	0.102	0.004
85990	4.898	0.053	9.828	0.087	0.214	0.014	0.335	0.007

Table 35: Orbital parameters of ARCS stars.

ARCS	R_{min} kpc	σR_{min} kpc	R_{max} kpc	σR_{max} kpc	$\lvert Z_{max}\rvert$ kpc	$\sigma\lvert Z_{max}\rvert$ kpc	ecc.	σecc
86342	7.505	0.072	11.392	0.154	0.323	0.017	0.206	0.009
87095	5.937	0.020	8.958	0.198	0.256	0.009	0.203	0.011
87502	6.898	0.054	9.755	0.079	0.995	0.056	0.172	0.006
87975	8.400	0.069	8.603	0.022	0.204	0.019	0.012	0.004
88083	7.676	0.050	10.862	0.105	0.213	0.015	0.172	0.006
89114	6.964	0.157	9.098	0.095	0.896	0.090	0.133	0.011
89776	6.688	0.106	9.690	0.101	0.597	0.027	0.183	0.009
90080	6.327	0.062	8.737	0.107	0.491	0.021	0.160	0.008
90594	7.042	0.047	8.567	0.007	0.815	0.092	0.098	0.003
90969	8.423	0.050	9.854	0.125	0.231	0.017	0.078	0.008
92706	7.903	0.069	8.776	0.040	0.226	0.012	0.052	0.005
93719	7.482	0.085	8.842	0.051	0.197	0.012	0.083	0.006
94058	8.446	0.016	9.541	0.071	0.163	0.009	0.061	0.004
94279	6.887	0.088	8.597	0.015	0.222	0.014	0.110	0.006
94363	4.657	0.152	8.724	0.030	0.448	0.057	0.304	0.015
94402	7.517	0.071	8.959	0.057	0.099	0.010	0.088	0.006
94738	8.451	0.008	10.563	0.055	0.251	0.010	0.111	0.003
95740	8.119	0.074	8.650	0.039	0.155	0.009	0.032	0.005
95849	8.299	0.084	9.000	0.140	0.150	0.017	0.041	0.009
96694	7.696	0.029	8.714	0.016	0.276	0.010	0.062	0.002
96720	6.410	0.094	8.531	0.008	0.232	0.014	0.142	0.007

Table 36: Orbital parameters of ARCS stars.

ARCS	R_{min} kpc	σR_{min} kpc	R_{max} kpc	σR_{max} kpc	$\lvert Z_{max}\rvert$ kpc	$\sigma\lvert Z_{max}\rvert$ kpc	ecc.	σecc
97197	6.428	0.114	9.158	0.087	0.245	0.018	0.175	0.010
97443	8.234	0.193	9.146	0.276	0.764	0.040	0.052	0.018
98399	6.733	0.123	9.063	0.081	0.181	0.012	0.148	0.009
99055	8.465	0.005	9.379	0.035	0.079	0.004	0.051	0.002
99648	8.283	0.008	9.671	0.025	0.065	0.003	0.077	0.001
99651	8.471	0.016	9.025	0.066	0.123	0.007	0.032	0.004
99873	8.146	0.094	9.697	0.204	0.214	0.022	0.087	0.012
100822	5.857	0.106	8.515	0.004	0.185	0.010	0.185	0.009
100920	8.474	0.001	9.666	0.025	0.163	0.006	0.066	0.001
100975	8.018	0.060	8.535	0.013	0.351	0.012	0.031	0.004
101154	8.425	0.017	9.657	0.068	0.138	0.008	0.068	0.004
102274	5.921	0.260	9.154	0.198	0.199	0.022	0.215	0.023
102928	8.117	0.020	8.782	0.017	0.246	0.009	0.039	0.001
104677	3.624	0.135	8.483	0.006	0.214	0.019	0.402	0.016
105089	7.174	0.065	8.495	0.004	0.182	0.009	0.084	0.004
105900	6.317	0.034	9.194	0.035	0.221	0.009	0.185	0.004
105911	6.759	0.238	13.080	0.457	1.009	0.047	0.318	0.024
106498	7.050	0.105	8.719	0.044	0.222	0.012	0.106	0.007
106775	7.840	0.062	8.595	0.022	0.239	0.011	0.046	0.004
107036	8.212	0.060	8.649	0.052	0.222	0.012	0.026	0.004
109014	7.436	0.265	12.073	0.176	0.857	0.041	0.238	0.021

Table 37: Orbital parameters of ARCS stars.

ARCS	R_{min} kpc	σR_{min} kpc	R_{max} kpc	σR_{max} kpc	$\lvert Z_{max} \rvert$ kpc	$\sigma \lvert Z_{max} \rvert$ kpc	ecc.	σecc
112048	5.923	0.024	8.941	0.017	0.288	0.012	0.203	0.002
112281	8.166	0.053	8.669	0.043	0.164	0.007	0.030	0.003
112992	8.423	0.009	10.517	0.044	0.193	0.008	0.111	0.002
113564	8.277	0.026	9.480	0.085	0.439	0.013	0.068	0.004
113595	4.149	0.195	8.473	0.015	1.357	0.100	0.343	0.020
116817	7.627	0.030	8.909	0.024	0.412	0.010	0.078	0.002
118219	8.458	0.002	12.182	0.095	0.285	0.008	0.180	0.004
119373	5.373	0.174	9.241	0.103	0.237	0.017	0.265	0.015
119461	6.814	0.222	8.427	0.009	0.155	0.014	0.106	0.016
120967	7.846	0.052	9.618	0.096	0.251	0.015	0.101	0.006
123509	6.639	0.063	8.959	0.036	0.418	0.015	0.149	0.004
128200	7.525	0.091	8.789	0.064	0.509	0.030	0.077	0.006
129887	7.996	0.040	9.203	0.081	0.238	0.016	0.070	0.004
131455	8.320	0.019	9.976	0.108	0.221	0.018	0.090	0.005
132132	7.799	0.029	10.572	0.076	0.113	0.010	0.151	0.004
136380	7.795	0.025	11.033	0.086	0.286	0.015	0.172	0.003
136514	6.153	0.077	8.670	0.011	0.081	0.005	0.170	0.006
138562	7.655	0.045	8.444	0.004	0.098	0.004	0.049	0.003
139308	7.639	0.092	8.697	0.063	0.157	0.015	0.065	0.005
140489	8.250	0.023	8.625	0.037	0.143	0.009	0.022	0.002
143857	5.434	0.113	8.121	0.028	1.051	0.071	0.198	0.010

Table 38: Orbital parameters of ARCS stars.

ARCS	R_{min} kpc	σR_{min} kpc	R_{max} kpc	σR_{max} kpc	$\|Z_{max}\|$ kpc	$\sigma\|Z_{max}\|$ kpc	ecc.	σecc
148287	8.065	0.024	9.366	0.048	0.074	0.006	0.075	0.003
148684	6.438	0.105	8.289	0.012	0.228	0.018	0.126	0.008
150066	5.750	0.111	8.766	0.036	0.143	0.014	0.208	0.008
152484	4.241	0.045	9.974	0.037	0.588	0.045	0.403	0.004
196346	6.426	0.151	10.190	0.255	0.934	0.128	0.226	0.014
197421	7.474	0.091	13.868	0.549	4.523	0.380	0.299	0.018
199442	6.248	0.035	8.449	0.006	0.049	0.006	0.150	0.003
203222	8.378	0.009	9.428	0.052	0.177	0.008	0.059	0.003
205423	8.259	0.019	9.020	0.037	0.138	0.006	0.044	0.002
206660	5.765	0.095	11.738	0.212	2.581	0.154	0.341	0.010
207435	6.860	0.067	9.488	0.075	0.245	0.011	0.161	0.006
207653	5.314	0.084	8.555	0.018	0.136	0.012	0.234	0.007
207920	8.424	0.008	9.857	0.068	0.107	0.006	0.078	0.004
208671	8.374	0.017	9.470	0.092	0.261	0.015	0.061	0.005
209321	7.330	0.109	9.196	0.114	0.264	0.024	0.113	0.010
210185	5.354	0.175	8.212	0.033	0.905	0.060	0.211	0.015
210434	7.364	0.073	9.021	0.059	0.080	0.005	0.101	0.005
212474	6.227	0.131	11.105	0.234	0.145	0.014	0.281	0.014
212927	6.951	0.093	8.598	0.035	0.199	0.011	0.106	0.006
215749	8.268	0.019	9.453	0.059	0.233	0.010	0.067	0.003
216401	7.690	0.066	8.989	0.060	0.226	0.014	0.078	0.005

Table 39: Orbital parameters of ARCS stars.

ARCS	R_{min} kpc	σR_{min} kpc	R_{max} kpc	σR_{max} kpc	$\lvert Z_{max}\rvert$ kpc	$\sigma\lvert Z_{max}\rvert$ kpc	ecc.	σecc
217187	8.467	0.009	10.098	0.066	0.188	0.012	0.088	0.003
217591	6.010	0.109	8.449	0.007	0.236	0.015	0.169	0.009
220858	7.018	0.087	8.514	0.008	0.103	0.007	0.096	0.006
220859	1.252	0.241	9.529	0.144	1.218	0.977	0.769	0.039
221296	5.871	0.175	10.992	0.288	1.070	0.066	0.304	0.016
222455	7.274	0.205	12.975	0.590	0.397	0.066	0.281	0.026
222754	8.422	0.016	10.211	0.082	0.382	0.016	0.096	0.004
222936	7.810	0.081	8.878	0.064	0.213	0.012	0.064	0.006
223252	7.390	0.090	8.908	0.055	0.095	0.007	0.093	0.006
223336	8.493	0.006	10.346	0.062	0.274	0.014	0.098	0.003
223870	8.191	0.035	10.884	0.112	0.408	0.021	0.141	0.006
224776	8.397	0.021	10.393	0.096	0.258	0.013	0.106	0.005

Table 40: PARAM ages for 144 ARCS stars.

	ARCS χ^2										PARAM							
ARCS	T_{eff}	σ_{Teff}	$logg$	σ_{logg}	[M/H]	$\sigma_{M/H}$	V	σ_V	phot.π	σ_π	Age	σ_{Age}	Mass	σ_{Mass}	$logg$	σ_{logg}	R	σ_R
	K	K	dex	dex	dex	dex	mag	mag	mas	mas	Gyr	Gyr	$M_\odot$	$M_\odot$	dex	dex	$R_\odot$	$R_\odot$
6	4743	47	2.57	0.07	0.15	0.17	6.420	0.010	8.41	0.39	3.3	2.4	1.12	0.27	2.44	0.11	10.1	0.5
3819	5095	43	3.04	0.09	-0.04	0.14	8.074	0.013	3.72	0.17	1.0	0.2	1.89	0.39	2.84	0.11	8.4	0.4
4621	4636	45	2.47	0.11	-0.12	0.17	8.119	0.014	3.83	0.18	5.7	2.7	1.09	0.15	2.41	0.08	10.4	0.6
5822	4798	52	2.43	0.13	-0.19	0.13	7.791	0.012	4.46	0.21	5.6	3.8	1.08	0.15	2.48	0.08	9.5	0.5
7736	4834	44	2.58	0.09	-0.13	0.08	7.362	0.011	5.19	0.24	5.0	3.4	1.07	0.21	2.45	0.09	9.8	0.4
8337	4620	47	2.45	0.08	0.11	0.15	7.748	0.012	4.58	0.21	5.2	2.5	1.09	0.19	2.40	0.08	10.5	0.5
9261	4918	56	2.73	0.13	-0.06	0.13	7.153	0.011	5.97	0.28	1.5	1.0	1.15	0.37	2.54	0.18	9.2	0.6
9649	4329	56	1.82	0.14	-0.21	0.12	8.017	0.013	1.06	0.02	0.4	0.2	1.80	0.33	1.24	0.11	51.2	2.7
9959	4683	55	2.51	0.07	-0.29	0.11	7.892	0.012	4.27	0.20	5.9	2.5	1.02	0.09	2.44	0.06	9.8	0.6
10642	4957	45	3.49	0.09	0.19	0.09	8.017	0.013	4.02	0.19	1.1	0.2	2.01	0.15	2.84	0.06	8.6	0.4
11037	4874	61	2.60	0.12	-0.18	0.10	6.013	0.010	10.09	0.47	4.2	3.8	1.12	0.21	2.52	0.11	9.2	0.6
11455	4556	41	2.44	0.14	-0.48	0.14	8.076	0.015	3.91	0.18	8.4	2.5	0.96	0.03	2.30	0.05	11.1	0.6
12254	4643	45	2.58	0.12	0.06	0.18	7.981	0.011	4.12	0.19	5.2	2.6	1.09	0.19	2.41	0.08	10.4	0.5
12513	5103	43	2.86	0.14	0.01	0.16	7.656	0.012	4.72	0.22	1.0	0.2	1.96	0.18	2.89	0.06	8.0	0.4
13468	4924	43	2.85	0.10	0.40	0.15	6.040	0.010	9.95	0.47	1.1	0.2	2.06	0.16	2.82	0.05	8.9	0.5

Table 41: PARAM ages for 144 ARCS stars.

	ARCS χ^2										PARAM							
ARCS	T_{eff} K	σ_{Teff} K	$logg$ dex	σ_{logg} dex	[M/H] dex	$\sigma_{M/H}$ dex	V mag	σ_V mag	phot.π mas	σ_π mas	Age Gyr	σ_{Age} Gyr	Mass $M_\odot$	σ_{Mass} $M_\odot$	$logg$ dex	σ_{logg} dex	R $R_\odot$	σ_R $R_\odot$
15005	4610	56	2.23	0.10	-0.18	0.13	7.003	0.011	6.41	0.30	6.1	2.7	1.06	0.11	2.39	0.08	10.4	0.7
16467	4787	43	2.51	0.14	-0.16	0.11	6.348	0.010	8.65	0.40	6.1	3.7	1.09	0.15	2.49	0.07	9.5	0.5
16672	4854	50	2.39	0.13	-0.08	0.09	7.745	0.011	4.56	0.21	2.5	2.2	1.08	0.24	2.49	0.13	9.5	0.5
16708	4746	71	2.52	0.10	-0.32	0.12	7.196	0.011	5.86	0.27	5.9	2.9	1.02	0.10	2.46	0.06	9.5	0.5
17806	4623	43	2.45	0.12	-0.21	0.15	7.790	0.014	4.48	0.21	6.1	2.7	1.06	0.12	2.39	0.07	10.4	0.6
18145	4895	59	2.10	0.12	0.11	0.10	6.644	0.011	7.23	0.33	1.2	0.3	1.30	0.45	2.54	0.18	9.7	0.6
18682	4605	57	2.69	0.13	-0.26	0.09	7.898	0.013	4.25	0.20	6.5	2.6	1.00	0.07	2.37	0.07	10.3	0.7
18739	5016	43	2.98	0.13	-0.15	0.08	8.196	0.016	3.69	0.17	1.1	0.2	1.21	0.42	2.61	0.20	8.6	0.6
19847	5092	46	2.89	0.10	-0.18	0.09	8.020	0.012	3.62	0.17	1.0	0.2	1.19	0.46	2.56	0.19	9.1	0.5
21838	4755	43	2.46	0.08	-0.24	0.16	8.160	0.012	3.76	0.18	5.9	3.3	1.06	0.13	2.47	0.06	9.6	0.5
21887	4875	56	2.89	0.12	0.03	0.09	7.286	0.011	5.62	0.26	1.5	0.9	1.06	0.30	2.47	0.15	9.6	0.6
21976	4466	56	2.62	0.09	0.23	0.12	7.951	0.012	4.33	0.40	6.5	2.8	1.10	0.16	2.34	0.10	11.3	1.1
22149	4705	57	2.91	0.11	0.05	0.11	7.637	0.011	4.82	0.22	5.3	2.9	1.09	0.19	2.43	0.09	10.1	0.5
22797	4486	69	2.43	0.14	0.13	0.13	7.615	0.012	4.86	0.23	6.1	2.6	1.09	0.15	2.34	0.08	11.2	0.8
22819	4876	45	2.62	0.12	-0.08	0.12	6.232	0.010	9.12	0.42	2.1	1.8	1.07	0.26	2.49	0.14	9.4	0.6
22853	4489	72	2.28	0.08	0.10	0.08	7.391	0.011	5.38	0.25	6.1	2.6	1.09	0.12	2.34	0.08	11.3	0.8
23223	4532	61	2.29	0.07	-0.04	0.09	7.140	0.018	5.74	0.27	5.5	2.5	1.06	0.10	2.30	0.07	11.6	0.8

Table 42: PARAM ages for 144 ARCS stars.

	ARCS χ^2										PARAM							
ARCS	T_{eff}	σ_{Teff}	*logg*	σ_{logg}	[M/H]	$\sigma_{M/H}$	V	σ_V	phot.π	σ_π	Age	σ_{Age}	Mass	σ_{Mass}	*logg*	σ_{logg}	R	σ_R
	K	K	dex	dex	dex	dex	mag	mag	mas	mas	Gyr	Gyr	$M_\odot$	$M_\odot$	dex	dex	$R_\odot$	$R_\odot$
23887	4665	53	2.75	0.11	0.39	0.15	6.041	0.009	10.43	0.96	4.4	2.3	1.25	0.29	2.45	0.11	10.6	0.7
24120	4425	55	1.95	0.14	-0.25	0.15	7.886	0.013	1.12	0.01	0.3	0.1	1.94	0.46	1.34	0.13	47.3	2.3
25041	4692	53	2.48	0.09	-0.28	0.18	7.193	0.011	5.89	0.27	6.0	2.9	1.07	0.13	2.44	0.07	9.9	0.6
26606	5030	55	2.59	0.09	-0.05	0.09	7.426	0.014	4.84	0.22	1.0	0.2	1.36	0.54	2.61	0.20	9.2	0.6
27146	4836	53	2.52	0.10	-0.04	0.12	7.340	0.012	5.49	0.26	2.7	2.4	1.07	0.24	2.47	0.12	9.6	0.6
27324	4842	54	2.38	0.12	-0.11	0.08	7.942	0.014	4.15	0.19	4.1	3.6	1.11	0.23	2.50	0.11	9.4	0.5
27531	5081	54	2.81	0.09	0.01	0.11	9.172	0.018	4.00	0.19	2.1	0.6	1.34	0.14	3.19	0.07	4.7	0.3
27574	4867	44	2.53	0.11	-0.19	0.13	7.521	0.013	5.04	0.23	3.8	3.5	1.10	0.20	2.51	0.11	9.2	0.5
27719	4773	43	2.52	0.11	0.04	0.12	7.407	0.012	5.33	0.25	3.6	2.8	1.06	0.21	2.44	0.10	9.9	0.5
28037	4563	56	2.29	0.10	-0.40	0.09	7.572	0.011	4.92	0.23	8.1	2.5	0.96	0.03	2.33	0.05	10.7	0.6
28054	4439	47	2.65	0.10	0.15	0.15	7.909	0.014	4.42	0.41	6.7	2.7	1.09	0.13	2.30	0.09	11.7	1.1
28322	4803	41	2.50	0.13	0.06	0.10	6.253	0.010	9.05	0.42	2.2	1.6	1.04	0.22	2.43	0.11	9.9	0.5
28959	4123	53	1.35	0.09	-0.41	0.15	8.081	0.012	1.03	0.02	1.7	0.7	1.13	0.22	0.89	0.11	61.1	3.5
29583	4148	48	1.75	0.11	-0.31	0.15	7.378	0.011	1.43	0.03	1.3	0.6	1.27	0.25	0.96	0.10	59.5	3.1
29913	4772	53	2.56	0.12	-0.02	0.16	8.113	0.013	3.88	0.18	4.2	3.3	1.09	0.21	2.46	0.10	9.8	0.6

Table 43: PARAM ages for 144 ARCS stars.

	ARCS χ^2										PARAM							
ARCS	T_{eff}	σ_{Teff}	*logg*	σ_{logg}	[M/H]	$\sigma_{M/H}$	V	σ_V	phot.π	σ_π	Age	σ_{Age}	Mass	σ_{Mass}	*logg*	σ_{logg}	R	σ_R
	K	K	dex	dex	dex	dex	mag	mag	mas	mas	Gyr	Gyr	$M_\odot$	$M_\odot$	dex	dex	$R_\odot$	$R_\odot$
31693	5039	56	2.92	0.12	0.13	0.12	7.772	0.012	4.48	0.21	1.1	0.2	2.00	0.19	2.86	0.06	8.3	0.4
32393	4581	53	2.69	0.11	0.58	0.09	5.991	0.010	10.33	0.48	6.1	2.5	1.20	0.21	2.39	0.08	11.2	0.4
35220	4452	44	1.95	0.09	-0.18	0.15	8.096	0.013	1.02	0.01	0.3	0.1	2.41	0.56	1.47	0.12	45.8	1.8
70435	3976	46	1.11	0.10	-0.32	0.11	7.870	0.012	1.12	0.01	1.6	0.5	1.12	0.19	0.72	0.10	73.7	5.0
73413	5739	78	2.96	0.12	-0.11	0.16	7.884	0.013	4.25	0.20	0.9	0.1	1.99	0.08	3.19	0.04	5.7	0.4
75175	6054	47	2.99	0.14	-0.28	0.09	7.032	0.010	6.34	0.29	1.1	0.1	1.81	0.06	3.26	0.03	5.0	0.3
75193	5012	39	2.66	0.10	-0.23	0.16	7.414	0.011	5.28	0.20	1.2	0.5	1.38	0.36	2.70	0.14	8.4	0.5
76366	5958	61	2.86	0.13	0.35	0.16	7.035	0.010	6.34	0.29	1.0	0.1	2.03	0.06	3.29	0.04	5.1	0.3
77894	4268	52	1.48	0.07	-0.43	0.18	7.369	0.011	1.43	0.02	1.2	0.7	1.27	0.27	1.06	0.11	53.3	2.6
78421	5114	50	2.98	0.12	-0.17	0.08	7.186	0.011	5.85	0.27	1.0	0.2	1.83	0.32	2.88	0.11	7.9	0.4
79567	4549	54	2.62	0.09	0.32	0.12	7.931	0.013	4.22	0.20	6.0	2.5	1.09	0.18	2.36	0.07	11.0	0.5
81490	5038	50	2.81	0.07	-0.03	0.11	7.720	0.012	4.38	0.20	1.1	0.2	1.65	0.57	2.74	0.19	8.7	0.5
82957	4807	75	2.67	0.11	0.10	0.17	7.510	0.011	5.09	0.24	2.5	2.0	1.19	0.36	2.50	0.16	9.8	0.6
83024	4870	55	3.29	0.07	0.11	0.09	8.017	0.013	4.02	0.19	1.5	0.7	1.22	0.43	2.53	0.19	9.6	0.7
83161	4815	62	2.52	0.10	-0.19	0.12	7.134	0.010	6.02	0.28	5.5	3.9	1.09	0.16	2.49	0.08	9.4	0.5
83453	4830	50	2.52	0.11	-0.14	0.12	7.825	0.011	4.39	0.20	4.6	3.9	1.09	0.19	2.50	0.10	9.4	0.5
83536	4730	62	2.46	0.08	-0.09	0.16	7.683	0.011	4.70	0.22	5.3	3.3	1.09	0.17	2.45	0.08	9.9	0.6
83581	4805	40	2.39	0.12	-0.26	0.09	7.423	0.010	5.28	0.25	6.3	3.7	1.05	0.11	2.48	0.05	9.4	0.5
83618	4241	48	1.70	0.10	-0.12	0.10	4.036	0.009	6.21	0.14	0.3	0.1	2.08	0.33	1.19	0.09	58.5	3.0

Table 49: Orbital parameters of ARCS stars.

ARCS	U (km s^{-1})	V (km s^{-1})	W (km s^{-1})	R_{MIN} (kpc)	R_{MAX} (kpc)	ecc	$\lvert z_{MAX} \rvert$ (kpc)	[M/H] (dex)	Age Gyrs
28037	9.53	44.15	−31.06	8.644±0.012	12.606±0.311	0.229±0.012	0.566±0.040	−0.40 ±0.09	8.1 ±2.5
87502	53.82	−11.46	54.71	6.898±0.054	9.755±0.079	0.172±0.006	0.995±0.056	−0.22 ±0.10	10.0 ±1.6
105900	−43.11	−19.56	−14.89	6.317±0.034	9.194±0.035	0.185±0.004	0.221±0.009	−0.54 ±0.09	8.9 ±2.2
113564	−11.84	14.42	−28.11	8.277±0.026	9.480±0.085	0.068±0.004	0.439±0.013	−0.34 ±0.11	10.7 ±1.1
118219	4.99	44.37	18.00	8.458±0.002	12.182±0.095	0.180±0.004	0.285±0.008	−0.56 ±0.17	7.1 ± 2.1
131455	−5.86	15.15	−11.97	8.320±0.019	9.976±0.018	0.090±0.005	0.221±0.018	−0.48 ±0.10	8.4 ±2.5
224776	13.98	25.28	3.56	8.397±0.021	10.393±0.096	0.106±0.005	0.258±0.013	−0.36 ±0.13	9.7 ±1.8

BIBLIOGRAPHY

[1] A. Acker and B. Stenholm. Misclassified planetary nebulae. A&AS, 86:219–225, December 1990.

[2] S. J. Adelman. On the Photometric Variability of Red Clump Giants. *Baltic Astronomy*, 10:593–597, 2001.

[3] D. A. Allen. A catalogue of symbiotic stars. *Proceedings of the Astronomical Society of Australia*, 5:369–421, 1984.

[4] A. Alonso-Herrero, G. H. Rieke, M. J. Rieke, L. Colina, P. G. Pérez-González, and S. D. Ryder. Near-Infrared and Star-forming Properties of Local Luminous Infrared Galaxies. ApJ, 650:835–849, October 2006.

[5] D. R. Alves. K-Band Calibration of the Red Clump Luminosity. ApJ, 539:732–741, August 2000.

[6] D. R. Alves, M. Rejkuba, D. Minniti, and K. H. Cook. K-Band Red Clump Distance to the Large Magellanic Cloud. ApJ, 573:L51–L54, July 2002.

[7] D. R. Alves and A. Sarajedini. The Age-dependent Luminosities of the Red Giant Branch Bump, Asymptotic Giant Branch Bump, and Horizontal Branch Red Clump. ApJ, 511:225–234, January 1999.

[8] T. Antoja, F. Figueras, D. Fernández, and J. Torra. Origin and evolution of moving groups. I. Characterization in the observational kinematic-age-metallicity space. A&A, 490:135–150, October 2008.

[9] T. Antoja, O. Valenzuela, B. Pichardo, E. Moreno, F. Figueras, and D. Fernández. Stellar Kinematic Constraints on Galactic Structure Models Revisited: Bar and Spiral Arm Resonances. ApJ, 700:L78–L82, August 2009.

[10] C. Babusiaux and G. Gilmore. Near-Infrared red clump distances to the Galactic Bar. In F. Combes, D. Barret, T. Contini, F. Meynadier, and L. Pagani, editors, *SF2A-2004: Semaine de l'Astrophysique Francaise*, pages 515–+, December 2004.

[11] C. Babusiaux and G. Gilmore. Red clump distances to the inner Galactic structures. *ArXiv Astrophysics e-prints*, June 2005.

[12] M. J. Barlow, J. E. Drew, J. Meaburn, and R. M. Massey. The Shock-Excited P-Cygni Nebula. MNRAS, 268:L29+, May 1994.

[13] D. Barrado y Navascués and E. L. Martín. An Empirical Criterion to Classify T Tauri Stars and Substellar Analogs Using Low-Resolution Optical Spectroscopy. AJ, 126:2997–3006, December 2003.

[14] J.-P. Beaulieu and P. D. Sackett. Red Clump Morphology as Evidence against a New Intervening Stellar Population as the Primary Source of Microlensing toward the Large Magellanic Cloud. AJ, 116:209–219, July 1998.

[15] K. Belczyński, J. Mikołajewska, U. Munari, R. J. Ivison, and M. Friedjung. A catalogue of symbiotic stars. A&AS, 146:407–435, November 2000.

[16] M. Bellazzini, R. Ibata, N. Martin, G. F. Lewis, B. Conn, and M. J. Irwin. The core of the Canis Major galaxy as traced by red clump stars. MNRAS, 366:865–883, March 2006.

[17] M. Bellazzini, R. Ibata, L. Monaco, N. Martin, M. J. Irwin, and G. F. Lewis. Detection of the Canis Major galaxy at (l;b) = (244deg $-8deg and in the background of Galactic open clusters.$MNRAS, 354
$1263 - -1278, November 2004.$

[18] D. P. Bennett. Red Clump Stars as a Tracer of Microlensing Optical Depth. ApJ, 493:L79+, February 1998.

[19] T. Bensby, M. S. Oey, S. Feltzing, and B. Gustafsson. Disentangling the Hercules Stream. ApJ, 655:L89–L92, February 2007.

[20] T. Bensby, M. S. Oey, S. Feltzing, and B. Gustafsson. Hercules-stream stars and the metal-rich thick disk. In G. Israelian & G. Meynet, editor, *The Metal-Rich Universe*, pages 62–+, 2008.

[21] D. Bersier. The Distance to the Fornax Dwarf Galaxy Using Red Clump Stars and the Discrepancy between Red Clump and Tip of the Red Giant Branch Distances. ApJ, 543:L23–L26, November 2000.

[22] O. Bienaymé, C. Soubiran, T. Mishenina, V. Kovtyukh, and A. Siebert. Chemistry and Kinematics in the Solar Neighbourhood. In C. Turon, K. S. O'Flaherty, and M. A. C.

Perryman, editors, *The Three-Dimensional Universe with Gaia*, volume 576 of *ESA Special Publication*, pages 149–+, January 2005.

[23] O. Bienaymé, C. Soubiran, T. V. Mishenina, V. V. Kovtyukh, and A. Siebert. Vertical distribution of Galactic disk stars. A&A, 446:933–942, February 2006.

[24] G. Bono and V. Castellani. A theoretical investigation of population II red giant clumps. A&A, 258:385–388, May 1992.

[25] J. Bovy, D. W. Hogg, and S. T. Roweis. The Velocity Distribution of Nearby Stars from Hipparcos Data. I. The Significance of the Moving Groups. ApJ, 700:1794–1819, August 2009.

[26] A. Bragaglia, E. Carretta, R. G. Gratton, M. Tosi, G. Bonanno, P. Bruno, A. Calì, R. Claudi, R. Cosentino, S. Desidera, G. Farisato, M. Rebeschini, and S. Scuderi. Metal Abundances of Red Clump Stars in Open Clusters. I. NGC 6819. AJ, 121:327–336, January 2001.

[27] A. Bressan, F. Fagotto, G. Bertelli, and C. Chiosi. Evolutionary sequences of stellar models with new radiative opacities. II - Z = 0.02. A&AS, 100:647–664, sep 1993.

[28] A. Cabrera-Lavers, P. L. Hammersley, C. González-Fernández, M. López-Corredoira, F. Garzón, and T. J. Mahoney. Tracing the long bar with red-clump giants. A&A, 465:825–838, April 2007.

[29] V. Caloi, D. Cardini, F. D'Antona, M. Badiali, A. Emanuele, and I. Mazzitelli. Kinematics and age of stellar populations in the solar neighbourhood from Hipparcos data. A&A, 351:925–936, November 1999.

[30] D. Calzetti, R. C. Kennicutt, C. W. Engelbracht, C. Leitherer, B. T. Draine, L. Kewley, J. Moustakas, M. Sosey, D. A. Dale, K. D. Gordon, G. X. Helou, D. J. Hollenbach, L. Armus, G. Bendo, C. Bot, B. Buckalew, T. Jarrett, A. Li, M. Meyer, E. J. Murphy, M. Prescott, M. W. Regan, G. H. Rieke, H. Roussel, K. Sheth, J. D. T. Smith, M. D. Thornley, and F. Walter. The Calibration of Mid-Infrared Star Formation Rate Indicators. ApJ, 666:870–895, September 2007.

[31] D. Calzetti, K. Sheth, E. Churchwell, and J. Jackson. Star Formation Rate Determinations in the Milky Way and

Nearby Galaxies. In *The Evolving ISM in the Milky Way and Nearby Galaxies*, January 2009.

[32] R. D. Cannon and C. Lloyd. The main sequence gap and red giant clump of NGC 6939. MNRAS, 144:449–+, 1969.

[33] K. W. Carrell and R. Wilhelm. Horizontal Branch and Red Clump Stars in the Southern Arm of the Sagittarius Stream. In *Bulletin of the American Astronomical Society*, volume 38 of *Bulletin of the American Astronomical Society*, pages 926–+, December 2007.

[34] V. Castellani, A. Chieffi, and O. Straniero. The evolution through H and He burning of Galactic cluster stars. ApJS, 78:517–536, February 1992.

[35] D. Chakrabarty. Phase space structure in the solar neighbourhood. A&A, 467:145–162, May 2007.

[36] D. Chakrabarty and I. V. Sideris. Chaos in models of the solar neighbourhood. A&A, 488:161–165, September 2008.

[37] C. Chiosi. *Struttura Stellare*.

[38] C. Chiosi, G. Bertelli, and A. Bressan. New developments in understanding the HR diagram. ARA&A, 30:235–285, 1992.

[39] G. Clementini, A. Bragaglia, M. Maio, E. Carretta, R. Gratton, and L. di Fabrizio. CMD's, RR Lyrae's, clump stars and reddening in the LMC. In T. Lejeune and J. Fernandes, editors, *Observed HR Diagrams and Stellar Evolution*, volume 274 of *Astronomical Society of the Pacific Conference Series*, pages 391–+, 2002.

[40] A. A. Cole. Age, Metallicity, and the Distance to the Magellanic Clouds from Red Clump Stars. ApJ, 500:L137+, June 1998.

[41] A. A. Cole and M. D. Weinberg. The Red Clump as a Probe of the Galactic Dust Distribution. In *Bulletin of the American Astronomical Society*, volume 34 of *Bulletin of the American Astronomical Society*, pages 573–+, December 2001.

[42] M. J. Collinge and T. Sumi. Geometry and Kinematics of the Galactic Bar using RR Lyrae and Red Clump Giants from OGLE. In *Bulletin of the American Astronomical Society*, volume 36 of *Bulletin of the American Astronomical Society*, pages 1474–+, December 2004.

[43] F. Combes, P. Boissé, A. Mazure, and A. Blanchard. *Galaxies and Cosmology, second edition.*

[44] R. L. M. Corradi. Large-Scale Ionized Outflows from Symbiotic Stars: A Real Link with Planetary Nebulae? In R. L. M. Corradi, J. Mikolajewska, & T. J. Mahoney, editor, *Astronomical Society of the Pacific Conference Series*, volume 303 of *Astronomical Society of the Pacific Conference Series*, pages 393–+, 2003.

[45] R. L. M. Corradi, E. R. Rodríguez-Flores, A. Mampaso, R. Greimel, K. Viironen, J. E. Drew, D. J. Lennon, J. Mikolajewska, L. Sabin, and J. L. Sokoloski. IPHAS and the symbiotic stars. I. Selection method and first discoveries. A&A, 480:409–419, March 2008.

[46] P. A. Crowther and L. J. Smith. NaSt1: a Wolf-Rayet star cloaked by an eta Car-like nebula? MNRAS, 308:82–96, September 1999.

[47] R. M. Cutri, M. F. Skrutskie, S. van Dyk, C. A. Beichman, J. M. Carpenter, T. Chester, L. Cambresy, T. Evans, J. Fowler, J. Gizis, E. Howard, J. Huchra, T. Jarrett, E. L. Kopan, J. D. Kirkpatrick, R. M. Light, K. A. Marsh, H. McCallon, S. Schneider, R. Stiening, M. Sykes, M. Weinberg, W. A. Wheaton, S. Wheelock, and N. Zacarias. *2MASS All Sky Catalog of point sources.* The IRSA 2MASS All-Sky Point Source Catalog, NASA/IPAC Infrared Science Archive. http://irsa.ipac.caltech.edu/applications/Gator/, June 2003.

[48] R. De Simone, X. Wu, and S. Tremaine. The stellar velocity distribution in the solar neighbourhood. MNRAS, 350:627–643, May 2004.

[49] W. Dehnen. The Effect of the Outer Lindblad Resonance of the Galactic Bar on the Local Stellar Velocity Distribution. AJ, 119:800–812, February 2000.

[50] J. E. Drew, R. Greimel, M. J. Irwin, A. Aungwerojwit, M. J. Barlow, R. L. M. Corradi, J. J. Drake, B. T. Gänsicke, P. Groot, A. Hales, E. C. Hopewell, J. Irwin, C. Knigge, P. Leisy, D. J. Lennon, A. Mampaso, M. R. W. Masheder, M. Matsuura, L. Morales-Rueda, R. A. H. Morris, Q. A. Parker, S. Phillipps, P. Rodriguez-Gil, G. Roelofs, I. Skillen, J. L. Sokoloski, D. Steeghs, Y. C. Unruh, K. Viironen, J. S. Vink, N. A. Walton, A. Witham, N. Wright, A. A. Zijlstra, and A. Zurita. The INT Photometric Hα Survey of the

Northern Galactic Plane (IPHAS). MNRAS, 362:753–776, September 2005.

[51] M. Durant and M. H. van Kerkwijk. Distances to Anomalous X-Ray Pulsars Using Red Clump Stars. ApJ, 650:1070–1081, October 2006.

[52] B. Famaey, A. Jorissen, H. Dejonghe, S. Udry, and M. Mayor. Three-Integral Models of the Milky Way Disk. In G. G. Byrd, K. V. Kholshevnikov, A. A. Myllri, I. I. Nikiforov, & V. V. Orlov, editor, *Order and Chaos in Stellar and Planetary Systems*, volume 316 of *Astronomical Society of the Pacific Conference Series*, pages 337–+, November 2004.

[53] B. Famaey, A. Jorissen, X. Luri, M. Mayor, S. Udry, H. Dejonghe, and C. Turon. Radial velocities for 6691 K and M giants (Famaey+, 2005). *VizieR Online Data Catalog*, 343:165–+, October 2004.

[54] B. Famaey, A. Jorissen, X. Luri, M. Mayor, S. Udry, H. Dejonghe, and C. Turon. Dynamical Streams in the Solar Neighbourhood. In C. Turon, K. S. O'Flaherty, & M. A. C. Perryman, editor, *The Three-Dimensional Universe with Gaia*, volume 576 of *ESA Special Publication*, pages 129–+, January 2005.

[55] B. Famaey, A. Jorissen, X. Luri, M. Mayor, S. Udry, H. Dejonghe, and C. Turon. Local kinematics of K and M giants from CORAVEL/Hipparcos/Tycho-2 data. Revisiting the concept of superclusters. A&A, 430:165–186, January 2005.

[56] B. Famaey, F. Pont, X. Luri, S. Udry, M. Mayor, and A. Jorissen. Using The Geneva-Copenhagen Survey To Study The Nature Of The Hyades Stream. In *IAU Joint Discussion*, volume 13 of *IAU Joint Discussion*, August 2006.

[57] B. Famaey, F. Pont, X. Luri, S. Udry, M. Mayor, and A. Jorissen. The Hyades stream: an evaporated cluster or an intrusion from the inner disk? A&A, 461:957–962, January 2007.

[58] B. Famaey, A. Siebert, and A. Jorissen. On the age heterogeneity of the Pleiades, Hyades, and Sirius moving groups. A&A, 483:453–459, May 2008.

[59] M. Fiorucci and U. Munari. The Asiago Database on Photometric Systems (ADPS). II. Band and reddening parameters. A&A, 401:781–796, April 2003.

[60] E. L. Fitzpatrick. Correcting for the Effects of Interstellar Extinction. PASP, 111:63–75, January 1999.

[61] W. L. Freedman, B. F. Madore, B. K. Gibson, L. Ferrarese, D. D. Kelson, S. Sakai, J. R. Mould, R. C. Kennicutt, Jr., H. C. Ford, J. A. Graham, J. P. Huchra, S. M. G. Hughes, G. D. Illingworth, L. M. Macri, and P. B. Stetson. Final Results from the Hubble Space Telescope Key Project to Measure the Hubble Constant. ApJ, 553:47–72, May 2001.

[62] K. Freeman. Dynamical History of the Galaxy. In *Bernard's Cosmic Stories: From Primordial Fluctuations to the Birth of Stars and Galaxies*, 2006.

[63] K. Freeman and J. Bland-Hawthorn. The New Galaxy: Signatures of Its Formation. ARA&A, 40:487–537, 2002.

[64] K. C. Freeman. *Stellar Disks*, pages 3–+. 2007.

[65] J. A. Frogel and A. E. Whitford. M giants in Baade's window - Infrared colors, luminosities, and implications for the stellar content of E and S0 galaxies. ApJ, 320:199–237, September 1987.

[66] R. Fux. Order and chaos in the local disc stellar kinematics induced by the Galactic bar. A&A, 373:511–535, July 2001.

[67] R. Fux, T. Axelrod, and P. Popowski. The 3D Structure of the Galactic Bulge from the MACHO Red Clump Stars. In L. P. Ossipkov and I. I. Nikiforov, editors, *Stellar Dynamics: from Classic to Modern*, pages 21–27, 2001.

[68] P. M. Garnavich and K. Stanek. Red clump stars - further improved distance indicator. *Highlights of Astronomy*, 12:688–+, 2002.

[69] P. M. Garnavich and K. Z. Stanek. Red Clump Stars - Further Improved Distance Indicator. *HIPPARCOS and the Luminosity Calibration of the Nearer Stars, 24th meeting of the IAU, Joint Discussion 13, August 2000, Manchester, England, meeting abstract.*, 13, 2000.

[70] L. Girardi. A secondary clump of red giant stars: why and where. MNRAS, 308:818–832, September 1999.

[71] L. Girardi. Fine Structure of the Red Clump in Local Group Galaxies. In J. Bergeron and A. Renzini, editors, *From Extrasolar Planets to Cosmology: The VLT Opening Symposium*, pages 294–+, 2000.

[72] L. Girardi. Theoretical expectations for clump red giants as distance indicators. *HIPPARCOS and the Luminosity Calibration of the Nearer Stars, 24th meeting of the IAU, Joint Discussion 13, August 2000, Manchester, England, meeting abstract.*, 13, 2000.

[73] L. Girardi. Theoretical expectations for clump red giants as distance indicators. *Highlights of Astronomy*, 12:689–693, 2002.

[74] L. Girardi, M. A. T. Groenewegen, A. Weiss, and M. Salaris. Fine structure of the red giant clump from HIPPARCOS data, and distance determinations based on its mean magnitude. MNRAS, 301:149–160, November 1998.

[75] L. Girardi, J.-C. Mermilliod, and G. Carraro. On the peculiar red clump morphology in the open clusters NGC 752 and NGC 7789. A&A, 354:892–898, February 2000.

[76] L. Girardi and M. Salaris. Population effects on the red giant clump absolute magnitude, and distance determinations to nearby galaxies. MNRAS, 323:109–129, May 2001.

[77] A. E. Gomez, X. Luri, S. Grenier, F. Figueras, P. North, F. Royer, J. Torra, and M. O. Mennessier. The HR-diagram from HIPPARCOS data. Absolute magnitudes and kinematics of BP - AP stars. A&A, 336:953–959, August 1998.

[78] E. Griv, M. Gedalin, and D. Eichler. The Stellar Velocity Distribution in the Solar Neighborhood: Deviations from the Schwarzschild Distribution. AJ, 137:3520–3528, March 2009.

[79] A. J. Grocholski and A. Sarajedini. WIYN Open Cluster Study: The Absolute K Band Magnitude of the Red Clump as a Distance Indicator. In *Bulletin of the American Astronomical Society*, volume 33 of *Bulletin of the American Astronomical Society*, pages 1385–+, December 2001.

[80] A. J. Grocholski and A. Sarajedini. WIYN Open Cluster Study. X. The K-Band Magnitude of the Red Clump as a Distance Indicator. AJ, 123:1603–1612, March 2002.

[81] A. J. Grocholski, A. Sarajedini, K. A. G. Olsen, G. P. Tiede, and C. L. Mancone. Distances to Populous Clusters in the Large Magellanic Cloud via the K-band Luminosity of the Red Clump. AJ, 134:680–693, August 2007.

[82] M. A. T. Groenewegen. The red clump absolute magnitude based on revised Hipparcos parallaxes. A&A, 488:935–941, September 2008.

[83] V. V. Gvaramadze, S. Fabrika, W.-R. Hamann, O. Sholukhova, A. F. Valeev, V. P. Goranskij, A. M. Cherepashchuk, D. J. Bomans, and L. M. Oskinova. Discovery of a new Wolf-Rayet star and its ring nebula in Cygnus. MNRAS, 400:524–530, November 2009.

[84] I. Hachisu, M. Kato, K. Nomoto, and H. Umeda. A New Evolutionary Path to Type IA Supernovae: A Helium-rich Supersoft X-Ray Source Channel. ApJ, 519:314–323, July 1999.

[85] D. Hatzidimitriou. A new age calibrator for red horizontal branch populations. MNRAS, 251:545–554, August 1991.

[86] D. Hatzidimitriou and M. R. S. Hawkins. Stellar populations and large-scale structure of the SMC. II - Geometry of the north-eastern and south-western outlying regions. MNRAS, 241:667–690, December 1989.

[87] A. Helmi. Velocity Trends in the Debris of Sagittarius and the Shape of the Dark Matter Halo of Our Galaxy. ApJ, 610:L97–L100, August 2004.

[88] X. Hernandez, D. Valls-Gabaud, and G. Gilmore. The recent star formation history of the Hipparcos solar neighbourhood. MNRAS, 316:605–612, August 2000.

[89] F. V. Hessman and E. W. Guenther. The highly veiled T Tauri stars DG Tau, DR Tau, and DI Cep. A&A, 321:497–512, May 1997.

[90] E. Hoeg, G. Bässgen, U. Bastian, D. Egret, C. Fabricius, V. Großmann, J. L. Halbwachs, V. V. Makarov, M. A. C. Perryman, P. Schwekendiek, K. Wagner, and A. Wicenec. The TYCHO Catalogue. A&A, 323:L57–L60, July 1997.

[91] N. L. Homeier, R. D. Blum, A. Pasquali, P. S. Conti, and A. Damineli. Results from a near infrared search for emission-line stars in the Inner Galaxy: Spectra of new Wolf-Rayet stars. A&A, 408:153–159, September 2003.

[92] R. Ibata, M. Irwin, G. F. Lewis, and A. Stolte. Galactic Halo Substructure in the Sloan Digital Sky Survey: The Ancient Tidal Stream from the Sagittarius Dwarf Galaxy. ApJ, 547:L133–L136, February 2001.

[93] R. A. Ibata, G. F. Lewis, and J.-P. Beaulieu. Reexamination of the Possible Tidal Stream in Front of the Large Magellanic Cloud. ApJ, 509:L29–L32, December 1998.

[94] I. Iben, Jr. Age and Initial Helium Abudance of Stars in the Globular Cluster M15. Nature, 220:143–+, October 1968.

[95] A. Ibukiyama and N. Arimoto. HIPPARCOS age-metallicity relation of the solar neighbourhood disc stars. A&A, 394:927–941, November 2002.

[96] E. Jilinski, V. G. Ortega, R. de la Reza, N. A. Drake, and B. Bazzanella. Dynamical Evolution and Spectral Characteristics of the Stellar Group Mamajek 2. ApJ, 691:212–218, January 2009.

[97] R. Jimenez, C. Flynn, and E. Kotoneva. HIPPARCOS and the age of the Galactic disc. MNRAS, 299:515–519, September 1998.

[98] K. V. Johnston, D. R. Law, and S. R. Majewski. A Two Micron All Sky Survey View of the Sagittarius Dwarf Galaxy. III. Constraints on the Flattening of the Galactic Halo. ApJ, 619:800–806, February 2005.

[99] S. Jordan, W. Schmutz, B. Wolff, K. Werner, and U. Muerset. Extragalactic symbiotic systems. IV. The supersoft X-ray source SMC 3. A&A, 312:897–904, August 1996.

[100] R. C. Kennicutt, Jr. Star Formation in Galaxies Along the Hubble Sequence. ARA&A, 36:189–232, 1998.

[101] R. C. Kennicutt, Jr., D. Calzetti, F. Walter, G. Helou, D. J. Hollenbach, L. Armus, G. Bendo, D. A. Dale, B. T. Draine, C. W. Engelbracht, K. D. Gordon, M. K. M. Prescott, M. W. Regan, M. D. Thornley, C. Bot, E. Brinks, E. de Blok, D. de Mello, M. Meyer, J. Moustakas, E. J. Murphy, K. Sheth, and J. D. T. Smith. Star Formation in NGC 5194 (M51a). II. The Spatially Resolved Star Formation Law. ApJ, 671:333–348, December 2007.

[102] M. Kim, E. Kim, M. G. Lee, A. Sarajedini, and D. Geisler. Determination of the Distance to M33 Based on the Tip of

the Red Giant Branch and the Red Clump. AJ, 123:244–254, January 2002.

[103] C. R. King, G. S. Da Costa, and P. Demarque. The luminosity function on the subgiant branch of 47 Tucanae A comparison of observation and theory. ApJ, 299:674–682, December 1985.

[104] J. R. King, A. R. Villarreal, D. R. Soderblom, A. F. Gulliver, and S. J. Adelman. Stellar Kinematic Groups. II. A Reexamination of the Membership, Activity, and Age of the Ursa Major Group. AJ, 125:1980–2017, April 2003.

[105] J. D. Kirkpatrick, T. J. Henry, and D. W. McCarthy, Jr. A standard stellar spectral sequence in the red/near-infrared - Classes K5 to M9. ApJS, 77:417–440, November 1991.

[106] C. Koen and F. Lombard. Some statistical aspects of estimating the local red clump absolute magnitude. MNRAS, 343:241–248, July 2003.

[107] L. Kohoutek. Hamburg Schmidt-camera survey of faint planetary nebulae. *Bulletin of the Astronomical Institutes of Czechoslovakia*, 16:221–+, 1965.

[108] L. Kohoutek and R. Wehmeyer. Catalogue of H-alpha emission stars in the Northern Milky Way. A&AS, 134:255–256, January 1999.

[109] V. V. Kovtyukh, C. Soubiran, O. Bienayme, T. V. Mishenina, and S. I. Belik. Effective temperatures of 215 FGK giants (Kovtyukh+, 2006). *VizieR Online Data Catalog*, 837:10879–+, November 2006.

[110] O. Krause, D. Lemke, L. V. Tóth, U. Klaas, M. Haas, M. Stickel, and R. Vavrek. A very young star forming region detected by the ISOPHOT Serendipity Survey. A&A, 398:1007–1020, February 2003.

[111] P. Kroupa. On the variation of the initial mass function. MNRAS, 322:231–246, April 2001.

[112] P. Kroupa. The initial mass function of simple and composite stellar populations. *ArXiv Astrophysics e-prints*, March 2007.

[113] P. Kroupa. The IMF of Simple and Composite Populations. In J. H. Knapen, T. J. Mahoney, and A. Vazdekis, editors,

Pathways Through an Eclectic Universe, volume 390 of *Astronomical Society of the Pacific Conference Series*, pages 3–+, June 2008.

[114] P. Kroupa, S. Röser, and U. Bastian. On the motion of the Magellanic Clouds. MNRAS, 266:412–+, January 1994.

[115] P. Kroupa, C. A. Tout, and G. Gilmore. The distribution of low-mass stars in the Galactic disc. MNRAS, 262:545–587, June 1993.

[116] M. Kubiak, A. McWilliam, A. Udalski, and K. Gorski. Metal Abundance of Red Clump Stars in Baade's Window. *Acta Astronomica*, 52:159–175, June 2002.

[117] H. J. G. L. M. Lamers, F.-J. Zickgraf, D. de Winter, L. Houziaux, and J. Zorec. An improved classification of B[e]-type stars. A&A, 340:117–128, December 1998.

[118] D. R. Law, K. V. Johnston, and S. R. Majewski. A Two Micron All-Sky Survey View of the Sagittarius Dwarf Galaxy. IV. Modeling the Sagittarius Tidal Tails. ApJ, 619:807–823, February 2005.

[119] Y. Lebreton. Stellar Structure and Evolution: Deductions from Hipparcos. ARA&A, 38:35–77, 2000.

[120] G. Liu and G. Zhao. Spectral analysis of red clump giants and the research on using them as the standard candles in I and K band. *Acta Astronomica Sinica*, 45:253–265, August 2004.

[121] G. Liu and G. Zhao. Spectral analysis of red clump giants and their use as standard candles in the wavebands I and K. *Chinese Astronomy and Astrophysics*, 29:39–52, January 2005.

[122] Y. J. Liu, G. Zhao, J. R. Shi, G. Pietrzyński, and W. Gieren. The abundances of nearby red clump giants. MNRAS, 382:553–566, December 2007.

[123] J. López-Santiago, G. Micela, and D. Montes. Quantifying the contamination by old main-sequence stars in young moving groups: the case of the Local Association. A&A, 499:129–135, May 2009.

[124] L. B. Lucy. Fluorescent excitation of (Ni II) lines in the spectra of gaseous nebulae. A&A, 294:555–567, February 1995.

[125] L. Magrini, R. L. M. Corradi, and U. Munari. A Search for Symbiotic Stars in the Local Group. In R. L. M. Corradi, J. Mikolajewska, & T. J. Mahoney, editor, *Astronomical Society of the Pacific Conference Series*, volume 303 of *Astronomical Society of the Pacific Conference Series*, pages 539–+, 2003.

[126] S. R. Majewski, M. F. Skrutskie, M. D. Weinberg, and J. C. Ostheimer. A Two Micron All Sky Survey View of the Sagittarius Dwarf Galaxy. I. Morphology of the Sagittarius Core and Tidal Arms. ApJ, 599:1082–1115, December 2003.

[127] S. Mao and B. Paczyński. Constraining the Galactic bar parameters with red clump giants. MNRAS, 337:895–900, December 2002.

[128] A. Massarotti, D. W. Latham, R. P. Stefanik, and J. Fogel. Rotational and Radial Velocities for a Sample of 761 HIPPARCOS Giants and the Role of Binarity. AJ, 135:209–231, January 2008.

[129] P. Massey. The Initial Mass Function of Massive Stars in the Local Group. In G. Gilmore & D. Howell, editor, *The Stellar Initial Mass Function (38th Herstmonceux Conference)*, volume 142 of *Astronomical Society of the Pacific Conference Series*, pages 17–+, 1998.

[130] M. Mateo and D. Hatzidimitriou. The Evolution of the Red Giant Clump and the Structure of the Small Magellanic Cloud. In B. Barbuy and A. Renzini, editors, *The Stellar Populations of Galaxies*, volume 149 of *IAU Symposium*, pages 454–+, 1992.

[131] A. McWilliam. High-resolution spectroscopic survey of 671 GK giants. I - Stellar atmosphere parameters and abundances. ApJS, 74:1075–1128, December 1990.

[132] M. R. Meyer, F. C. Adams, L. A. Hillenbrand, J. M. Carpenter, and R. B. Larson. The Stellar Initial Mass Function: Constraints from Young Clusters, and Theoretical Perspectives. *Protostars and Planets IV*, pages 121–+, May 2000.

[133] G. E. Miller and J. M. Scalo. The initial mass function and stellar birthrate in the solar neighborhood. ApJS, 41:513–547, November 1979.

[134] Y. Momany, S. R. Zaggia, P. Bonifacio, G. Piotto, F. De Angeli, L. R. Bedin, and G. Carraro. Probing the Canis

Major stellar over-density as due to the Galactic warp. A&A, 421:L29–L32, July 2004.

[135] U. Munari and L. M. Buson. The ultraviolet spectra of the symbiotic stars MWC 960, FN Sgr, SS 29 and Draco C-1. A&A, 287:87–94, July 1994.

[136] U. Munari, R. Sordo, F. Castelli, and T. Zwitter. An extensive library of 2500 10 500 Å synthetic spectra. A&A, 442:1127–1134, nov 2005.

[137] U. Munari and T. Zwitter. A multi-epoch spectrophotometric atlas of symbiotic stars. A&A, 383:188–196, January 2002.

[138] J. F. Navarro, A. Helmi, and K. C. Freeman. The Extragalactic Origin of the Arcturus Group. ApJ, 601:L43–L46, January 2004.

[139] H. J. Newberg, B. Yanny, C. Rockosi, E. K. Grebel, H.-W. Rix, J. Brinkmann, I. Csabai, G. Hennessy, R. B. Hindsley, R. Ibata, Z. Ivezić, D. Lamb, E. T. Nash, M. Odenkirchen, H. A. Rave, D. P. Schneider, J. A. Smith, A. Stolte, and D. G. York. The Ghost of Sagittarius and Lumps in the Halo of the Milky Way. ApJ, 569:245–274, April 2002.

[140] S. Nishiyama, T. Nagata, S. Sato, D. Kato, T. Nagayama, N. Kusakabe, N. Matsunaga, T. Naoi, K. Sugitani, and M. Tamura. The Distance to the Galactic Center Derived from Infrared Photometry of Bulge Red Clump Stars. ApJ, 647:1093–1098, August 2006.

[141] B. Nordström, J. Andersen, J. Holmberg, B. R. Jørgensen, M. Mayor, and F. Pont. The Geneva-Copenhagen Survey of the Solar Neighbourhood. *Publications of the Astronomical Society of Australia*, 21:129–133, 2004.

[142] B. Nordström, M. Mayor, J. Andersen, J. Holmberg, F. Pont, B. R. Jørgensen, E. H. Olsen, S. Udry, and N. Mowlavi. The Geneva-Copenhagen survey of the Solar neighbourhood. Ages, metallicities, and kinematic properties of 14 000 F and G dwarfs. A&A, 418:989–1019, May 2004.

[143] D. E. Osterbrock and G. J. Ferland. *Astrophysics of gaseous nebulae and active galactic nuclei.* 2006.

[144] B. Paczynski. Metallicity of Red Clump Giants in Baade's Window. *Acta Astronomica*, 48:405–412, September 1998.

[145] B. Paczynski and B. Rudak. Symbiotic stars - Evolutionary considerations. A&A, 82:349–351, February 1980.

[146] B. Paczynski and K. Z. Stanek. Galactocentric Distance with the Optical Gravitational Lensing Experiment and HIPPARCOS Red Clump Stars. ApJ, 494:L219+, February 1998.

[147] B. Paczynski and K. Z. Stanek. Galactocentric Distance with the Optical Gravitational Lensing Experiment and HIPPARCOS Red Clump Stars. ApJ, 494:L219+, February 1998.

[148] S. M. Percival and M. Salaris. An empirical test of the theoretical population corrections to the red clump absolute magnitude. MNRAS, 343:539–546, August 2003.

[149] M. A. C. Perryman, L. Lindegren, J. Kovalevsky, E. Hoeg, U. Bastian, P. L. Bernacca, M. Crézé, F. Donati, M. Grenon, F. van Leeuwen, H. van der Marel, F. Mignard, C. A. Murray, R. S. Le Poole, H. Schrijver, C. Turon, F. Arenou, M. Froeschlé, and C. S. Petersen. The HIPPARCOS Catalogue. A&A, 323:L49–L52, July 1997.

[150] M. Persic and Y. Rephaeli. Galactic star formation rates gauged by stellar end-products. A&A, 463:481–492, February 2007.

[151] A. E. Piatti, D. Geisler, E. Bica, J. J. Clariá, J. F. C. Santos, Jr., A. Sarajedini, and H. Dottori. A New Giant Branch Clump Structure in the Large Magellanic Cloud. AJ, 118:2865–2874, December 1999.

[152] G. Pietrzyński and W. Gieren. The ARAUCARIA Project: Deep Near-Infrared Survey of Nearby Galaxies. I. The Distance to the Large Magellanic Cloud from K-Band Photometry of Red Clump Stars. AJ, 124:2633–2638, November 2002.

[153] G. Pietrzy{ń}ski, W. Gieren, and A. Udalski. The Araucaria Project: Dependence of mean K, J, and I absolute magnitudes of red clump stars on metallicity and age. *ArXiv Astrophysics e-prints*, February 2003.

[154] G. Pietrzyński, W. Gieren, and A. Udalski. The Araucaria Project: Dependence of Mean K, J, and I Absolute Magnitudes of Red Clump Stars on Metallicity and Age. AJ, 125:2494–2501, May 2003.

[155] M. Popova, O. Dluzhnevskaia, A. Antov, and A. Piskunov. Clumps of red giants on the C-M diagrams of open clusters. *Astrofizicheskie Issledovaniya Sofia*, 5:60–63, 1989.

[156] M. Popova, O. Dluzhnevskaya, A. Antov, and A. Piskunov. On the clumps of red giants on the C-M diagrams of the open clusters. *Astrofiz. Issled., Vol. 5, p. 60 - 63*, 5:60–63, 1989.

[157] P. Ranalli, A. Comastri, and G. Setti. The 2-10 keV luminosity as a Star Formation Rate indicator. A&A, 399:39–50, February 2003.

[158] N. J. Rattenbury, S. Mao, V. P. Debattista, T. Sumi, O. Gerhard, and F. de Lorenzi. Proper motion dispersions of red clump giants in the galactic bulge: observations and model comparisons. MNRAS, 378:1165–1176, July 2007.

[159] N. J. Rattenbury, S. Mao, T. Sumi, and M. C. Smith. Erratum: Modelling the Galactic bar using OGLE-II red clump giant stars. MNRAS, 382:1376–1376, December 2007.

[160] N. J. Rattenbury, S. Mao, T. Sumi, and M. C. Smith. Modelling the Galactic bar using OGLE-II red clump giant stars. MNRAS, 378:1064–1078, July 2007.

[161] I. N. Reid. The Substellar Mass Function after 2MASS. In *Bulletin of the American Astronomical Society*, volume 30 of *Bulletin of the American Astronomical Society*, pages 1375–+, December 1998.

[162] T. H. Robertson and T. M. Jordan. Faint H-alpha emission objects near the equatorial selected areas. AJ, 98:1354–1357, October 1989.

[163] H. J. Rocha-Pinto, C. Flynn, J. Scalo, J. Hänninen, W. J. Maciel, and G. Hensler. Chemical enrichment and star formation in the Milky Way disk. III. Chemodynamical constraints. A&A, 423:517–535, August 2004.

[164] M. Romaniello, M. Salaris, S. Cassisi, and N. Panagia. Hubble Space Telescope Observations of the Large Magellanic Cloud Field around SN 1987A: Distance Determination with Red Clump and Tip of the Red Giant Branch Stars. ApJ, 530:738–743, February 2000.

[165] S. P. Rybka. A catalogue of candidate Red Clump stars in the Tycho-2. *Kinematika i Fizika Nebesnykh Tel*, 23:102–+, 2007.

[166] S. P. Rybka. Candidate Red Clump stars in the Tycho-2 (Rybka+, 2007). *VizieR On-line Data Catalog: J/other/KFNT/23.102. Originally published in: 2007KFNT...23..102R*, 30:2301–+, February 2007.

[167] S. P. Rybka. Peculiarities of galactic rotation in the solar neighborhood from the data on red clump giants. *Kinematics and Physics of Celestial Bodies*, 24:99–104, May 2008.

[168] R. Sagar, T. Richtler, and K. S. de Boer. Two distinct supergiant branches in the young Large Magellanic Cloud star cluster NGC 2214. A&A, 249:L5–L8, September 1991.

[169] M. Salaris and L. Girardi. Population effects on the red giant clump absolute magnitude: the K band. MNRAS, 337:332–340, November 2002.

[170] M. Salaris, S. Percival, and L. Girardi. A theoretical analysis of the systematic errors in the red clump distance to the Large Magellanic Cloud (LMC). MNRAS, 345:1030–1038, November 2003.

[171] S. E. Sale, J. E. Drew, Y. C. Unruh, M. J. Irwin, C. Knigge, S. Phillipps, A. A. Zijlstra, B. T. Gänsicke, R. Greimel, P. J. Groot, A. Mampaso, R. A. H. Morris, R. Napiwotzki, D. Steeghs, and N. A. Walton. High spatial resolution Galactic 3D extinction mapping with IPHAS. MNRAS, 392:497–513, January 2009.

[172] S. Salim, R. M. Rich, S. Charlot, J. Brinchmann, B. D. Johnson, D. Schiminovich, M. Seibert, R. Mallery, T. M. Heckman, K. Forster, P. G. Friedman, D. C. Martin, P. Morrissey, S. G. Neff, T. Small, T. K. Wyder, L. Bianchi, J. Donas, Y.-W. Lee, B. F. Madore, B. Milliard, A. S. Szalay, B. Y. Welsh, and S. K. Yi. UV Star Formation Rates in the Local Universe. ApJS, 173:267–292, December 2007.

[173] E. E. Salpeter. The Luminosity Function and Stellar Evolution. ApJ, 121:161–+, January 1955.

[174] M. Santander-García, R. L. M. Corradi, A. Mampaso, C. Morisset, U. Munari, M. Schirmer, B. Balick, and M. Livio. Hen 2-104: a close-up look at the Southern Crab. A&A, 485:117–126, July 2008.

[175] A. Sarajedini. WIYN Open Cluster Study. III. The Observed Variation of the Red Clump Luminosity and Color with Metallicity and Age. AJ, 118:2321–2326, November 1999.

[176] A. Sarajedini, A. J. Grocholski, J. Levine, and E. Lada. K-Band Red Clump Distances to the Large Magellanic Cloud Clusters Hodge 4 and NGC 1651. AJ, 124:2625–2632, November 2002.

[177] J. M. Scalo. The stellar initial mass function. *Fundamentals of Cosmic Physics*, 11:1–278, May 1986.

[178] M. Schmidt. The Rate of Star Formation. ApJ, 129:243–+, March 1959.

[179] H. R. Schmitt, D. Calzetti, L. Armus, M. Giavalisco, T. M. Heckman, R. C. Kennicutt, Jr., C. Leitherer, and G. R. Meurer. Ultraviolet-to-Far-Infrared Properties of Local Star-forming Galaxies. ApJ, 643:173–185, May 2006.

[180] G. M. Seabroke and G. Gilmore. Revisiting the relations: Galactic thin disc age-velocity dispersion relation. MNRAS, 380:1348–1368, October 2007.

[181] E. Seidel, P. Demarque, and D. Weinberg. The evolution of red clump stars - Theoretical sequences. ApJS, 63:917–945, April 1987.

[182] A. Siebert, O. Bienaymé, and C. Soubiran. Spectroscopic survey of Red Clump stars and the vertical shape of the Galactic potential. In C. M. Boily, P. Pastsis, S. Portegies Zwart, R. Spurzem, and C. Theis, editors, *EAS Publications Series*, volume 10 of *EAS Publications Series*, pages 49–+, 2003.

[183] A. Siebert, O. Bienaymé, and C. Soubiran. Vertical distribution of Galactic disk stars. II. The surface mass density in the Galactic plane. A&A, 399:531–541, February 2003.

[184] J. Skuljan. A study of moving groups of stars in our Galaxy. *Publications de l'Observatoire Astronomique de Beograd*, 75:135–136, October 2003.

[185] J. Skuljan, J. B. Hearnshaw, and P. L. Cottrell. Velocity distribution of stars in the solar neighbourhood. MNRAS, 308:731–740, September 1999.

[186] J. Skuljan, J. B. Hearnshaw, and P. L. Cottrell. High-Precision Radial Velocity Measurements of Some Southern Stars. PASP, 112:966–976, July 2000.

[187] J. L. Sokoloski. Rapid Variability as a Diagnostic of Accretion and Nuclear Burning in Symbiotic Stars and Supersoft

X-Ray Sources (invited review talks). In R. L. M. Corradi, J. Mikolajewska, & T. J. Mahoney, editor, *Astronomical Society of the Pacific Conference Series*, volume 303 of *Astronomical Society of the Pacific Conference Series*, pages 202–+, 2003.

[188] C. Soubiran, O. Bienaymé, T. V. Mishenina, and V. V. Kovtyukh. Vertical distribution of Galactic disk stars. IV. AMR and AVR from clump giants. A&A, 480:91–101, March 2008.

[189] C. Soubiran, O. Bienaymé, and A. Siebert. Vertical distribution of Galactic disk stars. I. Kinematics and metallicity. A&A, 398:141–151, January 2003.

[190] K. Z. Stanek and P. M. Garnavich. Distance to M31 with the Hubble Space Telescope and HIPPARCOS Red Clump Stars. ApJ, 503:L131+, August 1998.

[191] K. Z. Stanek and P. M. Garnavich. Distance to M31 with the Hubble Space Telescope and HIPPARCOS Red Clump Stars. ApJ, 503:L131+, August 1998.

[192] K. Z. Stanek and P. M. Garnavich. Red Clump Stars - Further Improved Distance Indicator. In *Bulletin of the American Astronomical Society*, volume 31 of *Bulletin of the American Astronomical Society*, pages 1391–+, December 1999.

[193] K. Z. Stanek, J. Kaluzny, A. Wysocka, and I. Thompson. UBVI Color-Magnitude Diagrams in Baade's Window Metallicity Range, Implications for the Red Clump Method, Color "Anomaly" and the Distances to the Galactic Center and the Large Magellanic Cloud. *Acta Astronomica*, 50:191–210, June 2000.

[194] K. Z. Stanek, M. Mateo, A. Udalski, M. Szymanski, J. Kaluzny, and M. Kubiak. Color-magnitude diagram distribution of the bulge red clump stars: Evidence for the galactic bar. ApJ, 429:L73–L76, July 1994.

[195] K. Z. Stanek, M. Mateo, A. Udalski, M. Szymanski, J. Kaluzny, M. Kubiak, and W. Krzeminski. Evidence for the Galactic Bar from the Two Color Photometry of the Bulge Red Clump Stars. *ArXiv Astrophysics e-prints*, October 1994.

[196] K. Z. Stanek, M. Mateo, A. Udalski, M. Szymański, J. Kaluzny, M. Kubiak, and W. Krzemiński. Evidence for

the Galactic Bar from the Two Color Photometry of the Bulge Red Clump Stars. In L. Blitz and P. J. Teuben, editors, *Unsolved Problems of the Milky Way*, volume 169 of *IAU Symposium*, pages 103–+, 1996.

[197] K. Z. Stanek, M. Mateo, A. Udalski, M. Szymanski, J. Kaluzny, M. Kubiak, and W. Krzeminski. Modelling the Galactic Bar using Red Clump Stars. In R. Buta, D. A. Crocker, and B. G. Elmegreen, editors, *IAU Colloq. 157: Barred Galaxies*, volume 91 of *Astronomical Society of the Pacific Conference Series*, pages 545–+, 1996.

[198] K. Z. Stanek, A. Udalski, M. Szymanski, J. Kaluzny, M. Kubiak, M. Mateo, and W. Krzeminski. Modeling the Galactic Bar Using Red Clump Giants. ApJ, 477:163–+, March 1997.

[199] K. Z. Stanek, D. Zaritsky, and J. Harris. A "Short" Distance to the Large Magellanic Cloud with the Hipparcos-calibrated Red Clump Stars. ApJ, 500:L141+, June 1998.

[200] K. Z. Stanek, D. Zaritsky, and J. Harris. A "Short" Distance to the Large Magellanic Cloud with the Hipparcos-calibrated Red Clump Stars. ApJ, 500:L141+, June 1998.

[201] V. Straizys and G. Kuriliene. Fundamental stellar parameters derived from the evolutionary tracks. Ap&SS, 80:353–368, December 1981.

[202] C. Sturch and H. L. Helfer. Upgren's unclassified stars A: a new type of G-giant stars ? AJ, 76:334–+, May 1971.

[203] T. Sumi, L. Eyer, and P. Wozniak. Measurements of streaming motions of the Galactic Bar with Red Clump Giants. In *Bulletin of the American Astronomical Society*, volume 34 of *Bulletin of the American Astronomical Society*, pages 1148–+, December 2002.

[204] T. Sumi, L. Eyer, and P. R. Woźniak. Measurements of streaming motions of the Galactic bar with red clump giants. MNRAS, 340:1346–1352, April 2003.

[205] G. Tautvaišienė, B. Edvardsson, E. Puzeras, E. Stasiukaitis, and I. Ilyin. *Chemical Abundances and Mixing in Red Clump Stars of the Galaxy*, pages 11–+. Chemical Abundances and Mixing in Stars in the Milky Way and its Satellites, ESO ASTROPHYSICS SYMPOSIA. ISBN 978-3-540-34135-2. Springer-Verlag, 2006, p. 11, 2006.

[206] G. Tautvaišiene, E. Stasiukaitis, E. Puzeras, D. F. Gray, and I. Ilyin. High resolution spectroscopic study of red clump stars in the Galaxy: main atmospheric parameters. In F. Favata, G. A. J. Hussain, and B. Battrick, editors, *13th Cambridge Workshop on Cool Stars, Stellar Systems and the Sun*, volume 560 of *ESA Special Publication*, pages 989–+, March 2005.

[207] H.-C. Thomas. Sternentwicklung VIII. Der Helium-Flash bei einem Stern von 1. 3 Sonnenmassen. *Zeitschrift fur Astrophysik*, 67:420–+, 1967.

[208] T. Tomov. Spectroscopic Evidence for High Velocity Bipolar Outflows in Symbiotic Binaries. In R. L. M. Corradi, J. Mikolajewska, & T. J. Mahoney, editor, *Astronomical Society of the Pacific Conference Series*, volume 303 of *Astronomical Society of the Pacific Conference Series*, pages 376–+, 2003.

[209] A. V. Torres and P. Massey. An atlas of optical spectrophotometry of Wolf-Rayet carbon and oxygen stars. ApJS, 65:459–483, November 1987.

[210] C. Turon. The HIPPARCOS results. In T. R. Bedding, A. J. Booth, and J. Davis, editors, *Fundamental Stellar Properties*, volume 189 of *IAU Symposium*, pages 9–+, 1998.

[211] A. V. Tutukov and L. R. Iungelson. On the origin and evolutionary stage of symbiotic stars. *Astrofizika*, 12:521–530, August 1976.

[212] A. Udalski. The Optical Gravitational Lensing Experiment. Population Effects on the Mean Brightness of the Red Clump Stars. *Acta Astronomica*, 48:383–404, September 1998.

[213] A. Udalski. The Optical Gravitational Lensing Experiment: Red Clump Stars as a Distance Indicator. ApJ, 531:L25–L28, March 2000.

[214] A. Udalski, M. Kubiak, and M. Szymanski. Optical Gravitational Lensing Experiment. OGLE-2 – the Second Phase of the OGLE Project. *Acta Astronomica*, 47:319–344, July 1997.

[215] A. Udalski, M. Szymanski, M. Kubiak, G. Pietrzynski, P. Wozniak, and K. Zebrun. Optical Gravitational Lensing Experiment. Distance to the Magellanic Clouds with the

Red Clump Stars: Are the Magellanic Clouds 15% Closer than Generally Accepted? *Acta Astronomica*, 48:1–17, January 1998.

[216] L. Valdivielso, E. L. Martín, H. Bouy, E. Solano, J. E. Drew, R. Greimel, R. Gutiérrez, Y. C. Unruh, and J. S. Vink. An IPHAS-based search for accreting very low-mass objects using VO tools. A&A, 497:973–981, April 2009.

[217] M. Valentini, R. Barbon, U. Munari, M. Fiorucci, and A. Siviero. ARCS: the Asiago Red Clump Spectroscopic Survey. In A. Vallenari, R. Tantalo, L. Portinari, and A. Moretti, editors, *From Stars to Galaxies: Building the Pieces to Build Up the Universe*, volume 374 of *Astronomical Society of the Pacific Conference Series*, pages 205–+, December 2007.

[218] V. van Helshoecht and M. A. T. Groenewegen. Influence of Metallicity on Distance Indicators in the Near Universe: the Red Clump. In C. Aerts and C. Sterken, editors, *Astrophysics of Variable Stars*, volume 349 of *Astronomical Society of the Pacific Conference Series*, pages 363–+, April 2006.

[219] V. van Helshoecht and M. A. T. Groenewegen. K-band magnitude of the red clump as a distance indicator. A&A, 463:559–565, February 2007.

[220] F. van Leeuwen. Rights and wrongs of the Hipparcos data. A critical quality assessment of the Hipparcos catalogue. A&A, 439:805–822, August 2005.

[221] F. van Leeuwen, editor. *Hipparcos, the New Reduction of the Raw Data*, volume 350 of *Astrophysics and Space Science Library*, 2007.

[222] F. van Leeuwen, editor. *Hipparcos, the New Reduction of the Raw Data*, volume 250 of *Astrophysics and Space Science Library*, 2007.

[223] F. van Leeuwen. Validation of the new Hipparcos reduction. A&A, 474:653–664, November 2007.

[224] F. van Leeuwen. Hipparcos, the New Reduction (van Leeuwen, 2007). *VizieR Online Data Catalog*, 1311:0–+, September 2008.

[225] F. van Leeuwen and E. Fantino. A new reduction of the raw Hipparcos data. A&A, 439:791–803, August 2005.

[226] J. S. Vink, J. E. Drew, D. Steeghs, N. J. Wright, E. L. Martin, B. T. Gänsicke, R. Greimel, and J. Drake. IPHAS discoveries of young stars towards Cyg OB2 and its southern periphery. MNRAS, 387:308–318, June 2008.

[227] S. D. M. White. Simulations of merging galaxies. MNRAS, 184:185–203, July 1978.

[228] S. D. M. White and C. S. Frenk. Galaxy formation through hierarchical clustering. ApJ, 379:52–79, September 1991.

[229] P. A. Whitelock and U. Munari. Photometric properties of symbiotic stars and the nature of the cool component. A&A, 255:171–180, February 1992.

[230] A. R. Witham, C. Knigge, J. E. Drew, R. Greimel, D. Steeghs, B. T. Gänsicke, P. J. Groot, and A. Mampaso. The IPHAS catalogue of Hα emission-line sources in the northern Galactic plane. MNRAS, 384:1277–1288, March 2008.

[231] M. S. Yun, N. A. Reddy, and J. J. Condon. Radio Properties of Infrared-selected Galaxies in the IRAS 2 Jy Sample. ApJ, 554:803–822, June 2001.

[232] G. Zhao, H. M. Qiu, and S. Mao. High-Resolution Spectroscopic Observations of Hipparcos Red Clump Giants: Metallicity and Mass Determinations. ApJ, 551:L85–L88, April 2001.

[233] G. Zhao, H. M. Qiu, and S. Mao. High-Resolution Spectroscopic Observations of Hipparcos Red Clump Giants: Metallicity and Mass Determinations. ApJ, 551:L85–L88, April 2001.

[234] G. Zhao, H.-M. Qiu, and H.-W. Zhang. Alpha element abundances in the red clump giants. *Acta Astrophysica Sinica*, 20:389–394, 2000.

[235] G. Zhao, H.-M. Qiu, and H.-W. Zhang. Abundance of α-elements in red clump giants. *Chinese Astronomy and Astrophysics*, 25:59–64, April 2001.

[236] G. Zhao, H.-M. Qiu, and H.-W. Zhang. Abundance of α-elements in red clump giants. *Chinese Astronomy and Astrophysics*, 25:59–64, April 2001.

[237] J. Zhao, G. Zhao, and Y. Chen. A Catalog of Moving Group Candidates in the Solar Neighborhood. ApJ, 692:L113–L117, February 2009.

[238] B. Zuckerman and R. A. Webb. Identification of a Nearby Stellar Association in theHipparcos Catalog: Implications for Recent, Local Star Formation. ApJ, 535:959–964, June 2000.